Shape Variation in the Growing Non-Adult Tibia

by

Sean Gordon Swaters

A thesis submitted in partial fulfillment of the requirements for the degree of

Master of Arts

Department of Anthropology
University of Alberta

Abstract

The degree of diaphyseal curvature in the human tibia has been shown to significantly correlate with activity levels in archaeological populations. Specifically, tibial anteroposterior curvature is greatest in physically active populations and decreases in less active populations. Interestingly, recent research has shown that the tibial anterior crest's sigmoid curvature increases as diaphyseal anteroposterior decreases. Tibial curvature is theorized to be the product of developmental plasticity during non-adult growth. This hypothesis was tested with 3D geometric morphometrics to determine if the non-adult anterior crest demonstrates age-related shape variation, and if a consistent pattern of shape change is identifiable during growth. A cross-sectional sample of non-adults (n = 41) from four archeological populations was analyzed. A second cross-sectional sample of adults (n = 24) from the four populations was included for two reasons. First, as an endpoint in a maturation analysis of anterior crest size and shape, and second, to determine if sexual dimorphism was present in the adult anterior crest. Age estimates were calculated from dental age atlases. A portion of the anterior crest was traced between 70-40% of tibial diaphyseal length. This portion overlapped the diaphyseal area previously observed to display the greatest degree of morphological change in the tibia. Twelve sliding 3D semi-landmarks were then derived from these traces to capture the shape and outline of the anterior crest. Statistical tests of age (dental age) and size (Csize) were conducted on the semi-landmark data to determine the possible presence of growth-related shape variation. For the results, non-adult anterior crest shape variation was observed to primarily occur in the mediolateral and anteroposterior planes, which coincided with previous research on the adult anterior crest. Age had a non-significant correlation with non-adult

anterior crest shape variation. Further, a consistent pattern of shape change during growth was not observed. Age and size were significantly correlated. No significant differences were detected between adult male and female anterior crests. Regarding the maturation analysis, non-adult shape maturation continued into adulthood as size maturation leveled off during adolescence. From the results of this thesis, non-adult anterior crest shape variation was not significantly correlated with dental age, despite shape maturation continuing into adulthood. This suggests that non-adult anterior crest shape variation may be influenced by other factors of developmental plasticity.

Dedication

This thesis is dedicated to my fiancée Holly Bray, whose love, support, and smile saw this thesis through to completion. Without her this undertaking would not have been possible. With all my heart, thank you.

Acknowledgments

I would like to thank and acknowledge my supervisor Dr. Lesley Harrington (UofA) and co-supervisor Dr. Helen Kurki (UVic) for their unwavering support during the entire course of my MA. In addition, I want to thank the other members of my examination committee, Pamela Mayne Correia and Dr. Robert Losey.

Table of Contents

List of Tables

List of Figures

Chapter 1: Introduction

This thesis explores shape change in the anterior crest of the non-adult human tibia. The tibial anterior crest is a pronounced sigmoid border that commences distal to the tibial tuberosity, and terminates at the distal-most point of the medial malleolus. Tibial shape change is an area of interest to bioarchaeologists because the tibia develops diaphyseal curvature in response to mechanical weight-bearing stress. As noted by Macintosh and colleagues (2015), the morphological plasticity of the tibia's curvature is unique, as it allows researchers to make inferences about behaviour (for example, population mobility and physical activity) in archaeological populations. Brzobohatá and colleagues (2019) published the first dedicated study on the relationship between physical activity levels and tibial anterior crest shape change. The results of their study demonstrated that physical activity levels influence both anterior crest shape and diaphyseal curvature in the tibia. Specifically, decreased levels of physical activity result in the anteroposterior straightening and mediolateral accentuation of anterior crest shape (Brzobohatá et al., 2019). Since adult lower limb morphology develops in response to physical activity during non-adult growth, Brzobohatá et al. (2019), Macintosh et al. (2015), De Groote (2011) and Trinkaus (1993) have pointed out that lower limb ontogenetic studies are fundamental to understanding the development of lower limb morphology in relation to behaviour. Currently, there are no dedicated studies on shape change in the non-adult[1] tibia.

[1] As noted by Beauchesne and colleagues (2018), the duration of childhood, if childhood has more than one stage, and when maturity is obtained, vary between different cultures and societies. Therefore, 'non-adult' is used in this thesis to refer to all individuals below a dental age of 18 years.

Due to a lack of prominent features on the tibia's diaphysis there are challenges to analyzing non-adult and adult tibial morphology (Brzobohatá et al., 2016). Recently, the anterior crest has been shown to be a diaphyseal feature that can be reliably studied in adult tibiae using geometric morphometrics (GM) to analyze the movement of three-dimensional (3D) semi-landmarks to explore changes in shape (Brzobohatá et al., 2019). This thesis attempts to apply the approach of Brzobohatá et al. (2019) to non-adult tibiae so that shape change during growth can be examined.

Recent research on archaeological populations has observed that anterior crest shape differs between those populations that are engaged in greater levels of weight-bearing activity as compared with populations engaged in lower levels of weight-bearing activity (Brzobohatá et al., 2016; Brzobohatá et al., 2019; Macintosh et al., 2015; Frelat and Mitteroecker, 2011). These studies looked exclusively at adult tibiae and did not consider non-adult remains. The exclusion of non-adults in tibia and lower limb research represents a gap in the available literature. This thesis seeks to address this gap by studying non-adult tibiae to answer two key questions. First, is there age-related shape variation in the non-adult anterior crest? Second, how does the tibial anterior crest change in shape during growth? These two primary research questions relate to the development of the anterior crest during non-adult growth.

The anterior crest is a prominent feature on the anterior surface of the tibial diaphysis and is the primary attachment site for the deep fascia of the lower leg. The deep fascia is a connective tissue structure that envelops and attaches to muscles of the calf (Benjamin, 2009; Meissner et al., 2007). The deep fascia helps distribute load-related stress across the calf muscles, and some of the muscular stress is transmitted into the connected deep fascia

(Benjamin, 2009). This stress transfer into other muscles and connected tissue structures is called myofascial transfer (Benjamin, 2009). Due to this, the weight-bearing stress placed on the deep fascia is also transmitted to the fascia's attachment point on the anterior crest, possibly contributing to morphological changes in diaphyseal curvature (Benjamin, 2009).

The importance of the developmental period is noted by Brzobohatá et al. (2019) when discussing the importance of growth disruptions as a possible cause of anterior crest gracility observed in their adult 20th century population. Further, Macintosh et al. (2015) state that the mechanical performance of the tibia and its morphology are derived from external pressures, such as activity, that influence the shape of the tibia during non-adult growth. In addition, studies by De Groote (2011) and Trinkaus (1993) (in relation to variation between Neanderthal and human femoral morphology) state the importance of non-adult physical activity as a determinant of adult morphology.

The studies of Brzobohatá et al. (2019), Macintosh et al. (2015), De Groote (2011) and Trinkaus (1993) note that to fully understand adult morphology, it is necessary to study how exposure to intensive physical and environmental pressures during growth can influence the tibia's later adult morphology. Bone morphology is influenced by external factors, such as activity levels and climate during growth. Using cross-sectional geometry to explore declining tibial diaphyseal curvature from hunter-gatherer to agricultural populations, Macintosh et al. (2015) noted that the tibiae of agricultural populations display reduced diaphyseal curvature compared to hunter-gatherers. The hypothesis for this change in curvature was that adoption of agriculture reduced the amount of weight-bearing stress placed on the tibia due to increased sedentism (Macintosh et al., 2015). The influence of external pressures, such as physical

activity, sedentism and environment, guide and alter the developing skeletal biology; this phenomenon is termed “developmental plasticity” (Gollin, 1981; West-Eberhard, 2005). Therefore, to understand the differences in shape observed in adult tibiae, it is crucial to observe non-adult morphological development and the effect of developmental plasticity on the developing non-adult bone.

A study by Marchi (2007) on hominoid and modern human tibiae demonstrates that tibial morphology is intricately linked to locomotion pattern (bipedalism, semi-bipedalism or quadrupedalism) and to engagement in intensive weight-bearing activity (Brzobohatá et al., 2016; Brzobohatá et al., 2019; Macintosh et al., 2015). Marchi (2007) observes that arboreal locomotion used by orangutans, chimpanzees and gibbons results in a more gracile tibiae and more robust fibulae than in hominoids (humans and gorillas) who engage in terrestrial locomotion forms. Marchi (2007) notes that arboreal locomotion transmits an increased degree of weight into the fibula due to more exaggerated adducted lower-limb movements. As such, this form of locomotion results in a more gracile tibia and more robust fibula. In terrestrial locomotion, due to reduced adducted movements in the lower limb, a greater degree of weight is transmitted into the tibia, resulting in a stronger and more robust tibia (Marchi, 2007).

High levels of weight-bearing physical activity in human populations results in morphological changes in the shape and curvature of the tibial diaphysis and its anterior crest (Brzobohatá et al., 2019; Macintosh et al., 2015). In this regard, the tibia allows bioarchaeologists to observe how changes in the type and frequency of weight-bearing activity can directly alter skeletal morphology. As described in Chapter Two, physical activity and locomotion are important determinants of human tibia morphology. Additionally, the

relationship between physical activity in archaeological populations and the corresponding shape change in the tibia and anterior crest will be discussed.

In order to answer the two research questions outlined above, this study analyzes two groups: 1.) a non-adult tibiae sample, and 2.) an adult tibiae sample. Archaeological burials of people from four regions were selected for study: Nunavut (Sadlermiut); Kentucky (Indian Knoll); Alaska (Point Hope), and Later Stone Age foragers from South Africa. The skeletal remains studied represent non-sedentary people with diverse physical activity patterns. The non-adult tibiae are from individuals of 7 to 17 years of age, based on dental development. Combining the four populations increased the available non-adults in each age group, thereby creating a more representative ontogenetic sample. Using geometric morphometric analysis of 3D cartesian shape data, this thesis is able to analyze anterior crest shape change in three-dimensions, instead of only two-dimensions. 3D analysis is, therefore, the preferred means by which this thesis will study shape change in the non-adult anterior crest.

Chapter 2: Anatomy and Morphology of the Human Tibia

2.1 Anatomy of the Tibia

The human tibia is a long bone in the lower limb, sometimes referred to as the shinbone. The tibia articulates proximally with the distal condyles of the femur, and with the patella. The tibial articulation with the femur and patella together forms the synovial knee joint, in which several ligaments are housed. Laterally the tibia has proximal and distal articulations with the fibula. Distally, the tibia articulates with the talus, a tarsal bone of the foot.

The majority of soft tissue structures associated with the tibia are found on the proximal and posterior surface. The proximal surface of the tibia (called the tibial plateau) is the site of attachment for several structures associated with the knee joint. Due to this, the proximal tibia plays an important role in lower limb stability (Hu et al., 2019). These structures are: the anterior cruciate ligament (ACL); posterior cruciate ligament (PCL); medial collateral ligament (MCL); lateral collateral ligament (LCL), and; medial and lateral menisci (Kersh, Ploeg and Pandy, 2015; Hu et al., 2019). The ACL and PCL originate from the intercondylar fossa of the femur and insert on the tibia's anterior intercondylar area for the ACL, and the posterior intercondylar area for the PCL (Kersh et al., 2015). The MCL inserts along the medial surface of the tibial plateau, while the LCL inserts onto the fibula (Kersh et al., 2015). Kersh et al. (2015) state that these four ligaments act to stabilize the knee joint, by providing support to the knee joint and

by acting as a restraining force upon knee motion (Cristofolini et al., 2013; Yang et al., 2014). The medial and lateral menisci which articulate with the medial and lateral tibial condyles, also provide support to the knee by absorbing load-induced shock that might otherwise damage the cartilage surfaces of the knee found on the proximal tibial and distal femoral surfaces (Hu et al., 2019).

The proximal half of the posterior surface of the tibia is associated with a number of muscles that serve to highlight the importance of the tibia in facilitating bipedal locomotion. These include the soleus, popliteus, and gastrocnemius muscles, all of which, Brzobohatá et al. (2019) noted contract on the tibial diaphysis. The popliteus muscle inserts on the posterior surface along the soleal line and gives rise to the soleus muscle. The popliteus muscle acts to promote flexion in the knee, and assists in knee stabilization (Buitrago, Quintero and Ballesteros, 2018). While the gastrocnemius muscle does not insert along the posterior surface of the tibia; it, along with the soleus act as flexors for the foot (Tian et al., 2012; Bolsterlee et al., 2018; Vieira, Minetto, Hodson-tole and Botter, 2013). Both these muscles join together distally to form the calcaneal (Achilles) tendon and insert into the calcaneal tuberosity of the calcaneus bone of the foot (Tian et al., 2012; Bolsterlee et al., 2018; Vieria et al., 2013).

On the anterior surface of the tibia, the patellar ligament of the quadriceps femoris muscle group inserts into the tibial tuberosity. The quadriceps femoris is vital in the lower limb's ability to facilitate extension which is involved in walking and running (Zhang, 2018). Additionally, on the anterior surface of the tibia, distal to the tibial tuberosity, is the anterior crest, which is the site of attachment for the deep fascia of the leg. The deep fascia of the leg is a thick connective tissue that individually envelops several calf muscles, such as the soleus and

gastrocnemius muscles, and attaches onto the anterior surface of the tibia and the tibia's periosteum (Benjamin, 2009; Meissner et al., 2007) (Figure 2.0). The functions of the deep fascia are: to group the muscles of the lower limb into separate osteofascial compartments according to muscle function; to act as a point of attachment for these muscles, and; to transmit loads between these compartments (Benjamin, 2009). In addition to function, the osteofascial compartments are organized by position (anterior, posterior, medial and lateral) (Benjamin, 2009). The identical developmental origins of the deep fascia and periosteum result in the deep fascia attaching onto the bone when contact with bone is made (Benjamin, 2009). When overworked, fascial entheses, such as medial tibial stress syndrome and 'shin-splints', are common (Benjamin, 2009). Benjamin (2009) noted that tendons in the posterior flexor osteofascial compartment increase the tensile load of the deep fascia when eccentric muscular contraction occurs during exercise on hard surfaces. As reported by Benjamin (2009), the increased tensile load is transmitted into the deep fascia's attachment site on the anterior crest in an effort to promote shock dissipation.

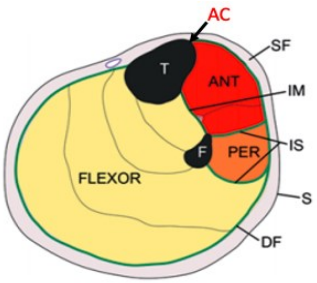

Figure 2.0. Cross-section depicting the fascia of the leg. Tibia (T); Fibula (F); Skin (S); Anterior Crest (AC); Superficial fascia (SF); Deep fascia (DF); Interosseous membrane (IM); Intermuscular septa (IS); Anterior (ANT), Peroneal (PER), and Flexor (Flexor) muscle compartments. Figure adapted from Benjamin (2009).

As previously stated, the tibia is vital to stabilizing the knee joint and facilitating bipedal locomotion. Biomechanical studies by researchers postulate that since the degree of curvature found in the anterior-posterior and medial-lateral planes of the tibia is variable, physical activity levels may drive curvature (Brzobohatá et al., 2016; Brzobohatá et al., 2019; Rantalainen et al., 2015; Ruff and Hayes, 1983; Macintosh et al., 2015). Cristofolini et al. (2013) using musculoskeletal models of *in vitro* measurements of joint force, stated that compressive axial and tensile mechanical stress is transmitted through the tibial plateau during physical activity into the diaphysis. Another area of mechanical stress, specifically from torsional strain, is the posterior surface of the tibia when the calf muscles are activated (Yang et al., 2014). Due to the calf muscles being located on the posterior surface of the tibia, Yang et al. (2014) reported that torsional strain was one of greatest mechanical forces acting on the diaphysis. Yang et al. (2014) theorized that long bone curvature can be further influenced by muscular contractions increasing the amount of bending stress experienced by a long bone. In the case of this thesis, the muscles on the posterior surface of the tibia could be contributing to increased curvature when repeatedly contracted during habitual physical activity. Macintosh et al. (2015) stated that populations that become increasingly more sedentary, display a corresponding decrease in anteroposterior curvature. Brzobohatá et al. (2019) demonstrated that, as diaphyseal anteroposterior curvature declines, the degree of mediolateral curvature in the anterior crest increases, in some populations. A possible explanation for the shape change seen in the anterior crest may relate to myofascial transfer in the deep fascia of the leg. According to Benjamin (2009) and Tian et al. (2012), the deep fascia helps offset load-related stress to other

calf muscles via myofascial transfer. Increased levels of myofascial transfer may play some role in the corresponding anterior crest curvature changes documented by Brzobohatá et al. (2019).

Whether or not the anterior crest curvature is predetermined at birth, or is a plastic response, is currently unknown. A tibial cross-sectional study by Rantalainen et al. (2015) noted that lower limb bones alter their mass and shape in response to load-related stress. Physical activity accrued additional bone mass, whereas decreased physical activity resulted in the loss of bone mass. As noted by Rantalainen et al. (2015), the tibial diaphysis of physically active pre-adolescent and adolescent boys were observed to have an increased amount of bone along the tibial shaft on the anterior and posterior surfaces. Rantalainen et al. (2015) observed that the accumulation or loss of bone mass along the anterior and posterior tibial surfaces corresponded to sagittal bending of the tibial shaft during “typical” weight bearing loading. The cross-sectional results of Rantalainen et al. (2015) showed that active individuals had larger tibial cross-sections with increased bone mineral levels, whereas non-active individuals had smaller cross-sections with decreased bone mineral levels. In addition, Rantalainen et al. (2015) reported that non-adult skeletal morphology is the most susceptible to load-related stress during growth than after growth cessation.

Due to the above, the study of lower-limb morphological shape change has increasingly advocated for the study of non-adult remains to observe how this shape change develops (De Groote, 2011; Macintosh et al., 2015). As non-adult growth coupled with elevated levels of physical activity are believed to exert the greatest influence on later adult tibia morphology, it is instructive to study how the tibial anterior crest changes in shape during growth towards the crest's final adult state.

2.2 The Development of the Non-Adult Tibia

Having described the adult tibia's context within the lower limb, it is necessary to briefly describe the non-adult tibia's development during growth. The non-adult tibia develops from a mesenchyme template around day 41 of embryonic development, with development of the lower limb's muscles and ligaments beginning by day 51 (Scheuer and Black, 2004). After the initial mesenchymal development, the tibia's primary centers of endochondral ossification begin forming during week 8 at the center of the mesenchymal template, and visibly expand proximally and distally (Scheuer and Black, 2004). During weeks 12-14, vascular invasion occurs and the growth plates of the metaphyses are formed (Scheuer and Black, 2004). From weeks 36-40 the secondary centers, which will form the proximal epiphysis, appear and continue to develop until birth (Scheuer and Black, 2004).

At birth, the tibia is usually represented by the tibial shaft and the proximal epiphysis (Scheuer and Black, 2004). However, as Scheuer and Black (2004) observe, the proximal epiphysis can be absent at birth, but in such cases develops shortly afterwards. Additionally, observed is the fact that females tend to develop the proximal epiphysis faster than do males (Scheuer and Black, 2004). The distal portion of the proximal epiphysis, which later forms the tibial tuberosity, first appears between 4.5-6 years of age, and commences proximal ossification between the ages of 8-14 years (Scheuer and Black, 2004). The distal epiphysis does not begin development until 3-4 months after birth, and by 14 months for females and 18 months for males the epiphyseal growth plate begins expanding towards the growth plate of the shaft (Scheuer and Black, 2004). Scheuer and Black (2004) observe that distal epiphyseal growth

occurs faster than that of proximal growth, and by 5-6.5 years the distal epiphysis is the same width as the distal metaphysis due to the ossification of the medial malleolus. By 4-5 years of age, both the proximal and distal metaphyseal surfaces bear ridged markings for later epiphyseal union with the appropriate epiphysis (Scheuer and Black, 2004). The distal section of the proximal epiphysis, which later forms the tibial tuberosity, first appears between 4.5-6 years of age, and commences proximal ossification between the ages of 8-14 years (Scheuer and Black, 2004). The medial malleolus ossification centers typically join the rest of the distal epiphysis between the ages of 10-12 years (Scheuer and Black, 2004). Distal epiphyseal fusion for both boys and girls completes prior to the completion of proximal fusion; distal fusion occurs between the ages of 14-16 years in females, and 15-18 in males (Scheuer and Black, 2004). Proximal epiphyseal fusion completes between the ages of 13-17 years for females, and 15-19 years for males (Scheuer and Black, 2004).

Theoretically, there may be a genetic cause for the degree of anteroposterior curvature seen in adult tibia by other researchers (Brzobohatá et al., 2019; Macintosh et al., 2015; Frelat and Mittereocker, 2011; Sládek et al., 2006), as the tibia, according to Scheuer and Black (2004), already demonstrates some degree of anteroposterior curvature by the prenatal stage of development. However, despite possessing some curvature at the prenatal stage, the non-adult tibia has shown to rapidly alter aspects of its morphology. For example, the angle of the tibial plateau relative to the shaft has been observed to vary at different ages (Scheuer and Black, 2004). In fetuses, the angle can be as high as 27°, but following birth, it declines rapidly until 2 years of age (Scheuer and Black, 2004). In relation to adults, Scheuer and Black (2004) noted high tibial plateau to shaft angles have been observed in populations that habitually squat.

However, Trinkaus (1975), in his study of Neanderthal tibiae, theorized that high plateau to shaft angles could just as likely result from increased levels of physical activity, as from squatting behaviour. Hyperdorsiflexion of the ankle and hyperflexion of the knee from habitual squatting during growth could alter the shape of the proximal tibial and talal condylar surfaces via deviation of the femur and tibia relative to the talus (Dewar and Pfeiffer, 2004). Dewar and Pfeiffer (2004) stated that the creation of lateral facets on the talus, and the rounding of the lateral proximal tibial condylar facet, are evidence of 'typical' human squatting behavior. This is from weight being channeled through the lateral side of the lower limb (Dewar and Pfeiffer, 2004). However, the South African Later Stone Age (LSA) individuals possessed a high frequency of squatting features on the medial side of the lower limb, which suggested that they utilized a modified squatting position, though with some variation according to the geographical region (Dewar and Pfeiffer, 2004). As such, habitual postural behaviour could produce unique lower limb morphological features specific to a group or region. Three LSA tibiae studied by Dewar and Pfeiffer (2004) were also studied in this thesis. In addition to the changing plateau to shaft angles, the degree of tibial shaft torsion has changed. Scheuer and Black (2004) noted that prenatal shaft torsion is initially medial in direction, but begins to alter in the first year of life before the onset of walking. Scheuer and Black (2004) observed a lateral rotation change of 25° by 2 years of age. Referencing the findings of Staheli and Engel (1972), Scheuer and Black (2004) reported a 10° rotation by mid-childhood, and a 14° rotation by adulthood. In contrast to this finding, Turner and Smilie (1981) noted that full adult torsion is usually reached by 5 years of age. According to Scheuer and Black (2004), these contradictory torsion findings could be due to differences in methods of measurement and research terminology.

Additionally, this change in tibial shape may be explained by the onset of walking. Using femoral cross-sections, Cowgill et al. (2010) reported that toddler femoral shape, which is initially circular, is heavily influenced by immature (non-adult) bipedal gait development. As toddlers develop the ability to efficiently walk via waddling, elevated levels of mediolateral bending stress are placed on the entirety of the lower limb until the cessation of waddling around 4 years of age (Cowgill et al., 2010). From 4 years of age on, a persistent decrease in mediolateral bending stress was observed that continued into late-adolescence and adulthood (Cowgill et al., 2010). While the degree of anteroposterior bending stress remained similar between toddlers and adults, Cowgill et al. (2010) theorized that reduced mediolateral bending stress led to the adult femur's tear-drop shape. From this, it is possible that the shape change observed by Scheuer and Black (2004) may also be due to the onset of walking.

2.3 Variation in Tibial Shape

The tibia has shown considerable morphological shape variation between early and contemporary human populations in the antero-posterior curvature of the proximal tibia, and in the medial-lateral curvature of the anterior crest (Sládek, Berner and Sailer, 2006; Brzobohatá et al., 2016; Brzobohatá et al., 2019). Previous research postulates that shape variation in the tibia may be the result of alterations in physical activity levels between more recent human populations and earlier hunter-gather groups (Brzobohatá et al., 2016; Brzobohatá et al., 2019; Macintosh et al., 2015; Frelat and Mitteroecker, 2011; Sládek et al., 2006). However, these previous studies focused on adult tibial morphology, which can be

considered the end-point of tibial development. De Groote (2011), in reference to the femur, and Macintosh et al. (2015) in reference to the tibia, theorize that to truly understand lower-limb curvature and its relation to physical activity, researchers need to study the morphological changes that occur during ontogeny.

It has been suggested that the human tibia demonstrates considerable morphological plasticity when environmental and physical activity related stress is placed upon the bone during growth at the onset of adolescence (Frelat and Mitteroecker, 2011; Frelat et al., 2012; Rantalainen, Weeks, Nogueira and Beck, 2015; Smith et al., 2008; Francis, 1939). The onset of walking, alongside the increased rate of skeletal growth during puberty and increased physical activity levels are believed to exert the greatest influence on the morphological development of the non-adult tibia (Cowgill et al., 2010; Brzobohatá et al., 2016; Brzobohatá et al., 2019; Rantalainen et al., 2015; Ruff and Hayes, 1983). As such, later adult tibial morphology is believed to be a direct consequence of the physical stresses placed upon the bone during adolescence.

In relationship to tibial shape variation, the importance of the need to explore the influence of behaviour (in this sense engagement in intensive weight-bearing physical-activity) on the growing tibia during the non-adult developmental period is emphasized by Brzobohatá et al. (2019), Macintosh et al. (2015), De Groote (2011) and Trinkaus (1993). As these studies all reference the importance of the non-adult developmental period in adult morphology, it is necessary to describe the concept of “developmental plasticity”.

Developmental plasticity refers to the behavioural and biological aspect that can cause variation during non-adult development (Gollin, 1981). Developmental plasticity as a term can

be further broken down, with *plasticity* being referred to as a changeable character of matter (Bateson and Gluckman, 2011). Gollin (1981) defines the concept of plasticity as the range of biological variation that occurs during an organism's individual growth and development. Additionally, the concept of plasticity has been referred to as the period in time where external force and pressure can cause the greatest amount of biological difference (variation) in an organism (Gollin, 1981). Meloni (2019) defines plasticity as a component of an organism (either biological, neurological or behavioural) that changes in form or state due to environmental input. From this, developmental plasticity can be interpreted as referring to an altering characteristic during non-adult development, in the case of this thesis, the tibia. These *aspects,* as referred to by Gollin (1981), are a wide array of external influences (pressures) that can influence skeletal morphological variation. These include pathological conditions, disease and intensity of physical activity (Gollin, 1981; Meloni, 2019).

Bateson and Gluckman (2011) describe the morphological variation that arises from the presence of these external pressures acting upon an organism, as an evolutionary method to increase an individual's robustness. The use of the term 'robust' by Bateson and Gluckman (2011) refers to the survival chances, or survival fitness, of an organism[2]. The morphological variation that arises from developmental plasticity increases the survivability (robustness) of an individual in the environment they inhabit. This is accomplished by altering biological structures, such as the tibia, to better withstand the external pressures, such as intensive physical activity acting upon the bone. Such external factors, primarily physical activity, can

[2] In bioarchaeology, 'robust' is used to describe structurally strong and overly-developed skeletal elements.

result in skeletal variation causing more robust or gracile bones. In anthropological contexts, long bones which are noted as being larger in size with greater cortical bone density and larger muscle attachment sites are typically classified as being robust (Rantalainen, Weeks, Nogueira and Beck, 2016). Structurally robust long bones are typically found in highly active individuals, who exercise their muscles to a greater extent, resulting in larger and more well-defined muscle attachment sites, and greater cortical bone density to withstand the increased stress placed upon the bone (Rantalainen et al., 2016; Pandey et al., 2009). In contrast, gracile bones indicate decreased activity-levels (Pandey et al., 2009). Gracile bones are thinner and more slender than robust bones, and structurally weaker due to decreased cortical bone density levels, with smaller less well-defined muscle attachment sites (Stavit, 2006; Pandey et al., 2009). As observed by Brzobohatá et al. (2019), tibial anterior-posterior (A-P) diaphyseal curvature, and medial-lateral (M-L) anterior crest curvature, are theorized to be a developmental response to intensive weight-bearing stress being placed on the tibia. The process of bone remodeling can alter diaphyseal curvature and cortical bone thickness to produce a more structurally robust bone that can accommodate elevated weight-bearing forces. As reported by Macintosh et al. (2015), there are three accepted biomechanical hypotheses for the occurrence of lower limb and tibial curvature; 1.) that A-P curvature results in greater bending predictability under intense loading conditions - physical activity (Lanyon, 1980); 2.) curvature translates bending stress into axial compression of the bone (Brzobohatá et al., 2019); and, 3.) that curvature might facilitate increased muscle packing around the bone (Lanyon and Bourn, 1979; Lanyon, 1980; De Groote, 2011). Within the framework of Gollin (1981) curvature, as a product of bone remodeling, is a plastic response to physical stress.

Macintosh et al. (2015) studied variation in tibial A-P curvature, in a study that was foundational to the research conducted by Brzobohatá et al. (2019). The hypothesis proposed by Macintosh et al. (2015) is that the adoption of agriculture would reduce the amount of A-P curvature in the diaphysis of the bone. Functional morphological adaptations in the bones of the lower limb are believed to result from mechanical stress during repeated engagement in a physically intensive activity (Macintosh et al., 2015). Due to this, adult lower limb morphology is considered by anthropologists to be the optimal way to derive inferences about behaviour and physical activity in archaeological populations (Macintosh et al. 2015). However, according to Macintosh et al. (2015) tibial morphology is derived from external pressures, such as activity, that act upon the bone during non-adult development. Despite this, Macintosh et al. (2015) solely considers adult tibiae, and excludes non-adult remains. It is this lack of consideration for non-adult remains and the shape change occurring in the anterior crest of the tibia, that this thesis seeks to address.

In humans, the femur and tibia are the primary weight-bearing bones of the lower limb. According to Marchi (2007), the importance of the tibia is largely based on locomotion type. Marchi (2007) notes that in hominoids employing arboreal locomotion, the fibula takes on a higher degree of weight than it normally would during bipedal locomotion. During bipedalism in both humans and in arboreal gorillas, (who employ occasional instances of bipedalism), Marchi (2007) observed (using cross-sectional geometry) that the increased weight transferred to the tibia results in a mechanically thicker and more robust bone with greater cortical density. Unlike with arboreal hominoids, the human tibia and fibula are spaced closer together and are relatively immobile to ensure greater stability of the talocrural (ankle) joint when upright

(Marchi, 2007). In comparison, the arboreal hominoid fibula and tibia are spaced farther apart to allow a wider range of movement. According to Marchi (2007), the occasional instances of terrestrial bipedalism result in Gorilla tibiae that are more gracile than human tibiae, but more robust than other fully arboreal hominoids. Additionally, Marchi (2007) notes that the greater space between the arboreal fibula and tibia allow for the fibula to 'detach' from the tibia during arboreal climbing. Due to this, arboreal hominoid tibiae bear concavity on the lateral diaphysis that human tibiae do not possess due to the fixed position of both the tibia and fibula (Marchi, 2007). The freedom of the fibula to move away from the tibia results in the arboreal tibia being more gracile and cortically thinner than in terrestrial bipeds which rely on the tibia for weight-bearing and stabilization during upright walking. Despite the morphological differences in robusticity and gracility in arboreal locomotion and terrestrial bipedal locomotion, Marchi (2007) and Ruff (2003) report that body size does not correlate with variation in tibial or fibular morphology in humans or in hominoids. Rather, according to Marchi (2007) and Ruff (2003), locomotion and the locomotion form's demands on the tibia to sustain greater or lesser amounts of weight-bearing stress, are instead the primary indicators of morphological shape variation in the tibia.

This thesis builds upon the work of Brzobohatá et al. (2019), as the primary study, due to their exploration of anterior crest shape variation in the adult tibia. The primary objective of their study was to explore whether a reduction in tibial loading (brought on by less intensive physical activity, such as decreased mobility) influenced anterior crest curvature (Brzobohatá et al., 2019). To test their hypothesis, seven tibiae datasets from the Czech Republic were studied using geometric morphometrics (GM), a statistical approach to analyzing shape variation (an

overview of the method is found in Chapter 3). These datasets represent (from oldest to most recent) the Eneolithic, Early Bronze Age, Late Iron Age, Early Medieval, Late Medieval, 20th century and 21st century (Brzobohatá et al., 2019). Brzobohatá et al. (2019) theorize that the oldest of these datasets would contain the greatest amount of A-P and M-L anterior crest curvature, and that this curvature would gradually decrease in the more recent datasets. The rationale for the hypothesized reduction in anterior crest curvature is that decreased population mobility, intensification of agriculture, and adoption of urbanization and technological advancements would impact the curvature of the anterior crest (Brzobohatá et al., 2019).

Brzobohatá et al. (2019) observed that the degree of anterior crest curvature was greatest in the Eneolithic, Early Bronze Age and Late Iron Age datasets. These datasets were theorized to have experienced the greatest amount of tibial loading during the initial adoption of agriculture (Brzobohatá et al., 2019). However, Brzobohatá et al. (2019) note that the Late Iron Age population, while nearly identical to the early groups, possessed a slight straightening in the anterior crest in the A-P plane that continued to straighten into the Early and Late Medieval populations. This straightening was attributed to lifestyle changes that resulted in less weight-bearing stress being placed on the tibia, and more favorable living conditions (Brzobohatá et al., 2019). The 20th and 21st century populations continued to exhibit A-P straightening in the crest and were the most gracile despite showing the greatest degree of M-L curvature (Brzobohatá et al., 2019). As a result, Brzobohatá et al. (2019) claimed that A-P straightening and increased M-L curvature in the anterior crest were associated with decreased physical strain on the tibia. As such, Brzobohatá et al. (2019) theorized that tibial shape

variation was the result of repeated muscular contractions on the diaphysis during ontogenetic development. Finally, Brzobohatá et al. (2019) also looked at sexual dimorphism in anterior crest shape and size. The results showed that outside of the Early Medieval and 20th century populations, there were no statistically significant differences in shape or size between male and female tibiae.

In an earlier study by Sládek, Burner and Sailer (2006) on tibial cross-sectional geometry, a lack of tibial diaphyseal curvature variation was noted between the more mobile Late Eneolithic populations of the Central European Corded Ware period and later sedentary populations of the Central European Early Bronze Age. Sládek et al. (2006) concluded that Corded Ware populations may have engaged in behaviour practices that placed similar amounts of stress on their tibiae as the populations of the later Early Bronze Age. According to Brzobohatá et al. (2019) and Sládek et al. (2006), a shift in behaviour from a highly mobile to sedentary agricultural lifestyle would be supported by variation in tibial curvature.

Similar to Brzobohatá et al. (2019), the oldest tibiae studied by Macintosh et al. (2015), derived from early and middle Neolithic populations characterized by high levels of mobility and population migration, possessed the greatest degree of A-P diaphyseal curvature, while the more recent Early Medieval sedentary agricultural populations exhibited comparatively straighter tibiae with less A-P curvature (Macintosh et al., 2015). Cross-sections taken at 65, 50 and 40% of diaphyseal bone length showed that the older, and theoretically more mobile, populations exhibited an oval or elongated circular internal diaphyseal shape while the diaphyseal cross-sections of the Iron and Medieval populations were noticeably more circular (Macintosh et al., 2015). Essentially, elongated tibiae with oval cross-sections belong to tibiae

that are more curved, while smaller circular cross-sections belong to tibiae that are straighter. The shape of the 25% cross-section did not vary substantially between any of the populations. This may be due to morphological constraints, such as limb-tapering, which according to Marchi (2007) and Ruff (2003) are required to ensure bipedal ankle stability (Macintosh et al., 2015).

Cross-section elongation is theorized to be an adaptive structural response to extensive weight loading in the lower limb (Macintosh et al., 2015; Stock, 2006). According to Macintosh et al. (2015), cross-sectional elongation indicates that the oldest populations were placing a substantial amount of weight-bearing stress on their tibiae, possibly due to terrestrial migration. In comparison, as the degree of cross-sectional elongation decreased in subsequent agricultural populations, the amount of A-P curvature diminished (Macintosh et al., 2015).

Both Macintosh et al. (2015) and Brzobohatá et al. (2019) concluded from their results that behaviour (migration and mobility) appeared to be the primary driver of tibial diaphyseal curvature, which reduced significantly with the adoption of sedentary agricultural farming. However, unlike Brzobohatá et al. (2019) who did not find considerable evidence of sex-specific differences in shape, Macintosh et al (2015) reported that morphological alterations in A-P curvature were more noticeable in males than in females (Macintosh et al., 2015). Further, Pearson correlation tests showed that A-P curvature did not correlate with body size or bone length (Macintosh et al., 2015).

Variation in A-P curvature is not isolated to the tibia. Using geometric morphometrics in her study on Neanderthal femoral curvature, De Groote (2011) demonstrated that Neanderthal femora possessed noticeably greater curvature than contemporary human femora. These results were surprising, as Neanderthals and early modern humans were hypothesized to have

employed near-identical subsistence hunting and scavenging strategies based on faunal assemblages from kill and processing sites (Lieberman, 1989; Sorensen and Leonard, 2001). Recalling from Macintosh et al. (2015) and Brzobohatá et al. (2019) that activity level correlates to increased or decreased A-P tibial curvature, the similar subsistence strategies between Neanderthals and early modern humans should, according to De Groote (2011), possess a similar degree of femoral curvature due to similar activity levels. This is based in part on the straighter femora of modern sedentary human populations relative to the more curved femora of more mobile early modern humans (De Groote, 2011). However, the results of De Groote (2011) demonstrate the opposite: that early modern human femora were noticeably straighter than Neanderthal femora.

As with Macintosh et al. (2015) in reference to the human tibia, Marchi (2007) and Ruff (2003) in reference to the hominoid tibia and fibula, De Groote (2011) found that body size did not correlate significantly with femoral curvature. Due to this discrepancy, De Groote (2011) theorizes that greater Neanderthal femoral curvature indicates that either the archaeological record under-represents the amount of physical activity Neanderthals undertook, or that Neanderthal and early modern human behaviour during ontogeny is markedly different and contributes to this morphological discrepancy. De Groote (2011) claims the latter explanation is more likely as a result of the lower femoral neck angle of Neanderthal femora relative to the higher neck angle in early modern human femora. As reported by Trinkaus (1993), a lower femoral neck angle indicated unusually high levels of physical stress being placed on the hip. Due to this, De Groote (2011) strongly advocates the need to expand lower limb curvature studies to include ontogenetic non-adult study samples, since the results of Trinkaus (1993)

imply that Neanderthal non-adults were more physically active than early modern human non-adults. The studies by Brzobohatá et al. (2019), Macintosh et al. (2015), De Groote (2011) and Trinkaus (1993) strongly support the theory that developmental plasticity, mainly via physical activity, has the capacity to influence adult morphology in the tibia. The decrease observed in adult tibial curvature from early modern humans to contemporary human populations can be at least partially explained by decreased activity levels and reduced population mobility.

Chapter 3. Using Geometric Morphometrics to Study Bony Shape Variation

Geometric morphometrics is a relatively new methodology to be employed in biological anthropology and bioarchaeology studies regarding bone shape. Before geometric morphometrics, fossil remains were commonly analyzed through traditional osteometric distance and angle measurements (Rein & Harvati, 2014); however, these methods are now less frequently used, since morphometrics allows researchers to extract more shape and morphology data (Rein & Harvati, 2014). Specifically, Zelditch and colleagues (2012) describe morphometrics as providing a highly detailed method to visualize and understand biological shape variation caused by trauma, disease and ontogeny. According to Rein and Harvati (2014), the advantages of applying geometric morphometrics to anthropological studies are that it allows the targeted morphology to be completely captured, and statistical shape differences to

be easily visualized. The mechanism for which geometric morphometric analysis is carried out is through the use of landmarks (Zelditch et al., 2012; Rein & Harvati, 2014). Landmark analysis can be conducted two-dimensionally (2D), via photographs or image scans, or three-dimensionally (3D), via complete models created through, for example, a series of CT scans or 3D surface scanning technologies (Rein & Harvati, 2014). By digitally reconstructing virtual models, objects can be studied without needing to be repeatedly handled (Rein & Harvati, 2014), which has the added benefit of reducing wear-and-tear on the remains (Rein & Harvati, 2014). In addition, unlike the traditional angle and distance measurements, morphometrics allows for curves, ridges and skeletal projections/protrusions to be included in the morphological analysis (Rein and Harvarti, 2014).

Morphometrics has been applied to other studies involving shape analysis in modern humans. Examples of such studies include: tooth loss and its effects on cranium shape (Small, Brits & Hemmingway, 2016); tooth morphology (Gomez-Robles et al., 2007; Woods et al., 2017); cranial variation (Kuzminsky, Tung, Hubbe, & Villaseñor-Marchal, 2016; Bertsatos et al., 2018); mandible shape (Oettle, Pretorius, & Steyn, 2005); and variation in the shape of postcranial elements (Bastir et al., 2019; Lynch, Cross and Heaton, 2017; Cavaignac et al., 2017; Aniol et al., 2014; De Groote, 2011; Brzobohatá et al., 2019; Sorrentino et al., 2020; Galletta et al., 2019; Wilson and Humphrey, 2015).

However, while the body of research regarding morphometrics in anthropology is broad and explores a wide array of topics regarding human, hominin and primate research, there are relatively few morphometric studies of non-adults. Morphometric research involving non-adults has examined skeletal sexual dimorphism and ontogeny, with a focus on the cranium and

pelvis (Noble et al., 2019; Wilson & Humphrey, 2017; Wilson, Ives & Humphrey, 2017) and application to age and sex estimation (Braga & Treil, 2007; Scholtz, Steyn & Pretorius, 2010; Estévez et al., 2017). Relative to adults, apart from the cranium and pelvis, there are fewer studies on non-adult skeletal elements. Some notable exceptions include: the non-adult talus (Hellier & Jeffery, 2006); non-adult scapula (Scholtz, 2007), and non-adult maxilla (Schuh et al., 2019). This thesis aims to expand upon this under-represented area of research relating to applying morphometrics to non-adult skeletal elements by studying the non-adult tibia.

3.1 Landmarks and Semi-landmarks

The definition of a landmark, as described by Zelditch et al. (2012), is that of a site or biological feature that is homologous in its location, provides coverage of the targeted morphology, and is present across all individuals. An example of a landmark in the human skull is the proximal-most point of the nasal aperture. Landmarks can be described by Cartesian coordinates, and variation in this Cartesian data represents shape variation (Zelditch et al., 2012; Webster and Sheets, 2010). For geometric morphometric analysis of photographs and other images, these landmarks consist of x and y coordinates. Landmarks of 3D models, like those analyzed in this thesis, consist of x, y and z coordinates. However, to accurately study shape variation, landmarks across a study sample must be placed on the exact same (homologous) feature for data to yield meaningful results. Within geometric morphometric research there are three types of landmark (Zelditch et al., 2012). Type One landmarks are found at locations of intersection, such as where the intermaxillary suture meets the interpalatine suture (Bookstein, 1992). Type Two landmarks are located at the maximum point

of a curvature, such as the crown tip of a human or animal tooth (Bookstein, 1992). Type Three landmarks are the broadest, and encompass morphology located at endpoints of a feature, intersections of interlandmark segments or contours, or are those located solely through relation to another set of Type One and Type Two landmarks (Bookstein, 1992). In terms of preference, Type One landmarks are the most desirable, with Type Three being usable, yet less desirable than Type One, as they are by their nature somewhat more subjective in location. However, Bookstein (1992) states that Type Three landmarks are optimal and highly desirable when defining the length or size of a targeted morphology to be analyzed.

A problem with landmarks is that they cannot be used on surfaces and features deficient in homologous definition (Gunz and Mitteröecker, 2013). This problem left many biological areas unable to be studied. To address this, a new type of landmark called a semi-landmark, was developed to study biological surfaces that traditionally were unsuitable for study due to their lack of definition.

Semi-landmarks as a concept were first proposed by Bookstein (1997) for use in 2D analysis. The semi-landmark methodology of Bookstein (1997) was later expanded and adapted for 3D analysis by Gunz et al. (2005). Bookstein (1997) placed semi-landmarks on 2D images to create a shape outline. The semi-landmarks, as Bookstein (1997) called them, were in effect traditional landmarks but placed as an outline defining a shape. The primary process Bookstein (1997) utilized to study the outline data was through thin-plate spline relaxation. Thin-plate spline relaxation allowed tangential variations in an individual's semi-landmark outline data to be weighted equally regardless of direction in shape space (Bookstein, 1997). In the study conducted by Bookstein (1997) where surface outlines were being landmarked, thin-plate

spline relaxation allowed a single individual's semi-landmarks to be used as a template and projected onto the surface of another individual (Bookstein, 1997). Traditional landmark analysis methods, such as Procrustes superimposition were then successfully used for the analysis of semi-landmark data (Bookstein, 1997). In order for semi-landmarks to be used, the surface or curve they are placed on must be present on each individual (Gunz et al., 2005). The concept of semi-landmark spline relaxation was adapted by Gunz et al. (2005) to the study of 3D curves and surfaces. Curve and surface semi-landmarks, since they are contained within the boundary of two or more fixed landmarks, remain homologous across individuals (Gunz and Mitteröecker, 2013). This fact allowed for surfaces and curves to be studied using geometric morphometrics where traditional landmarks could not be placed. For these reasons, Dubzik (2019) noted that surface and curve semi-landmarks have been particularly effective in studying morphological shape change during ontogeny in species and individuals who lack sufficient skeletal development to be landmarked traditionally.

Gunz et al. (2005) outlined the steps involved in the creation of semi-landmarks. This process is conducted by first placing a large number of points along a curve to act as an outline of the feature. Gunz et al. (2005) state that this outline must always contain more points defining the curve than the number of semi-landmarks derived from it. This ensures that the curve or outline is accurately depicted by the semi-landmarks. Once the outline is created, the desired number of semi-landmarks are then derived from the outline and placed equidistantly along the curve. However, Gunz et al. (2005) state that equidistant projection of semi-landmarks cannot be considered as optimally spaced, due to variations in the shape and elevation along the curve. To address this issue, Gunz et al. (2005) adapted semi-landmarks to

automatically ‘slide’ along the designated curve in accordance with the previously created outline. This ensures that the projected semi-landmarks are able to shift and resample along the curve and adjust position to better capture the shape of the curve (Gunz et al., 2005; Gunz and Mitteröecker, 2013). Due to the appropriateness of this technique to the current study, this thesis utilizes sliding semi-landmarks to study anterior crest shape change.

Brzobohatá et al. (2019) traced a single 3D curve from the proximal-most projection of the tibial tuberosity, distally along the anterior crest, before projecting medially at the termination of the crest to the distal-most point of the medial malleolus. The fixed start and end landmarks which define their curve are Type Three landmarks (Brzobohatá et al., 2019). This curve was then used to derive 20 semi-landmarks spanning the length of the tibia along the anterior crest (Brzobohatá et al., 2019). This thesis follows the approach of Brzobohatá et al. (2019) in using semi-landmarks to capture the shape of the anterior tibial crest, with some modifications to accommodate the less well-defined non-adult morphology. It expands on the research conducted by Brzobohatá et al. (2019) by looking at the growth and development of the non-adult anterior crest during growth.

3.2 Statistical Analysis of Landmark Data

Geometric morphometrics is a blend of biological study with the mathematical field of statistical analysis (Zelditch, Swiderski, Sheets & Fink, 2012). Geometric morphometrics was first used by biologists to understand biological shape change between individuals, populations and species. As expertly described by Zelditch et al. (2012), by applying mathematical operations to the extraction of biological shape data, morphometrics provides a highly detailed

method to visualize and understand variation among complex organisms. For the purposes of this thesis, the shape to be analyzed is the curvature of the anterior crest of the tibia.

Before proceeding, it is vital to briefly describe the definitions of shape and size in geometric morphometrics. Shape is defined as the configuration of a set of landmarks, with shape studies looking at variance within that configuration (Klingenberg, 2016). Size is defined as the 'geometric scale' of the landmark configuration, and is studied by analyzing the configuration's *centroid size* (Csize) (Zelditch et al., 2012). Csize is mathematically defined by Klingenberg (2016) as the square root of the sum of squared distances of all landmarks from the configuration's centroid (the single average 'location' of all Cartesian coordinate values). Through the analysis of Csize, differences in size among individuals and populations can be studied.

Generalized Procrustes Analysis (GPA) is the method by which morphometicians use information provided by 2D and 3D landmarks in analysis of shape and size (Zelditch et al., 2012). Briefly, the name Procrustes refers to a murderer of the same name from Greek mythology, who would "stretch" or "truncate" his victims to a bed before disposing of them (Zelditch et al., 2012). The same "stretching" and "truncating" is applied to the landmark configurations during GPA. GPA is a method to remove all information related to size, orientation, and location, to isolate differences in shape among individuals. This minimization of difference is accomplished computationally by rotating, scaling and translating the "raw" landmark data (Zelditch et al., 2012). Specifically, each individual configuration of landmarks is centered to an origin by way of subtracting the coordinates of its centroid from the corresponding coordinates of each landmark (Zelditch et al., 2012). By doing this, Zelditch et al.

(2012) stated that each centroid is translated to the origin, and each landmark's coordinates reflect their deviation from the centroid. Next, scaling is accomplished by dividing each coordinate of each landmark by the centroid size of that configuration (Zelditch et al., 2012). Finally, once the previous steps are complete, one configuration is chosen as a reference, and the rest of the configurations are rotated to it so that the overall Procrustes distance is minimized (Zelditch et al., 2012). Procrustes distance is defined as the square root of the sum of squared distances between corresponding landmarks of two or more landmark configurations (Klingenberg, 2020; Drydan and Mardia, 2016).

Geometric morphometrics allows shape change to be visualized in multiple ways such as scatter plots, thin-plate spline analysis, or the plotting of principal components (Webster and Sheets, 2010). These visualizations occur in what is called "tangential shape space" which is the space within which shape deviations from a mean shape can be visualized (Klingenberg, 2013). Mean shape can best be described as the consensus landmark configuration derived from GPA, to which all other landmark configurations are aligned (Klingeberg, 2020). Principal component analysis (PCA) is a powerful tool in geometric morphometric research, used for both simplifying shape variation for the researcher and for the ease with which this variation can be plotted and visualized using plots (Zelditch et al., 2012). As described by Zelditch et al. (2012), PCA is a method to interpret and simplify patterns of shape variation by replacing the variables of shape information with new variables called principal components (PCs). Principal components represent the highest amounts of shape variation in a study sample (Zelditch et al., 2012). A study sample can be visualized using a scatter plot to show how a study sample varies by PCs (Klingenberg, 2013). In practice, when creating a scatterplot of the most important PCs,

individuals who initially may have appeared to share no morphological similarities, may cluster together and reveal hidden morphological similarities that may otherwise have been overlooked (Zelditch et al., 2012). The principal components are ranked, with the two most prominent PCs referred to as PC1 and PC2. The structure of a PC scatter plot is straightforward, with PC1 scores conventionally running along the x-axis while PC2 scores run along the y-axis. Additionally, individuals that are plotted away from the PC trajectory may hold significant morphological variance that marks them as "unique" and different from the rest of the study sample, and are referred to as outliers (Zelditch et al., 2012). A simplified description of PCA is provided by Zelditch et al. (2012): PCA through the reduction of shape variables into their most significant parts (PCs) allows data to be viewed from different perspectives.

Chapter 4. Materials and Methods

4.1 Archaeological Groups Studied

4.1.1 Native Point

The site of Native Point is located on the southeastern coast of Southampton Island, Nunavut, Canada (Figure 4.0). Native Point is a relatively recent archaeological site. Its original inhabitants, known as the Sadlermiut, entirely perished after coming into contact with disease, speculated to be typhoid or typhus, during the winter of 1902-03 (Ryan and Young, 2013; Merbs, 2018). The site of Native Point consists of 150 limestone cairn burials containing the remains of adults and children. In addition, archaeologists have described limestone and

whalebone structures, and assorted tools made from whale bone and chipped stone (Merbs, 2018; Coltrain, 2009; Ryan and Young, 2013; Comer, 1910).

The geographic area encompassing Native Point is flat and sparsely vegetated, with gravel beaches (Clark, 1980). The Sadlermiut were first encountered by Lyon (1825) during his arctic expedition. Native Point was noted by Lyon (1825) to be unusually difficult to access due to dangerous currents surrounding the island. Despite these hazardous waters surrounding the settlement for much of the year, Lyon (1825) reported several kayak rests along the shoreline and Comer (1910) observed that the coastal waters immediately adjacent to the settlement's shoreline were calm. Additionally, Comer (1910) relayed that, when using bows, the Sadlermiut of Native Point were reported to be excellent whale hunters from ice and kayaks (Mathiassen, 1927). Despite the abundance of caribou and other terrestrial animals on the island, isotopic analysis of Sadlermiut skeletal remains has indicated that their diet was overwhelmingly marine based (due to their high trophic levels) and consisted of seal, and arctic birds (Coltrain, 2009) which were noted to nest in abundance near the settlement (Clark, 1980).

In their synthesis of archaeological research on Native Point, Ryan and Young (2013) related that Mathiassen (1927) concluded that the Sadlermiut were descended from the prehistoric Thule culture on Baffin Island, due to their unique circular whale bone structures not found on the mainland, and their use of bone tools in the Thule tradition (Comer, 1910). This conclusion by Mathiassen (1927) has been contested in subsequent studies by Collins (1958) and de Laguna (1947;1979) who, based on oral histories and the presence of non-Thule chipped stone tools (Merbs, 2018), argued that the Sadlermiut were instead descended from the Dorset Eskimo and had only been culturally influenced by the Thule. Comer (1910) reported that his

Inuit guides from the surrounding mainland recalled that they had great difficulty understanding the Sadlermiut dialect, as the island's inhabitants rarely interacted with other peoples. Merbs (2018) noted that surrounding Inuit groups described the Sadlermiut as "baby voiced and unable to pronounce words correctly".

Unlike Thule burials, the Sadlermiut chose to inter bodies extended in longer graves, rather than inter them in a flexed position within a smaller grave (Merbs, 2018). Thule graves typically orientated the head of the grave towards the southwest, if the interred was female, and to the northeast if male (Merbs, 2018). These graves were marked with headstones made from white rock, limestone or quartz (Merbs, 2018). In comparison, Native Point graves were orientated largely towards the east regardless if the interred was male or female, and were not marked with any sort of headstone (Merbs, 2018). While the Sadlermiut did not appear to differentiate between male and female in grave orientation, they did, however, differentiate the quality of the burial structure by sex and age. Interred adult males, as reported by Merbs (2018), were laid to rest in the most well-constructed graves, followed by adult females in slightly lower quality graves, and, finally, infants, who were interred in the poorest quality of grave. Some infants were found in what appeared to be an unaltered meat cache with a few animal bones.

A point of considerable interest is that the burial cairns were not always constructed solely for the purpose of a burial. The Sadlermiut initially used the stone cairns as caches for food, and later converted them into burial cairns as need arose (Merbs, 2018). The need to convert a food cache to a burial cairn coupled with the high rate of non-adult burials are, according to Merbs (2018), evidence that the Sadlmeriut underwent periods of sudden and

considerable stress that impacted children more so than adults. As such, these periods of sudden and intense stress required the Sadlermiut to quickly construct or convert a previous structure into a burial cairn (Merbs, 2018). Additionally, Sadlermiut skeletal remains revealed a high rate of various spinal pathological conditions and diseases. Merbs (2018) recorded that the Sadlermiut suffered from high rates of spinal spondylosis, attributed to unusual levels of lower back physical activity during adolescence; childhood osteopenia (bone mineral loss); degenerative joint disease, such as osteoarthritis of the spinal vertebrae, which affected Sadlermiut women more than men; osteoarthritis of the elbow and shoulder, and, vertebral compression fractures along the thoracic and vertebral sections of the spine. It was noted by Merbs (2018) that vertebral compression fractures that occur during adolescence often result in spondylosis during adulthood. Additionally, a high rate of lower limb pathological conditions and diseases, such as osteoarthritis of the knee and ankle, were observed. These included femoral, fibular and tibial longitudinal stress fractures (some of which incorrectly healed and altered the curvature and length of the element's diaphyses) and crushing injuries sustained by the tarsals and metatarsals of the foot (Merbs, 2018). Merbs (2018) concluded that these lower limb pathological conditions stemmed from physical activity, such as carrying heavy stones.

Regardless of the origins of the Native Point inhabitants, the prevailing theory is that the geographic isolation of Southampton Island allowed the Sadlermiut population to develop independently from other mainland groups (Ryan and Young, 2013; Comer, 1910; Mathiassen, 1927**;** Clark, 1980).

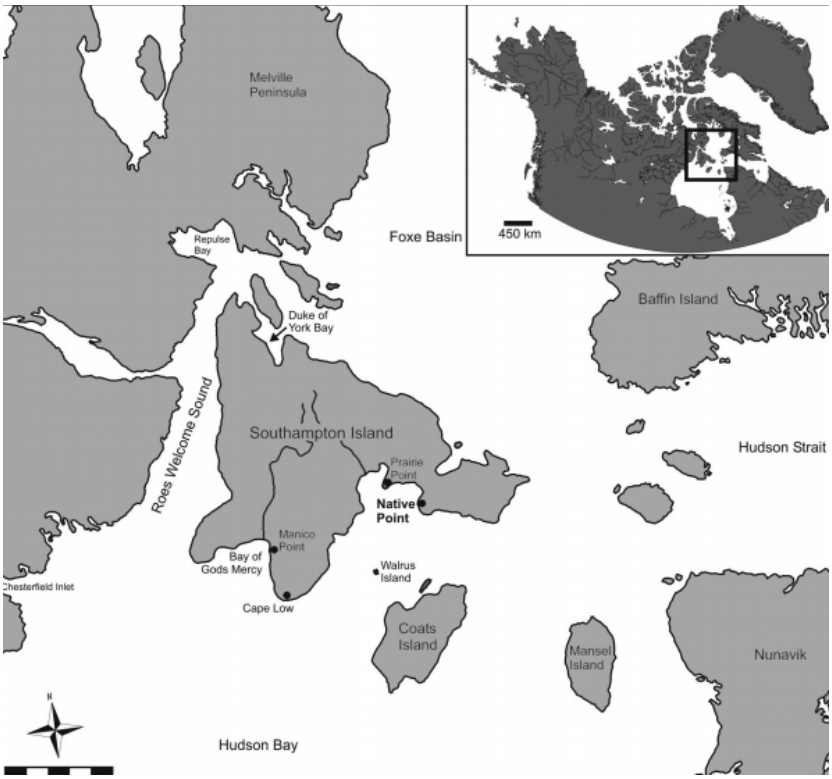

Figure 4.0. Map showing location of Native Point in Nunavut, Canada. Image from Ryan and Young (2013).

4.1.2 Indian Knoll

The Indian Knoll site is located in Kentucky, United States between Mammoth Cave and the Ohio River (Claassen, 2019) (Figure 4.1). Indian Knoll is currently the largest archaeological site located in North America, due to the large number of burial mounds with over 1,000 individuals, and over 55,000 recovered artefacts (Francis, 1961; Classen, 2019; Nealis and Seeman, 2015). Attributed to the Archaic period, the site has been radiocarbon dated to 5,000 B.P., and is theorized to have been used for around 500 years (Ruff, 1980; Webb 1946). The Indian Knoll people are believed to have been hunter-gatherers who made extensive use of local resources such as freshwater mussels for food and their shells for personal adornment (Rothschild, 1979; Winters, 1974).

Webb (1946) theorized that the individuals interred in the burials at Indian Knoll represent a single homogeneous group, who occupied the site for an unusually long period of time. This statement attracted the attention of Ruff (1980) who performed craniofacial metric analysis on a selection of Indian Knoll remains. Owing to the low craniofacial variability of the Indian Knoll burials relative to other contemporary burials sites, Ruff (1980) agreed with Webb (1946) that the individuals buried at the site were a single homogeneous people.

A unique aspect of the Indian Knoll site is the high proportion of infants included in the burials. Powell (1996) estimated from the excavated remains that 1 in 5 infants died before 1 year of age, and Cassidy (1984) concluded that few adults survived into their 50s over the 500-year occupation of the site. In addition to the high rates of infant mortality, dental wear and dental disease, such as pulp exposure and common presence of tooth loss among young adults, indicate the Indian Knoll group were under intense stress (Claassen, 2010; Ward, 2005; Belovich, 2005; Nealis and Seeman, 2015).

Despite this, the Indian Knoll people are believed to have been an egalitarian society with some evidence for social stratification. Rothschild (1979) reported the majority of the skeletal remains within the burial mounds are men and infants (of unknown sex) along with the rare inclusion of women. Selected male and infant burials are reported by Rothschild (1979) to have contained grave goods such as disk beads that may have served as markers of social status. Further evidence for social status comes from burial mound cluster 13, which Rothschild (1979) reported to have contained only stone tools, while the contents of mound cluster 17 were mostly mollusc shell bead ornaments. Women, according to Rothschild (1979) were not given multiple types of status marker artifacts.

Figure 4.1. Map showing location of the Indian Knoll site in Kentucky, United States of America. Image from Nealis and Seeman (2015).

4.1.3 Point Hope

First excavated in 1939 and 1941 by Froelich Rainey and Helge Larsen, Point Hope is the oldest continuously occupied archaeological site within North America (Rainey, 1941) (Figure 4.2). This Alaskan site is home to one of the largest non-adult skeletal assemblages in the world (Hilton et al., 2014; Cowgill, 2014). Rainey (1941) called the original inhabitants of Point Hope the Ipiutak and the subsequent inhabitants the Tigara. Point Hope is located north of the Bering Strait on a narrow strip of land between Cape Thompson and Cape Lisburne in northwestern Alaska (Rainey, 1941). Dated between 1,400-1,100 BP, the site itself is characterized by over 600 square houses and a large gravesite (Justice and Temple, 2019; Rainey, 1941).

The origins of the Ipiutak, like the Sadlermiut, are uncertain. Rainey (1941) reported that select graves of wealthy Point Hope residents contained ivory eyeballs and engraved ivory cup-shaped mouth coverings as burial goods. The engravings on the ivory mouth coverings,

according to Rainey (1941), are similar in style to those attributed to the Okvik site on the Punuk Islands in the northern Bering Sea. However, despite this similarity, also recovered from Point Hope was a series of unidentified engraved ivory spiral shaped artefacts that did not correlate to any other Arctic or North American culture (Rainey, 1941). Interestingly, the Ainu culture of Northern Japan employed moustache sticks that were engraved with a similar spiral pattern (Rainey, 1941). As a result, Rainey (1941) theorized that the Ipiutak and Ainu cultures might be related, and the Ipiutak must have migrated from Asia.

The square houses at Point Hope were constructed from driftwood, sod blocks and covered with animal hides (Rainey, 1941). Also discovered by Rainey (1941) were numerous detritus piles in the houses, along with 50 harpoons and over 500 arrowheads. Oddly, Rainey (1941) reported that very few ice picks were discovered. The skeletal detritus piles from the houses showed that Point Hope's primary food source was caribou followed by seal (Rainey, 1941). The large amount of terrestrial animal detritus, in conjunction with the few recovered harpoons, suggested that the Ipiutak were primarily inland caribou hunters who seasonally hunted coastal mammals (Rainey, 1941).

Contained within the Point Hope gravesite is a large number of adult skeletons and over 570 non-adult skeletons (Cowgill, 2014; Justice and Temple, 2019). An assortment of burial goods was recovered from the graves, such as blades and arrowheads constructed from ivory, bone and antler (Rainey, 1941). The graves were oriented either towards the west or south depending on age. Graves with individuals 4 years of age or older were orientated with the head of the grave facing west, while non-adults younger than 4 years of age were interred facing the south (Justice and Temple, 2019). Justice and Temple (2019) reported that the

number of burial goods placed in a non-adult grave was based on age; non-adults of 1-6 years of age were given a single animal-shaped burial artefact, while non-adults of 7-10 were buried with two animal artefacts.

Shackelford (2014) and Cowgill (2014) noted that Point Hope adults and non-adults were unique in their high level of postcranial skeletal robusticity and large body size, relative to other Arctic people. Shackelford (2014) reported that the humeri of both adult males and females were reinforced and strengthened with additional bone. The location of this reinforcement stems from habitual throwing movements, and led Shackleford (2014) to postulate that the Ipiutak may have also practised coastal whale hunting. Oval-shaped cross-sections showed substantial robusticity in the femoral midshaft's bone density levels which, according to Shackleford (2014), indicated extensive terrestrial mobility. These marks of Point Hope adult postcranial robusticity were also reported in the non-adult remains. The signs of mechanical stress in the lower limb and overall postcranial robusticity of the non-adult skeletons led Cowgill (2014) to conclude that Point Hope non-adults were highly active in foraging activities from an early age.

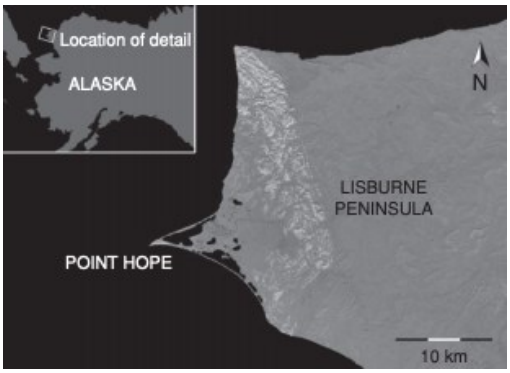

Figure 4.2. Map showing location of Point Hope, Alaska, United States of America. Image from Hilton et al. (2014).

4.1.4 South Africa

The South African Later Stone Age (LSA) hunter-gatherer skeletal remains studied for this thesis are from the following five institutional collections: National Museum Bloemfontein, McGregor Museum, Albany Museum, Iziko South African Museum, and University of Cape Town. Many of the LSA skeletons were recovered from archaeological sites located in the South African Greater Cape Floristic Region (GCFR) (Figure 4.3). The GCFR spans 80,000km^2 from the Cape Fold Mountains to South Africa's southern coast, and is believed to have been inhabited by humans for 195,000 years B.P. (Pfeiffer and Harrington, 2018). The LSA adult and non-adult remains studied in this thesis have been radiocarbon dated to between 8,000 and 800 years BP (Harrington, 2010). The ability for LSA hunter-gatherers to inhabit the area for such a prolonged period of time is due to the GCFR's abundant natural resources for the construction of tools, diverse array of edible flora, and sizable quantities of terrestrial animal and marine food sources (Pfeiffer and Harrington, 2018; Marean et al., 2014). The LSA people that lived in the GCFR were characterized by Woodburn (1982) as immediate-return hunter-gatherers who foraged and hunted to meet the needs of the day. Artefacts, including lithics and ostrich eggshells have been recovered from rock-shelter and open-air sites within the GCFR (Pfeiffer and Harrington, 2018).

Attributed to the GCFR are a substantial number of LSA sand dune and rock-shelter hunter-gatherer burials. These are largely individual burials and are described as having the body flexed, with an unmarked grave (Pfeiffer and Harrington, 2018). According to Pfeiffer and Harrington (2018), non-adult burials are rare relative to those of adults. Through skeletal and dental dimensions, the LSA hunter-gatherers of the GCFR were determined to be a single

homogenous people dispersed into multiple groups across the region (Pfeiffer and Harrington, 2018).

In regard to the skeletal remains themselves, GCFR adults are characterized by a small body size (measuring 178cm in height, on average) and a low body mass (Pfeiffer and Harrington, 2018). In spite of this, GCFR adults were observed to display substantial lower limb robusticity, such as high femoral torsional strength that indicates extensive terrestrial mobility (Stock and Pfeiffer, 2001; Pfeiffer and Harrington, 2018). Sexual dimorphism, theorized to be the result of a sexual division of labour, is indicated in the adult remains as well (Pfeiffer and Harrington, 2018). When analyzed via cross-sections of the humerus, adult female humeri demonstrate balanced levels of cortical bone strength throughout the bone, while male humeri display evidence of dominance-induced asymmetry (Pfeiffer and Harrington, 2018). This humeral sexual dimorphism is postulated in women to be the result of foraging behaviour that required balanced arm strength such as in the use of a digging stick (Pfeiffer and Harrington, 2018). In men, the dominance asymmetry is believed to be the result of hunting activities that required greater upper limb strength, such as the use of a bow and arrow (Pfeiffer and Harrington, 2018).

Aside from occasional instances of *cribra orbitalia*, osteomyelitis, tuberculosis, the relative lack of chronic disease markers including a lack of dental enamel hypoplasia, supports the theory that childhood was relatively stable and healthy in the GCFR (Pfeiffer and Harrington, 2018). Additionally, LSA infants were similar in size and rate of growth to European infants until 2 years of age, at which point LSA growth trajectory became distinctive, in keeping with the short-stature of LSA adults. LSA child growth is, however, comparable to modern

European children in terms of proportional stature-for-age, providing further evidence for a lack of chronic illness among children in the GCFR (Pfeiffer and Harrington, 2011; Pfeiffer and Harrington, 2018). Drawing on evidence from non-adult limb bone cross-sectional measures, Harrington (2010) concluded that GCFR non-adults were active participants in hunting and gathering activities well before adulthood.

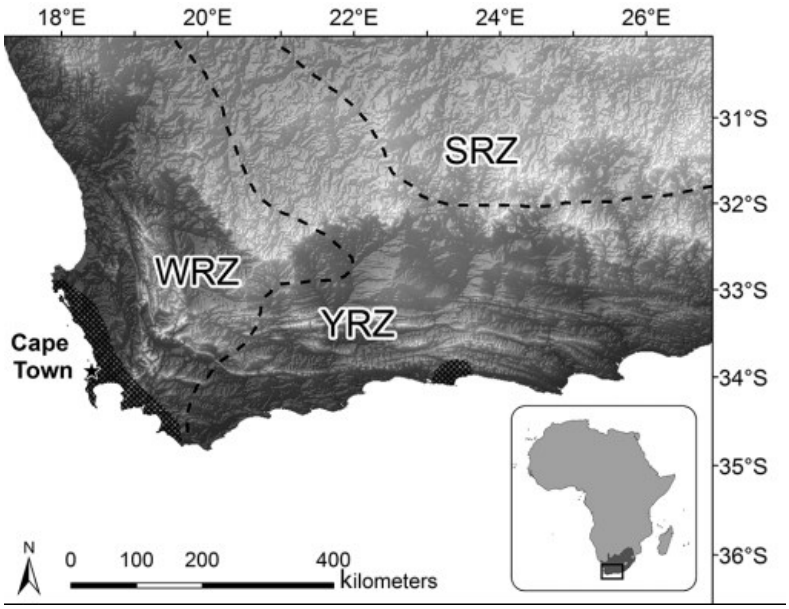

Figure 4.3. Map showing the location of the Greater Cape Floristic Region in South Africa (WRZ, SRZ, and YRZ indicate zones receiving winter, summer, or year-round rains, respectively.) Image from Pfeiffer and Harrington (2018).

4.2 Dental Age

This thesis explores shape change in anterior crest of the non-adult tibia. A key aspect of this research is the need to accurately estimate non-adult chronological age. Analyzing dental development and eruption to discern the age at death is widely employed by both forensic

anthropologists and for bioarchaeologists, as the deciduous and permanent dentition develop in a predictable sequence. The lengthy process that is dental development, spanning the fetal to late adolescent period, allows researchers to make accurate estimations of non-adults based on tooth crown and root development (Al Qahtani, Hector and Liversidge, 2010). For this reason, the non-adult tibiae selected for this current study are drawn from individuals with preserved dentitions.

Due to the relative accuracy that analysis of dental development provides, dental development rather than tibia bone length is used to estimate the chronological age of 41 non-adults in this thesis. Estimations of the age at death of the individuals analyzed in this thesis were conducted by Dr. Lesley Harrington in accordance with the dental age atlas developed by Al Qahtani et al. (2010) using crown and root formation stages developed by Moorrees et al. (1963a; 1963b). The use of a dental atlas follows a simple and straightforward approach: the developmental progress of a dentition is observed and matched to an atlas stage, with its associated age range (Al Qahtani et al., 2010). The atlas of Al Qahtani et al. (2010) was selected for use due to its increased accuracy (Al Qahtani, 2014) over preceding atlases, such as those developed by Ubelaker (1978). The Al Qahtani et al. atlas (2010) is derived from studying children of diverse ethnic backgrounds, and expanded on previous atlases to add data for the deciduous and wisdom teeth, to cover the full period of dental development.

The ages derived from Al Qahtani et al. (2010) were used to group the non-adult sample into 2-year age cohorts (Table 4.0). Age groups of 2 years reduced the number of non-adult groups consisting of only a single individual, given the sample size. The 24 individuals in the adult sample consists of individuals who had completed dental development, and adult sex

estimation was performed by H. Kurki (pers. communication) using standard morphological methods (Buikstra and Ubelaker, 1994). The sex of several adults could not be estimated due to poor preservation. The number of adult males, adult females and adults of unknown sex is listed in Table 4.1. Together, the 41 non-adults and 24 adults studied form a total sample of 65 individuals.

2 Year Age Groups	Native Point	Indian Knoll	Point Hope	LSA		Total
7-8.99	0	2	0	0		2
9-10.99	3	3	2	1		9
11-12.99	2	1	3	3		9
13-14.99	1	5	1	2		9
15-16.99	4	1	4	3		11
17-18.99	0	0	1	2		4
19-20.99	2	0	0	1		3
21-22.99	0	0	0	1		1
>=23	5	5	5	2		17
Total	17	17	16	15		65

Table 4.0. Breakdown of the 65 individuals of this thesis' study. Each site is separated by column, and the number of individuals from each site are provided at the bottom of the table. Age groups are separated by row, and the total number of individuals in each age group are provided on the far right of the table.

Adults (>18y)	n
Male	7
Female	7
Unknown	10
Total	24

Table 4.1. Breakdown of the biological sex of the 24 adult individuals of this thesis' study.

4.3 Tibia Alignment Protocol

As part of a larger research project, Dr. Lesley Harrington and Dr. Helen Kurki previously studied the collections from Native Point, Indian Knoll, Point Hope, and South Africa, and made 3D scans of the tibiae using a Next Engine or Konica Virtuoso structured-light laser scanner. Prior to the commencement of this thesis, these tibial scans were consolidated and fused into single models saved as an XRL file. The majority of the fused XRL models were of left tibiae, and they constitute the majority of this thesis' study sample. When encountered, right tibiae were mirrored to resemble left tibiae using Geomagic Design X software's "Mirror" function (3D Systems Inc. 2019). Each model was oriented to the same anatomical alignment and followed the steps outlined by Dr. Alison Murray's Protocol (Appendix A).

4.4 Anterior Crest Tracing Protocol

Of 65 tibiae selected for this study, 41 were non-adult tibiae and the remaining 24 were identified as belonging to adults. Tibiae were selected for the analysis according to the following criteria. First, all models are free of damage on the anterior, proximal and distal surfaces; this ensured that the model was not influenced by damage to the ends of the diaphysis or to the anterior crest (AC). Second, the anterior crest had sufficient surface definition to be automatically traced in GOM Inspect using the "Construct Surface Curve" function; this uses an algorithm that analyzes the vector values of the surface points adjacent to the trace's start point to detect changes in curvature. The function modifier "To Max. Curvature" ensured that the software's automatic trace adhered to the points of maximum

curvature along the anterior crest (Optical Measuring Techniques GOM, Germany, 2019). As the amount of crest definition decreased distal to the tibial tuberosity and in the lower third of the diaphysis, the algorithm used by "Construct Surface Curve" failed to detect a maximum point of curvature outside of 70-40% of diaphyseal length in the younger non-adults. Models with insufficient anterior crest definition were, therefore, not traced by the software. While a number of tibiae belonging to young children were analysed in GOM Inspect, ACs were found to be untraceable by the software due to a lack of definition in most individuals estimated to be below 9 years of age. Two tibiae, attributed to a 7.5 year-old and an 8.5 year-old, displayed adequate definition in the AC and were able to be traced. These represent the two youngest individuals found in this study. The third criterion for sampling concerned the adult tibiae. In addition to meeting the first two criteria, these models also had to preserve identifiable proximal and distal epiphyseal fusion lines/scars for use in measuring the diaphyseal length of the models.

Due to the variability in the amount and length of the AC definition among tibiae, particularly in the areas immediately distal to the tibial tuberosity and in the lower third of the diaphysis, it was determined that the AC could only be consistently traced between 70% and 40% of the unfused diaphysis' total length; therefore, the tracing was limited to within these measurements for all models (Figure 4.4). When loaded into GOM Inspect, all models were orientated to anterior using GOM Inspect's 3D rotation cross (red, green and blue cross in the bottom left of Figure 4.5) to visualize the AC. Then using the measurement grid overlay, tracing of the AC began proximally at 70% of diaphyseal length and extended distally along the crest, until terminating at 40%. The algorithm used in the "Construct Surface Curve" function (with

the “To. Max Curvature'' modifier) identified the x and z coordinates of the crest for the trace. This captured a tracing of 30% of the length of the diaphysis along the AC. The process for tracing a tibia with one or both epiphyses fused to the diaphysis is described in the next paragraph.

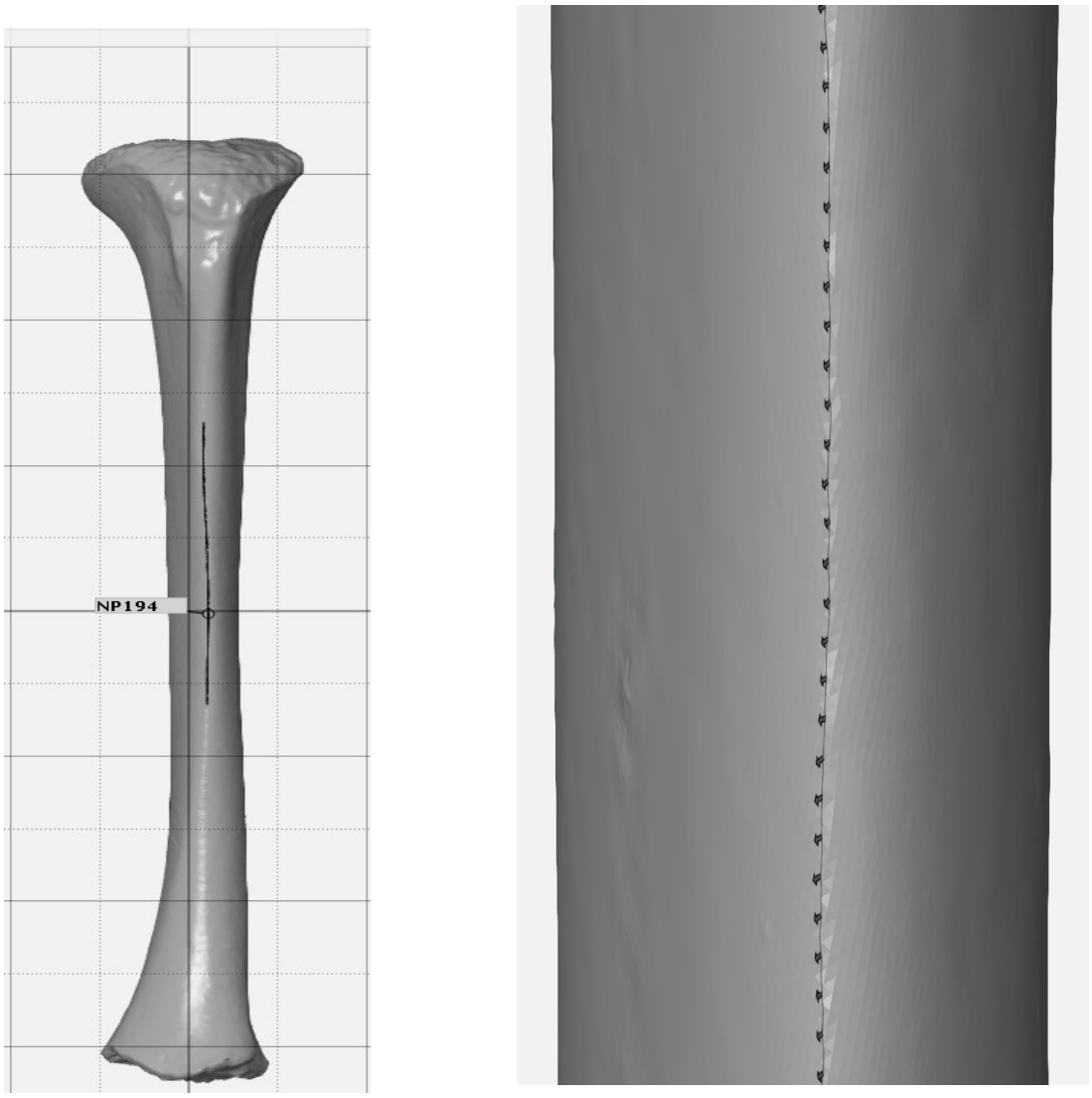

Figure 4.4. Left: A tibia model in GOM Inspect software depicting the trace along the anterior crest at 70% to 40% of diaphyseal length. Right: The same tibia, but zoomed in to display the individual Cartesian points of the AC trace created in GOM Inspect.

In tibiae that possessed one or both epiphyses fused, the distal and proximal epiphyseal scars were used as a guide to estimate where the diaphysis ceased and the epiphysis began. From this, 70% and 40% of the AC on the diaphysis was identified and traced. However, as the proximal and distal epiphyses differ in height, the 0mm mark on the grid overlay did not correspond to 50% of diaphyseal length. To ensure accurate tracing of the AC from 70% to 40%, the length of the diaphysis from distal to proximal epiphyseal scars was measured and divided by two; this gave a measurement on the grid overlay corresponding to 50% of diaphyseal length to use in locating the trace area of interest (70 to 40%). An image of a traced AC on a tibia with fused proximal and distal epiphyses is shown below (Figure 4.5). The traced line on each model was exported as an .asc file, which stores the traced line as a set of Cartesian points (Optical Measuring Techniques GOM, Germany, 2019) that varied in number (1,200-2,000) depending on the size of the individual. These sets of points captured the shape and size of the AC along 30% of diaphysis length.

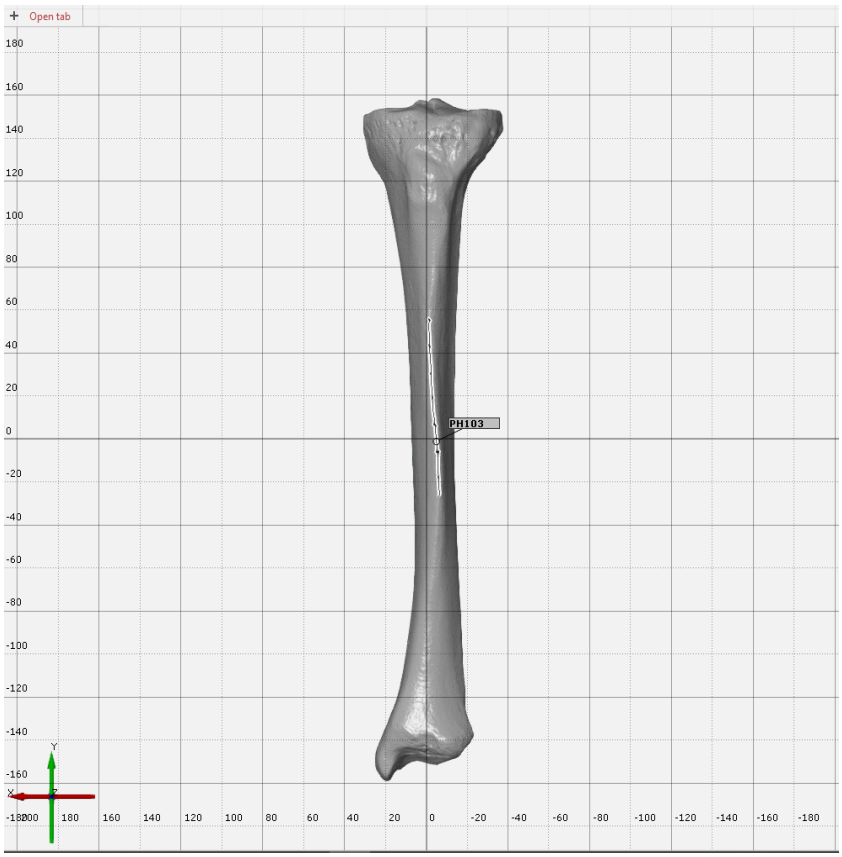

Figure 4.5. Depicts the tracing of 70% to 40% of the anterior crest on a tibia with fused proximal and distal epiphyses.

The .asc AC trace files were analysed in the R statistical environment (version 3.5.0; R Core Team, 2018; RStudio Team 2016) using function *digit.curves* in the package geomorph (version 3.1.0; Adams et al. 2019) to convert the 1,200-2,000 Cartesian points into ten new sliding semi-landmarks along the AC using the argument 'nPoints = 10' (Appendix B). These ten semi-landmarks were located between two fixed landmarks set by the function at the ends of the traced line using the argument 'closed = false', making a total of twelve landmarks (Figure 4.6). The number of semi-landmarks required to capture a curve's overall shape and outline is determined by the curve's complexity, with relatively simple curves requiring fewer semi-landmarks than more complex curves to capture their overall shape and outline (Bardua et al.,

2019; Brzobohatá et al., 2019). Bardua et al. (2019) reported that oversampling can decrease the accuracy of statistical analysis through the incorporation of unimportant shape data. This is reiterateded by Brzobohatá et al. (2019), who stated that increasing the twenty landmarks within their AC traces risked registering non-significant surface variables that could detract from otherwise relevant shape data. For this thesis, twelve landmarks were determined to be sufficient in capturing the overall shape and outline of the AC so as to not increase the risk of incorporating non-significant shape variables that would devalue any statistical analysis.

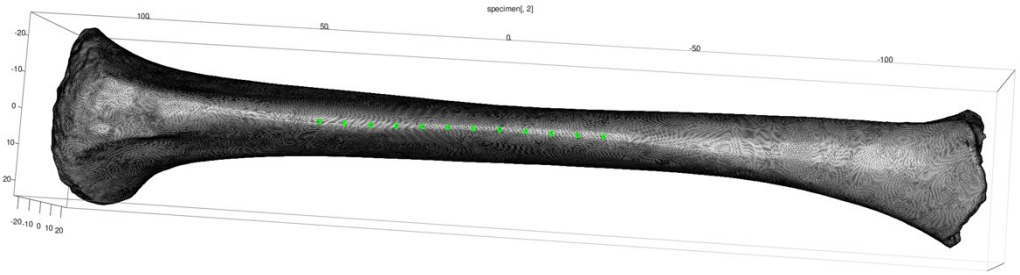

Figure 4.6. Example of the 12 landmarks (green points) derived from the anterior crest trace files created in GOM Inspect (Optical Measuring Techniques GOM, Germany, 2019).

4.5 Statistical Analysis of Data

The Cartesian coordinates of the 12 landmarks were saved in a .csv file for statistical analysis, converted into a matrix using the function *as.matrix,* and then converted into a 3D array using the geomorph function *arrayspecs* (Adams et al., 2019). Array conversion combined the data from the 65 individuals into the same data structure. 3D arrays were used for Generalized Procrustes Analysis (GPA) which was conducted separately on sub-groups: a non-

adult sample; an adult sample; and, a subsetted adult sample consisting of a male and a female group.

Generalized Procrustes Analysis was conducted using the geomorph function *gpagen*. During GPA, the data were analyzed by minimizing Procrustes distance, rather than thin-plate spline (TPS) bending energy. TPS bending energy has been noted to produce erroneous results when used on features that are in the process of development. As reported by Mitteroecker and Gunz (2009), TPS bending energy is ineffective if 3D shape differences among individuals are not subtle. For TPS bending energy to function correctly, a single landmark template is constructed from one individual, and then automatically mapped onto all other individuals (Mitteroecker and Gunz, 2009). As the anterior crest is a feature in the process of growth, a template could not be homologously mapped onto each model when this method was attempted.

Once GPA was completed, the resulting shape data were analyzed through Principal Components Analysis (PCA) using the geomorph function *plotTangentSpace* (Adams et al., 2019). As noted previously, PCA deconstructs GPA data into a set of axes describing the shape variation, called Principal Components (PCs) (Zelditch et al., 2012). Custom PC plots, using the package *ggplot2*, were created to highlight individuals by population and sex by assigning a separate symbol and color per variable (Wickham, 2016). The plots were created to explore PCs in non-adults, and by sex in adults. To help the reader visualize the shape variations associated with the PC plots, the minima and maxima of PCs were displayed. Grey points represent the minimum mean shape of PC1 and PC2, while black points represent their maximum shape

(Figure 5.1). The criteria to determine which PCs were retained for analysis were those that account for over 10% of total variation.

Three sets of Pearson correlation analyses were performed on the non-adult sample using the *cor.test* function. Of the three Pearson correlation analyses, the first two were conducted to explore the question of age-related shape variation in the non-adult anterior crest. The first correlation analysis of age (represented by dental age) with PC scores (shape) was conducted to determine whether age influenced AC shape. Next, in order to determine if AC size influenced shape, centroid size (Csize) with PC scores was analyzed. Lastly, in order to determine if the non-adult AC's size increased with dental age, a Pearson correlation analysis of Csize with age was conducted. As the growth plate is responsible for longitudinal increases in a bone's size, it is expected that Csize and dental age will demonstrate a significant correlation. Next, in order to answer the question of how the tibial anterior crest changes in shape during growth, visualizations of PC score by age were conducted in the non-adult sample.

For the adult sample, t-tests for sex-based differences in PC scores, and in Csize were conducted using the *t.test* function. These t-tests would indicate any possible evidence of sexual dimorphism in the AC. If significant differences were not detected between the male and female adults, then the adults were to be combined into a single sample for analysis. Next, Pearson correlation analysis was conducted on adult Csize by PC score to identify if size was associated with shape change.

To demonstrate the progression of the non-adult AC into its final adult shape and size, a maturation analysis was performed. Using the sliding average approach outlined by Wilson et

al. (2015) (Appendix C), shape maturation was illustrated by calculating the numeric Procrustes Distance (PD) between each non-adult individual's GPA coordinates using the Shapes package function *procdist* (Dryden, 2019; version 1.2.5). The mean GPA coordinates of the five youngest non-adults represented the maturational start point, and the adults' mean GPA coordinates represented the maturational end point. Wilson and colleagues' (2015) sliding approach assumes the shape of the youngest non-adult must progressively change into the shape of the second youngest before it changes into the shape of the third youngest, and so on. In order to reflect this ontogenetic progression, each progression of shape (represented by PD) occurs sequentially from the chronologically youngest individual to the chronologically oldest (Wilson et al., 2015). The identification of each non-adult's precise dental age for the maturation sequence was conducted by Dr. Lesley Harrington using dental development scores from Smith (1991), or from long bone regressions. This allowed each non-adult within the age stages described by Al Qahtani et al. (2010) to be ordered sequentially from youngest to oldest. In order to conduct the shape progressions, the PD of the maturation start point was determined by using *procdist* on the start point's mean GPA coordinates and the youngest non-adult's GPA coordinates. Next, the PD of the youngest non-adult was determined by using *procdist* on its GPA coordinates and those of the second youngest. This process continued sequentially until the last PD was obtained between the eldest non-adult and the adult sample (Dryden, 2019).

Next, in order to obtain each non-adult's 'sliding' PD (used in maturation groups), the PDs (which represent the shape transformations) were added together for each non-adult (Wilson et al., 2015). For example, the sliding PD of the youngest non-adult was obtained by adding its PD to the PD of the maturation's start point. The number derived from this

summation represented the sliding PD of the youngest individual. For the second youngest non-adult, the PDs of it and youngest non-adult were summed with the youngest's sliding PD to obtain the second non-adult's successive sliding PD. This process repeated for every non-adult to obtain the maturation's cumulative Procrustes distance (Wilson et al., 2015).

Once this was complete, a series of maturation groups, each containing five non-adults, was created in accordance with the method of Wilson et al. (2015). Each group contained an overlap of two non-adults, ensuring that each successive maturation group did not plot beyond the next group or behind the previous group (Wilson et al., 2015). For example, Group One contained the sliding PDs of non-adults 1 – 5; Group Two contained the sliding PDs of non-adults 3 – 7. This continued for all 41 non-adults. The average of the sliding PDs of each group was used as a percentage of the maturation's cumulative Procrustes distance. A loess trendline using the average dental age was used to help visualize the rates of maturation and any increases or decreases in maturation rate during growth. Size maturation followed the same steps as shape maturation, despite using Csize instead of PD for the size maturation. As PD was not used, a maximum cumulative trajectory length for Csize was not required.

4.6 Error Study

An error test was conducted to ensure the accuracy and reliability of the study landmarks. Twenty randomly selected non-adult tibiae and 12 adult tibiae were traced and landmarked twice with a three-day gap between each session. The two fixed landmarks and 10

semi-landmarks derived from the tracings were exported into a .csv file and compared in RStudio using *procD.lm* (RStudio Team, 2016; Adams et al., 2019). The function *summary* was used on the *procD.lm* results to display the mean square (MS) values (RStudio Team, 2016; Adams et al., 2019). Once the MS values were displayed, the MS measurement error equations provided by Zelditch et al. (2012) were used to compare the landmarks between the two non-adult and adult tracing sessions. These equations are provided below. As such, 2 is the number of replications. The repeatability was then re-expressed as an error percentage by subtracting the repeatability from 1. These equations were conducted twice, once for the non-adult sample and once for the adult sample.

Individual Variance = (MSindividual – MSerror)/2
Total Variance = MSerror + individual variance
Repeatability = individual variance / total variance
Percent Error = 1 – Repeatability

Chapter 5. Results

5.1 Error Analysis

The non-adult and adult samples were subjected to separate semi-landmark error tests generated from the trace line data. The error tests looked for coordinate variance between two measuring sessions, each three days apart. The results indicated a non-adult repeatability of 0.92 (8% error) and an adult repeatability of 0.90 (10% error).

5.2 Shape Change as described by Principal Component Analysis

Shape change in the non-adult and adult samples was analyzed with Principal Component Analysis (PCA). The first three principal components (PCs) represented over 71.4% of shape covariance in both samples (Table 5.2). The complete non-adult and adult PC summaries are found in Appendix D. This thesis focused on the first three PCs for analysis because the remaining have eigenvalues less than 0.1. Size and age were the primary variables of interest in the non-adult sample. For the adult sample, only size was of interest. Size was represented by centroid size (Csize), and age was represented by the dental age stage of each individual. Shape was studied by analyzing the PC axes' representation of the position of landmarks along the anterior crest (from 70-40% of diaphyseal length). Movement of these landmarks along a PC axis illustrates shape change, along with the minimum and maximum shift in landmarks relative to the axis mean.

	PC1	**PC2**	**PC3**
Non-adult	43.6%	18.0%	11.8%
Adult	37.7%	25.5%	11.2%

Table 5.2. Proportion of total variance accounted for by the first three principal components in the Non-adult, and in the Adult samples.

5.2.1 Non-Adult Sample

The first principal component (PC1) illustrates mediolateral variation along the entirety of the anterior crest (Figure 5.1). Specifically, the most proximal area displayed the greatest amount of lateral variation away from the minimum shape. Descending distally, a lengthy portion of medial variance is located along the middle length of the configuration. Medial variation then transitioned anteromedially toward the distal-most area where lateral variation resumed. When viewed in medial orientation, no anteroposterior variation is found in the most proximal area. The middle area of the configuration in medial-orientation showed a distally descending posterior to anterior variance from the shape minimum. In the medially-viewed distal-most aspect, a brief proximo-posterior variance was observed. Age did not correlate with any of the three PCs, while Csize had a low correlation with PC2 (Table 5.3).

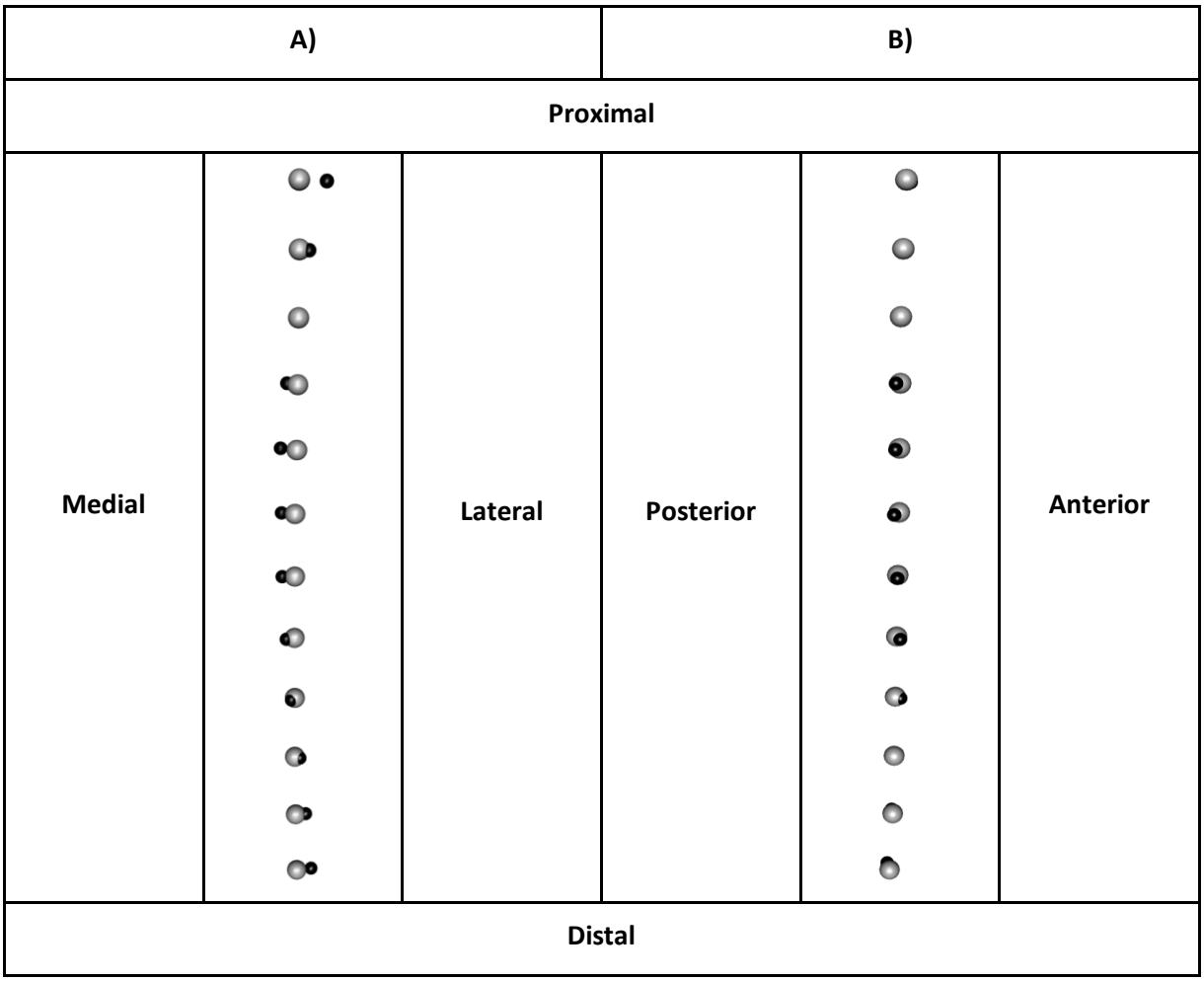

Figure 5.1. Minimum (grey) and maximum (black) landmark positions for PC1 in the non-adult sample.(2X magnification.) A) is in anterior orientation to depict mediolateral shape change. B) is in medial orientation to depict anteroposterior shape change.

	PC1	**PC2**	**PC3**
Age	r = 0.217 95% CI = -0.096, 0.492 p-value = 0.171	r = -0.199 95% CI = -0.476, 0.117 p-value = 0.215	r = -0.004 95% CI = -0.311, 0.303 p-value = 0.977
Csize	r = 0.227 95% CI = -0.032, 0.539 p-value = 0.078	r = -0.342 95% CI = -0.587, -0.038 **p-value = 0.028**	r = -0.154 95% CI = -0.440, 0.161 p-value = 0.335

Table 5.3. Pearson correlation test results in the non-adult sample. Age is represented by the dental age of the individuals. Size is represented by centroid size (Csize). The threshold for statistical significance is a p-value of 0.05. Significant p-value results are bolded.

Beginning proximally in PC2's anterior orientation and descending distally, no lateral or medial variation is observed except for a single instance of lateral variance in the configuration's distal-most aspect (Figure 5.2). When PC2 was viewed in medial orientation, sizable yet intermittent anteroposterior variance was displayed. The maximum's most proximal landmark varied posteriorly from the shape minimum. Distal to this, anterior variation transitioned posteriorly along the crest. The distal-most aspect of the medial-orientated configuration varied anteriorly. The anterior and medial oriented PC2 configurations predominantly demonstrated anteroposterior shape variation with no medial and limited anterolateral variation in the configuration's distal-most aspect.

In PC1, the degree of shape variation overall is more extensive than in PC2. Based on the minimum to maximum shape change observed, PC1 emphasized a mediolateral sigmoid accentuation in the anterior crest. In comparison, PC2 appeared to represent anteroposterior shape variation. PC2 correlated with Csize but not age (Table 5.3).

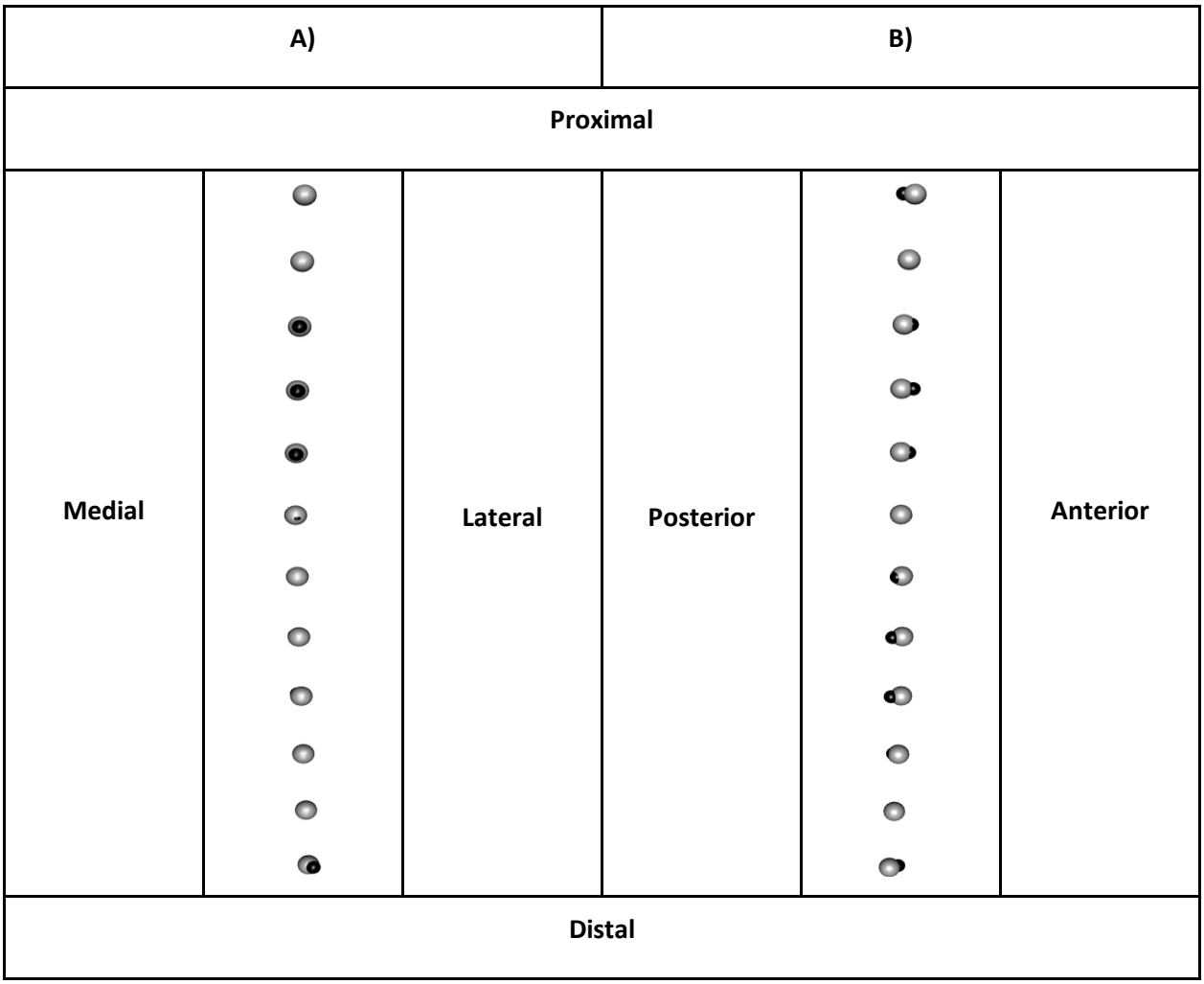

Figure 5.2. Minimum (grey) and maximum (black) landmark positions for PC2 in the non-adult sample.(2X magnification.) A) is in anterior orientation to depict mediolateral shape change. B) is in medial orientation to depict anteroposterior shape change.

The results of the correlation tests demonstrated that PC1 and PC3 did not significantly correlate with age or size, while size moderately correlated with PC2 (Table 5.3). As age does not correlate with any of the PCs, the correlation tests between PC1 and PC2 with age were visualized with scatter plots (Figure 5.3). This was conducted to observe if a hidden pattern of shape variance not detectable by the correlation tests was present in the sample. The results of these tests and scatter plots showed that age does not appear to be a significant factor in anterior crest shape change. A PC scatter plot of the non-adult sample for PC1 and PC2 is

displayed in Figure 5.4. Non-adults did not group according to population and instead grouped together. This indicated that some form of variation, or variable outside of age and size, was possibly present among the individuals. Since age did not correlate with either PC1, PC2 or PC3, and size exclusively correlated with PC2, it appears that anterior crest shape is not subject to statistically significant age-related shape variance. However, an additional correlation test was conducted that revealed that age and size themselves were significantly correlated (Table 5.4). This confirmed that the size of the anterior crest increased during growth.

	Csize
Age	r = 0.753 95% CI = 0.580, 0.861 **p-value = <0.001**

Table 5.4. Pearson correlation test results in the non-adult sample between age and size. Age is represented by the dental age of the individuals. Size is represented by centroid size. Significant p-value results are bolded.

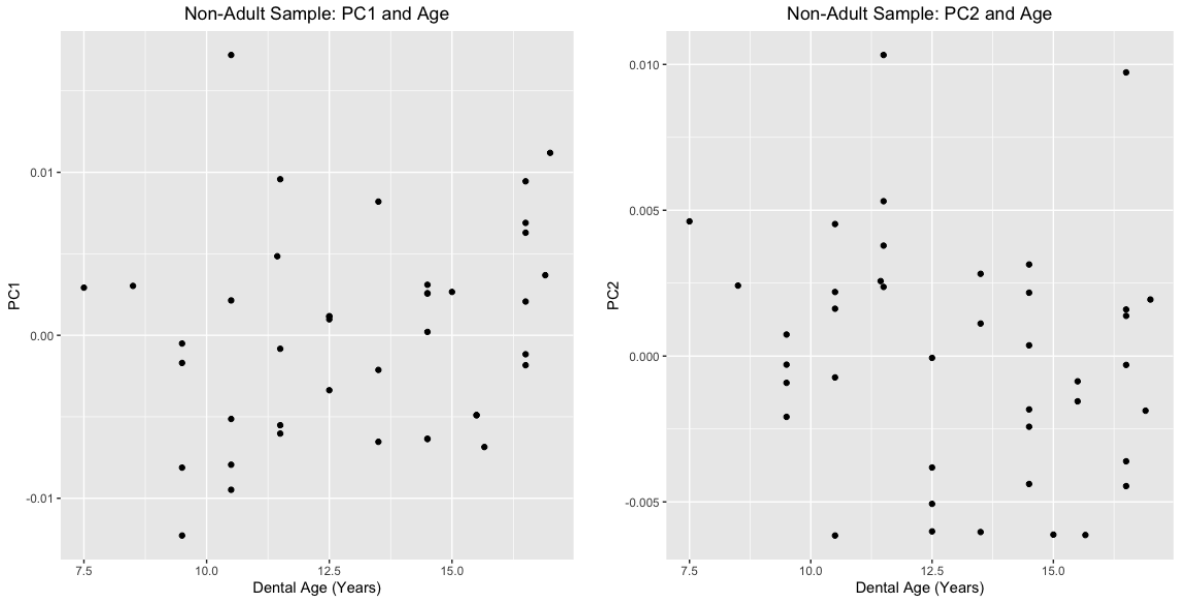

Figure 5.3. Scatter plots of the non-adult sample according to PC1 and PC2 against age.

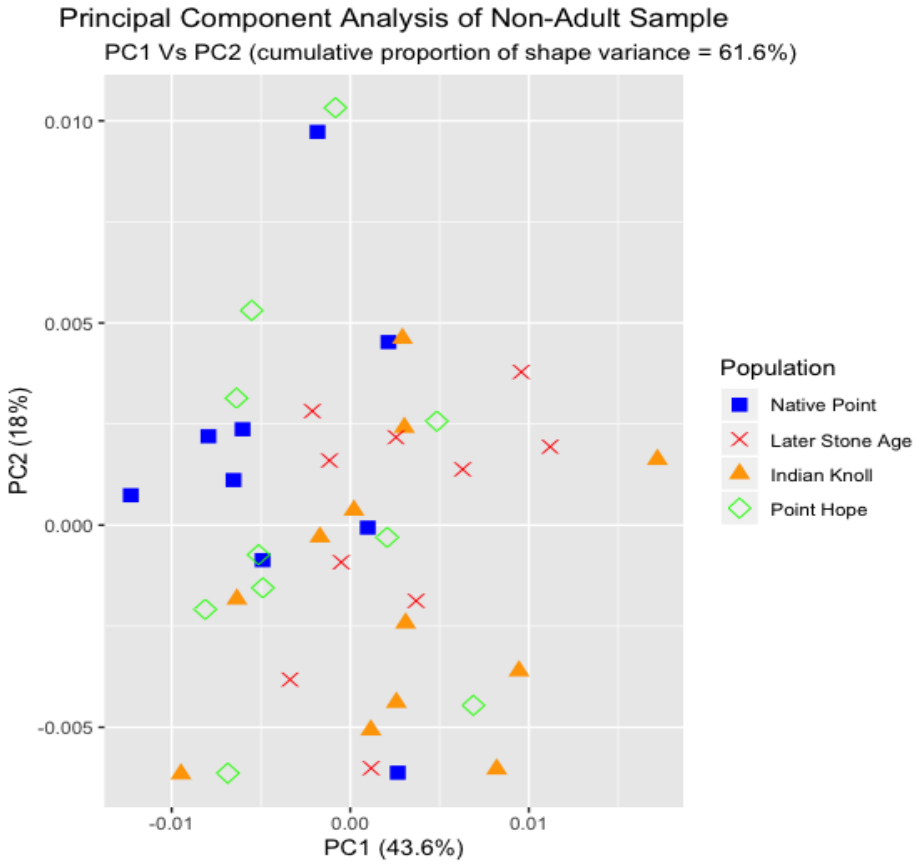

Figure 5.4. Principal Component Analysis scatter plot of the non-adult sample according to the first two principal components. Each individual's population is identified with a unique symbol and color.

5.2.2 Adult Sample

The results of the t-tests on the male and female adult samples demonstrated that centroid size (Table 5.5) and PC score (Table 5.6) were not significantly different between males and females. A scatter plot to visualize how males and females plotted according to PC is located in Figure 5.5. The scatter plot revealed that male and female adults do not group by

population or sex. Due to the lack of sexual dimorphism, all adults were combined into a single sample.

	Sex
Csize	t = 1.547 95% CI = -2.367, 13.978 df = 12 p-value = 0.147

Table 5.5. Depicts t-test results between centroid size (Csize) and sex. Significant results are in bold.

	PC1	**PC2**	**PC3**
Sex	t = -1.159 95% CI = -0.010, 0.003 df = 12 p-value = 0.268	t = 0.926 95% CI = -0.002, 0.007 df = 12 p-value = 0.377	t = 1.075 95% CI = -0.002, 0.005 df = 12 p-value = 0.303

Table 5.6. Depicts t-test results between sex and PCs. Significant results are in bold.

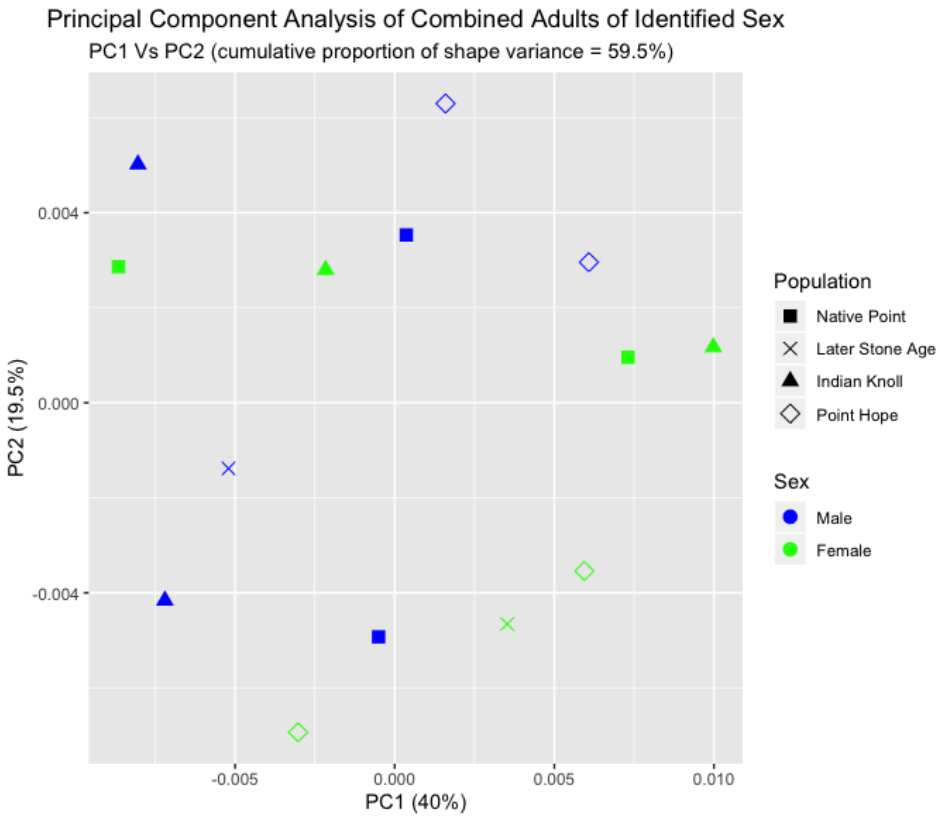

Figure 5.5. PC scatter plot of the adult males and females by population.

	PC1	**PC2**	**PC3**
Csize	r = 0.411 95% CI = 0.010, 0.699 **p-value = 0.045**	r = 0.127 95% CI = -0.290, 0.505 p-value = 0.552	r = 0.112 95% CI = -0.304, 0.493 p-value = 0.599

Table 5.7. Pearson correlation test results for centroid size (Csize) and PCs in the adult sample. Significant results are in bold.

In the combined adult sample, centroid size was found to have a low correlation with PC1, but not with PC2 or PC3 (Table 5.7). This indicated that the combined adult sample's PC1 shape was slightly influenced by anterior crest size. A PC scatter plot of PC1 and PC2 for the combined adult population is located in Figure 5.6. In this figure, the adults, similar to the non-

adults, did not group according to population. However, a visual comparison of Figure 5.6 revealed that the adult sample had a tendency to plot higher for both PC1 and PC2 than did the non-adults in Figure 5.3.

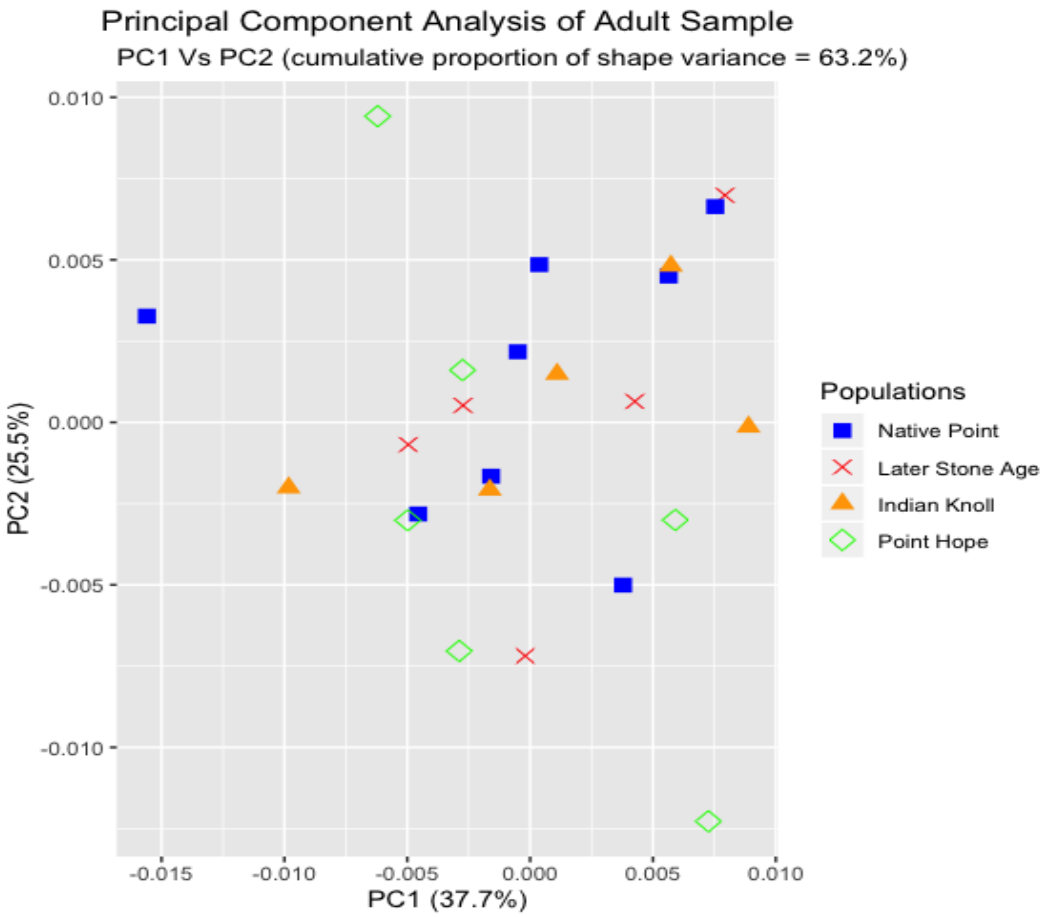

Figure 5.6. Principal Component Analysis scatter plot of the combined adult sample according to the first two principal components (PC1 and PC2). Each individual's population is identified with a unique symbol and color.

5.3 Maturation Analysis

The maturation trajectories for both shape and size along with their loess regression trend lines, were compared in Figure 5.7. The comparison between shape and size revealed a significant positive increase with age. The trajectory for shape was observed to be notably steeper than for size and suggested a greater increase in shape maturity during growth. The rate of shape maturation was constant until 12.5 years of age, when a brief slowdown in maturation occurred around 13.5 years of age. After this point, shape maturation consistently increased into adulthood. In comparison, the trajectory of size maturation was more gradual with increased variation among maturation groups after roughly 13 years of age. The previously noted slowdown in shape maturation partially overlapped with a period of increased size maturation from 13 to just before 15 years of age. For size, the period of increased maturation persisted longer than the period of decreased shape maturation. Two size maturation groups, attributed to around 14 years of age, displayed near complete adult maturity. This showed that average adult size could be achieved before 15 years of age. After 15 years of age, size maturation decreased and leveled off towards adulthood, leaving three size maturation groups congregated with the last having achieved full adult size. This stagnation is possibly due to decreased tibial growth towards the end of adolescence. Unlike for size, the final three shape maturation groups did not group together; neither slope for shape or size intersected the other. However, the trendline for shape remained in a steep incline towards adulthood where size did not. This suggested that shape maturation is unaffected by the decreased size maturation towards the end of adolescence.

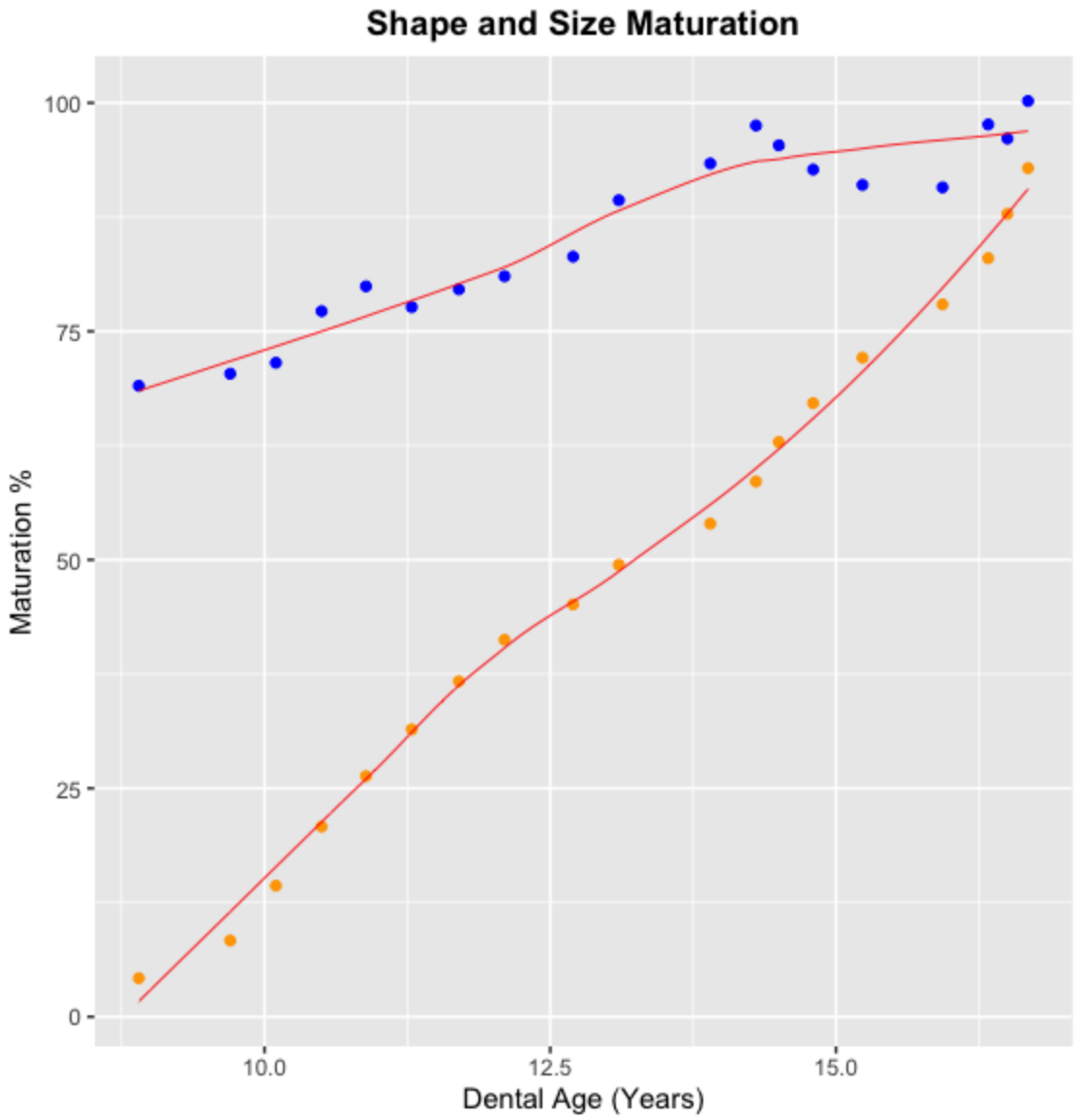

Figure 5.7. Depicts the shape and size percentage of each maturation sliding age group in the combined non-adult sample. Shape is represented by the orange series. Size is represented by the blue series. Loess regression lines are depicted in red for each series.

Chapter 6: Discussion

The two research questions this thesis endeavoured to answer were: first, if age-related shape variance was displayed in the non-adult anterior crest and second, if the anterior crest displayed a pattern of shape change during growth. The results of this thesis failed to find support for the hypothesis that anterior crest shape variation was patterned by dental age; nor was a consistent pattern of shape change identifiable during growth. In keeping with expectation, however, a correlation test revealed that anterior crest size increased during growth. The maturation analysis demonstrated that mean adult size can be obtained around 15 years of age. Further, the relatively early acquisition of adult size did not impede subsequent maturation of anterior crest shape.

6.1 Shape Variation with Dental Age

For the non-adult anterior crest, PC1 represented mediolateral shape change, and PC2 depicted anteroposterior shape change. The non-adult PC scatter plot revealed that individuals with high mediolateral curvature did not always have a correspondingly low degree of anteroposterior curvature, and vice versa. PC1 and PC2 did not correlate with dental age; this indicated that both forms of shape change are not age-related in the sample. Visualization of the correlation analyses via scatter plots did not reveal patterned shape change during growth. Given the results of the correlation analyses, it was expected that a pattern of shape change would not be visible when plotted.

Both this thesis and Brzobohatá et al. (2019) reported PC1 and PC2 as representing mediolateral and anteroposterior changes in curvature. This was expected due to the similarities between the two studies. Based on this and Brzobohatá et al. (2019), mediolateral and anteroposterior shape change are the primary forms of anterior crest shape variance during both non-adult growth and adulthood. Interestingly, individuals with high mediolateral curvature did not always have a consistently low degree of anteroposterior curvature, and individuals with low mediolateral curvature did not always have a corresponding high degree of anteroposterior curvature. This observation was unexpected due to the previous research conducted by Brzobohatá et al. (2016; 2019). According to Brzobohatá et al. (2016; 2019), accentuation of mediolateral curvature occurred when anteroposterior curvature decreased in response to reduced physical activity. Essentially, the reduction of physical activity caused less bending stress being placed on the anterior crest by the soleus, gastrocnemius and quadriceps femoris muscles, thereby decreasing anteroposterior curvature and increasing mediolateral curvature (Brzobohatá et al., 2019).

The lack of age-related shape variance in the anterior crest was a surprising result, as Brzobohatá et al. (2019) postulated that age could be an important non-genetic factor of anterior crest curvature. Further, the studies of Macintosh et al. (2015), De Groote (2011) and Trinkaus (1993) all strongly supported the theory that activity during development can dictate adult morphology in the lower limb.

A possible explanation for the lack of age-related shape variance or pattern during growth is that age by itself does not influence anterior crest morphology to the degree Brzobohatá et al. (2019) theorized. Ruff (2018), Brzobohatá et al. (2016; 2019) and Trinkaus

(1993) agreed that physical activity during growth could act as a powerful determinant of human lower limb morphology. Ruff et al. (2006), Holt et al. (2018) and Higgins (2014) demonstrated that the terrain upon which activity is conducted, whether 'flat', 'rough' or 'uneven', could have greatly influenced the degree of anteroposterior and mediolateral curvature that was developed in the tibia. Ancestry and climate also influenced lower limb morphology (Ruff, 2018; Frelat and Mitteroecker, 2011; Roseman and Auerbach, 2015). Therefore, lower limb morphology can be seen as a compromise among multiple factors during growth (Ruff, 2018). In regards to the four population samples drawn upon for this research, differences in terrain and activity could explain the lack of age-related shape variance and lack of shape pattern during growth in the combined non-adult sample.

Importantly, it was observed by Ruff (2018) that morphological change in the lower limb could persist into early adulthood after growth had concluded. With this observation, it is possible that morphological change in the anterior crest could occur both during growth and in the first few years after the cessation of growth. Possibly, a consistent pattern of shape change in the anterior crest may be only identifiable in older adolescents and younger adults.

6.2 Interaction between Size and Shape

Csize and dental age significantly correlated together in the non-adult sample, confirming that the size of the anterior crest increased during growth. Correlation between Csize and dental age was expected due to the growth plates' role in the longitudinal expansion of a growing bone. The t-tests conducted for this thesis in the adult sample showed a lack of

adult sexual dimorphism in anterior crest shape and centroid size (Csize). This result was expected and conformed to the reported results of Brzobohatá et al. (2019). From this it can be inferred that anterior crest shape change and size were not significantly different between males and females.

The size of the anterior crest, represented by Csize, showed a statistical correlation with PC2 (anteroposterior shape change) in the non-adult sample. However, this correlation can be described as low to moderate. Csize also correlated with shape change in the adult sample. However, adult Csize was associated with PC1 and not with PC2. Despite the correlation of Csize to shape change, this correlation was also classified as low in significance. As an increased Csize corresponds to an increase in age during growth, it appears that the anteroposterior shape change captured by PC2 was related to age by proxy of size increases in the anterior crest. These correlations between Csize and shape change may hint at a relationship with ontogenetic allometry.

Allometry refers to morphological variation being explained by a change in size (Klingenberg, 2016). Macintosh et al. (2015), De Groote (2011) and Brzobohatá et al. (2019) all reported a lack of interaction between size and shape in their adult lower limb studies. If an interaction between size and shape change was detected, these studies would be evidence of static allometry, the study of changes in size of a single developmental stage or population (Klingenberg, 2016; Rosas and Bastir, 2002), while ontogenetic allometry looks at shape changes associated with increased size over individual growth (Klingenberg, 2016; Loy, Catuadella and Corti, 1997; Mitteroecker et al., 2013). Importantly, these are two separate forms of allometry. As such, the presence or lack thereof for static allometry in the previous

research cannot be used to infer any possible role for ontogenetic allometry in the non-adult sample. Currently, a possible relationship with ontogenetic allometry is only hinted at in the data.

6.3 Maturation of Size and Shape

Growth is theorized to have been an important factor in determining lower limb morphology due to the plasticity of the skeleton during this period (Brzobohatá et al., 2019; Macintosh et al., 2015; De Groote, 2011; Trinkaus, 1993; Bateson and Gluckman, 2011). Maturation trajectories for anterior crest shape and size were constructed to detect if growth influenced anterior crest shape towards a mean adult size and shape. The creation of size and shape maturation groups with overlapping individuals ensured that no single group plotted beyond or behind the adjacent group. As described by Wilson et al. (2015), this acted as a smoothing function for maturation analysis. The direct comparison of size and shape showed that both trajectories had a significant positive association with increased age towards the mean adult anterior crest's size and shape.

The slope for size maturation was observed to be more gradual than the slope for shape, and began at a substantially high maturation rate towards adult size; neither trajectory intersected the other. In their pediatric surgical review of lower limb growth predictions to calculate when to conduct epiphysiodesis, Kelly and Diméglio (2008) reported that the tibia's diaphysis has achieved 65% of total size by 7 years of age, and close to 90% of size by the onset of puberty. As such, size's high maturation percentage towards mean adult size was not a surprising result. The large amount of tibial growth that has occurred by puberty may have

been the cause of the low correlation between Csize and PC2 anteroposterior shape change. Gindhart (1973) studied tibial growth standards and reported that males underwent a pubescent growth spurt from 12-15 years of age, and from 9-12 years of age for females. Kelly and Diméglio (2008) noted that size maturation increased in velocity once puberty had commenced, for a year and then decreased for a period of 2.5 years, after which all lower limb growth ceased so that spinal growth was not outpaced. If correct, this could explain the variable maturation rates observed among the size maturation groups, and why two maturation groups achieved near-complete adult size before 15 years of age.

A *loess* regression line for size showed that size maturation notably increased in velocity around 12.5 years of age, and gradually decreased after a year or so towards adulthood. This increased size maturation appears to have aligned with the increase recorded by Kelly and Diméglio (2008). A maturation increase was not observed before 12.5 years of age, when females undergo their growth spurts (Gindhart, 1973). This may indicate an imbalance of males over females in the non-adult sample. It is important to note that the determination of sex in non-adult skeletons, not including genetic analysis, remains highly difficult before puberty due to the lack of developed sex-specific skeletal features primarily located on the pelvis (Wilson et al., 2008; Navarro-Romero et al., 2020; Kanabur, 2012).

Shape's *loess* regression line was observed to exhibit a dramatically steeper incline with age and proceeded at a uniform rate towards mean adult shape, until a brief slowdown occured at 12.5 years of age. This period of decreased shape maturation partially overlapped with the period of increased size maturation, though the duration of this decrease was shorter and afterwards shape velocity dramatically increased. From this, and the non-adult correlation test

results, a limited interaction between size and shape may have been present around 12.5 years of age. Essentially, as size maturation increased, shape maturation towards the adult mean slightly decreased; as size maturation slowed, shape maturation accelerated sharply.

The regression lines illustrated size maturation at a slower rate than shape maturation, which is likely due to the large amount of growth that had already occurred by puberty (Kelly and Diméglio, 2008). Further, shape maturation appeared to be unimpeded by the obtaining of near-complete adult size. This observation appeared to support the theory by Ruff (2018) - that morphological change can persist after the cessation of growth. Additionally, shape maturation being unimpeded by size maturation could have been due to separate growth processes. For size, endochondral growth results in increased length through deposition of bone-tissue at the ends of the bone's diaphysis as it extends towards the epiphyseal growth plate (Mays, Ives and Brickley, 2009). Longitudinal growth will cease once the diaphysis and epiphyses fuse together. For shape, appositional growth causes increased bone width through deposition of bone-tissue beneath the diaphysis' periosteum (Mays, Ives and Brickley, 2009). However, appositional growth does not explain the maturation trajectory of shape after adult size has been achieved. Bone remodeling may also influence shape maturation in the anterior crest. Hadjidakis and Androulakis (2006) defined bone remodelling as the continuous resorption and replacement of old and damaged bone-tissue with new and healthy bone-tissue in response to changing mechanical loads and strains. As noted by Wolff (1986) remodelling occurs throughout life and alters the internal structure and external shape of a bone, such as increased diaphyseal curvature to withstand bending stress. Ruff and Hayes (1982; 1988) reported that bone remodeling in the tibia is crucial during adulthood to maintain the structural shape and strength

of areas, such as the mid-diaphysis, that experience high levels of mechanical stress from physical activity. As noted by Brzobohatá et al. (2019), the anterior crest around the mid-proximal and mid-diaphysis demonstrated the greatest amount of shape variation.

The hypothesis put forth by Brzobohatá et al. (2019) that age is an important factor in anteroposterior and mediolateral crest curvature was not supported by the results of this thesis. However, this could be due to sample size, sample composition, or the amount of the non-adult anterior crest that was traced. It should be noted that the traces in this study captured the region of greatest shape change reported by Brzobohatá et al. (2019). The results of this thesis showed age was significantly correlated with the maturation of anterior crest shape, but not with changes in curvature as theorized by Brzobohatá et al. (2019).

Chapter 7: Conclusions and Future Research

There were two research objectives of this thesis: first, to determine if age-related shape variance was present in the non-adult anterior crest and second, if a pattern of shape change was identifiable during growth. These research questions were derived from Brzobohatá et al. (2019), who hypothesized that age was an important factor in anterior crest morphology. Geometric morphometrics, which examines variance in the cartesian coordinates of landmarks and semi-landmarks along a biological feature, was essential to exploring shape variation along the anterior crest of the tibia. Brzobohatá et al. (2019) and this thesis were in agreement that changes in mediolateral and anteroposterior curvature were the primary

principal components of anterior crest shape change; however, neither PC correlated with dental age when subjected to correlation tests. As such, this thesis is unable to support the hypothesis of Brzobohatá et al. (2019) that anterior crest curvature was strongly influenced by age. No evidence of sexual dimorphism in Csize or shape change was discovered in the adult anterior crest, as with Brzobohatá et al. (2019). Both the non-adult and adult samples had a minor correlation between shape change and Csize, possibly hinting at a relationship ontogenetic allometry.

In regards to the second research question, no consistent pattern of shape change was identifiable in the anterior crest during growth. This was determined with correlation analyses of Csize with age, and through the use of scatter plots to image mediolateral and anteroposterior shape change by dental age in the non-adult sample. Further, these scatter plots showed that the morphological relationship observed by Brzobohatá et al. (2019) between the development of accentuated mediolateral curvature and the relaxation of anteroposterior curvature was not consistent in this study sample.

A maturation analysis of the anterior crest was conducted to study the trajectory, rate and interaction between size and shape during growth towards their adult mean. The analysis revealed these to have a significant positive association with age. Size maturation was considerably further developed than shape maturation, yet progressed at a slower rate. These observations were likely the result of 90% of tibial adult size being achieved by puberty (Kelly and Diméglio, 2008). Further, this explained why maturation groups 12 and 13 achieved near-adult size by 15 years of age. After 15 years of age, size maturation slowed and began to level off towards adulthood. Shape maturation was not as initially highly developed as that of size.

However, the trajectory of shape maturation was notably steeper and increased in incline towards adulthood as size slowed. Overall, size maturation did not impede continued shape maturation after adult size was obtained. Continued shape maturation might be the result of bone remodeling and of the different growth processes responsible for increased bone size and shape via longitudinal and appositional growth.

As a result of the findings of this thesis, there are multiple avenues of future research in this area. First, the correlation tests on both the non-adult and adult samples hinted at the possible presence of allometric shape change. Therefore, the question of ontogenetic allometry in the anterior crest should be explored with a future study. As noted previously, the current body of research on lower limb morphology has been performed on adult individuals, and showed no evidence of static allometry (Macintosh et al., 2015; De Groote, 2011; Brzobohatá et al., 2019). However, these studies exclusively examined adult remains. It is important to note that the type of allometry would likely be different between an adult and non-adult study, with the former an exploration of static allometry while the latter a study of ontogenetic allometry. A future research project should determine if an ontogenetic interaction between anterior crest size and shape change is present during growth. As noted by Klingenberg (2016), an allometric study would entail a multivariate regression of shape change on Csize to determine the existence of an association. Second, the results of the maturation analyses aligned with Ruff (2018) and showed that shape maturation towards the adult mean continued well after adult size was achieved. As such, an additional study which is specifically targeted towards the late adolescent and early adult age period could be undertaken to explore if a pattern of shape change is identifiable towards the end of growth.

Overall, while age is significantly associated with size and shape maturation towards an adult mean, the results of this thesis do not support Brzobohatá et al. (2019) who hypothesized age was a notably important factor in the development of mediolateral and anteroposterior anterior crest curvature. No consistent pattern of shape change was observed during growth. However, the analyses conducted in this thesis indicated the possible presence of anterior crest allometric shape change via correlation tests. It also revealed the continuation of shape maturation after adult size was achieved. Consequently, further study of the non-adult anterior crest is required to determine the influence, if any, of ontogenetic allometry and to explore anterior crest maturation shape change towards the end of non-adult growth.

Bibliography

Adams, D.C., M.L Collyer, and A. Kaliontzopoulou. (2019). Geomorph: Software for geometric morphometric analysis. (R package version 3.1.0) https://cran.r-project.org/package=geomorph

AlQahtani, S. J., Hector, M. P., & Liversidge, H. M. (2010). Brief communication: The London atlas of human tooth development and eruption. *American Journal of Physical Anthropology*, *142*(3), 481–490.

Aniol, P., Carme, R., Jacint, V., Joaquim, B., & Daniel, T. (2014). Ontogeny of the female femur: Geometric morphometric analysis applied on current living individuals of a Spanish population. *Journal of Anatomy*, *3*, 346-357.

Ardren, T., & Coşkunsu, G. (2015). *The archaeology of childhood: Interdisciplinary perspectives on an archaeological enigma*. State University of New York Press.

Bardua, C., Felice, R. N., Watanabe, A., Fabre, A.-C., & Goswami, A. (2019). A practical guide to sliding and surface semilandmarks in morphometric analyses. *Integrative Organismal Biology*, *1*(1), 1-34.

Bastir, M., Nicole Torres-Tamayo, Palancar, C. A., Stephanie Lois-Zlolniski, Daniel García-Martínez, Alberto Riesco-López, Vidal, D., Esther Blanco-Pérez, Barash, A., Nalla, S., Martelli, S., Juan Alberto Sanchis-Gimeno, & Schlager, S. (2019). Geometric morphometric studies in the human spine. *Spinal Evolution: Morphology, Function, and Pathology of the Spine in Hominoid Evolution*, 361–386.

Bateson, P., & Gluckman, P. (2011). *Plasticity, robustness, development and evolution*. Cambridge University Press.

Beauchesne, P., Agarwal, S. C., & Larsen, C. S. (2018). *Children and childhood in bioarchaeology: Bioarchaeological interpretations of the human past: Local, regional, and global perspectives*. University Press of Florida.

Belovich, S. (2005). Fractures in the Carlston Annis shell mound skeletal population. In W. Marquardt & P. Watson (Eds.), *Archaeology of the middle Green River Region, Kentucky* (pp. 505–514). University Press of Florida.

Benjamin, M. (2009). The fascia of the limbs and back--a review. *Journal of Anatomy*, *214*(1), 1–18.

Bertsatos, A., Valakos, E., Chovalopoulou, M.-E., & Papageorgopoulou, C. (2018). Investigating the sex-related geometric variation of the human cranium. *International Journal of Legal Medicine*, *132*(5), 1505–1514.

Bolsterlee, B., Finni, T., D'Souza, A., Eguchi, J., Clarke, E. C., & Herbert, R. D. (2018). Three-dimensional architecture of the whole human soleus muscle in vivo. *PeerJ*, *1-22*.

Bookstein, F. L. (1992). Landmarks. In *Morphometric tools for landmark data: Geometry and biology* (pp. 55–87). Cambridge University Press.

Bookstein, F. L. (1996). Biometrics, biomathematics and the morphometric synthesis. *Bulletin of Mathematical Biology*, *58*(2), 313-365.

Bookstein, F. L. (1997). Landmark methods for forms without landmarks: Morphometrics of group differences in outline shape. *Medical Image Analysis*, *1*(3), 225–243.

Bourn, S., & Lanyon, L. (1979). The influence of mechanical function on the development and remodeling of the tibia: An experimental study in sheep. *The Journal of Bone and Joint Surgery*, *61*, 263–273.

Braga, J., & Treil, J. (2007). Estimation of pediatric skeletal age using geometric morphometrics and three-dimensional cranial size changes. *International Journal of Legal Medicine*, *121*(6), 439-443.

Brzobohatá, H., Krajíček, V., Horák, Z., & Velemínská, J. (2016). Sexual dimorphism of the human tibia through time: Insights into shape variation using a surface-based approach. *PLoS ONE*,*11*(11), 1–21.

Brzobohatá, H., Krajíček, V., Velemínský, P., & Velemínská, J. (2019). Three-dimensional geometry of human tibial anterior curvature in chronologically distinct population samples of Central Europeans (2900 BC – 21st century AD). *Scientific Reports*, *9*(1), 1–10.

Buikstra, J., & Ubelaker, D. (1994). *Standards for data collection from human skeletal remains*. Arkansas Archaeological Survey Research Series 44: Fayetteville.

Buitrago, E., Quintero, I., & Ballesteros, L. (2018). Popliteus muscle. An anatomical study. *International Archives of Medicine*, *11*, 1-6.

Cassidy, C. (1984). Skeletal evidence for prehistoric subsistence adaptation in the central Ohio River Valley. In M. Cohen & G. Armelagos (Eds.), *Paleopathology at the Origins of Agriculture* (pp. 307–346). Academic Press.

Cavaignac, E., Savall, F., Chantalat, E., Faruch, M., Reina, N., Chiron, P., & Telmon, N. (2017). Geometric morphometric analysis reveals age-related differences in the distal femur of Europeans. *Journal of Experimental Orthopaedics*, *1*, 1-8.

Claassen, C. (2010). *Feasting with shellfish in the southern Ohio Valley*. University of Tennessee Press.

Claassen, C. (2019). The beads of Indian Knoll. *Southeastern Archaeology*, *38*(2), 95–112.

Clark, B. (1980). The Lake Site (KkHh-2), Southampton Island, N.W.T. and its position in Sadlermiut prehistory. *Canadian Journal of Archaeology*, *4*, 53-81.

Coltrain, J. B. (2009). Sealing, whaling and caribou revisited: Additional insights from the skeletal isotope chemistry of eastern Arctic foragers. *Journal of Archaeological Science*, *36*(3), 764–775.

Colnot, C., & Alliston, T. (2009). Tissue interactions in long bone development. In F. Bronner, M. Farach-Carson, & H. Roach (Eds.), *Bone and Development* (pp. 25–37). Springer London.

Comer, G. (1910). A geographical description of Southhampton Island and notes upon the Eskimo. *Bulletin of the American Geographical Society*, *42*(2), 84–90.

Cowgill, L. W., Warrener, A., Pontzer, H., & Ocobock, C. (2010). Waddling and toddling: The biomechanical effects of an immature gait. *American Journal of Physical Anthropology*, *143*(1), 52–61.

Cowgill, L. W. (2014). Postcranial growth and development of immature skeletons from Point Hope, Alaska. In B. M. Auerbach, C. E. Hilton, & L. W. Cowgill (Eds.), *The foragers of Point Hope: The biology and archaeology of humans on the edge of the Alaskan Arctic* (pp. 212–232). Cambridge University Press.

Cristofolini, L., Angeli, E., Juszczyk, J. M., & Juszczyk, M. M. (2013). Shape and function of the diaphysis of the human tibia. *Journal of Biomechanics*, *46*(11), 1882–1892.

De Groote, I. (2011). Femoral curvature in Neanderthals and modern humans: A 3D geometric morphometric analysis. *Journal of Human Evolution*, *60*(5), 540–548.

De Laguna, F. (1979). Therkel Mathiassen and the beginnings of Eskimo archaeology. In A. McCartney (Ed.), *Thule Eskimo culture: An anthropological retrospective* (Vol. 88, pp. 10–53). National Museum of Man Archaeological Survey of Canada.

De Laguna, F., & Donald, H. (1947). The prehistory of northern North America as seen from the Yukon. *Memoirs of the Society for American Archaeology*, *3*, iii – 360.

Dewar, G., & Pfeiffer, S. (2004). Postural behaviour of Later Stone Age people in South Africa. *The South African Archaeological Bulletin*, *59*(180), 52–58.

Dryden, I., & Mardia, K. (2016). *Statistical shape analysis: With applications in R* (2nd ed.). Wiley.

Dryden, I. (2019). *Shapes* (R package version 1.2.5). https://CRAN.R-project.org/package=shapes

Dudzik, B. (2019). Landmark and semilandmark data collection using digitizers and data processing. In *3D data acquisition for bioarchaeology, forensic anthropology, and archaeology* (pp. 59–69). Academic Press.

Estévez, E., López-Lázaro, S., López-Morago, C., Alemán, I., & Botella, M. (2017). Sex estimation of infants through geometric morphometric analysis of the ilium. *International Journal of Legal Medicine*, *131*(6), 1747–1756.

Francis, C. (1939). Growth of the human tibia. *American Journal of Physical Anthropology*, *25*, 323–331.

Francis, J. (1961). Sequence of epiphyseal union in a prehistoric Kentucky population from Indian Knoll. *Human Biology*, *33*(1), 66-81.

Frelat, M. A., & Mittereocker, P. (2011). Postnatal ontogeny of tibia and femur form in two human populations: A multivariate morphometric analysis. *American Journal of Human Biology*, *23*(6), 796–804.

Frelat, M., Katina, S., Weber, G. W., & Bookstein, F. L. (2012). Technical note: A novel geometric morphometric approach to the study of long bone shape variation. *American Journal of Physical Anthropology*, *149*(4), 628–638.

Galletta, L., Stephens, N. B., Bardo, A., Kivell, T. L., & Marchi, D. (2019). Three-dimensional geometric morphometric analysis of the first metacarpal distal articular surface in humans, great apes and fossil hominins. *Journal of Human Evolution*, *132*, 119–136.

Gindhart, P. S. (1973). Growth standards for the tibia and radius in children aged one month through eighteen years. *American Journal of Physical Anthropology*, *39*(1), 41–48.

Gollin, E. S. (1981). *Developmental plasticity: Behavioural and biological aspects of variation in development*. Academic Press.

Gomez-Robles, A., Martinon-Torres, M., de Castro, B., J., M., Margvelashvili, A., Bastir, M., Arsuaga, J. L., Perez-Perez, A., Estebaranz, F., & Martinez, L. M. (2007). A geometric morphometric analysis of hominin upper first molar shape. *Journal of Human Evolution*, *3*, 272-285.

Greska, L. P. (1996). Evidence for a genetic basis to the enhanced total lung capacity of Andean highlanders. *Human Biology*, *68*(1), 119–129.

Gunz, P., Mitteroecker, P., & Bookstein, F. (2005). Semilandmarks in three dimensions. In D. Slice (Ed.), *Modern morphometrics in physical anthropology* (pp. 73–98). Springer US.

Gunz, P., & Mitteroecker, P. (2013). Semilandmarks: A method for quantifying curves and surfaces. *Hystrix, the Italian Journal of Mammalogy*, *24*(1), 103–109.

Hadjidakis, D. J., & Androulakis, I. I. (2006). Bone remodeling. *Annals of the New York Academy of Sciences*, *1092*(1), 385–396.

Harrington, L. (2010). *Ontogeny of postcranial robusticity among holocene hunter-gatherers of southernmost Africa* (S. Pfeiffer (ed.)) [PhD]. University of Toronto.

Hellier, C. A., & Jeffery, N. (2006). Morphological plasticity in the juvenile talus. *Foot and Ankle Surgery: Official Journal of the European Society of Foot and Ankle Surgeons*, *3*, 139-147.

Higgins, R. (2014). The effects of terrain on long bone robusticity and cross-sectional shape in lower limb bones of bovids, Neandertals, upper paleolithic modern humans. In K. Carlson & D. Marchi (Eds.), *Mobility: Interpreting behavior from skeletal adaptations and environmental interactions.* (pp. 227–252). Springer.

Hilton, C. E., Auerbach, B. M., & Cowgill, L. W. (2014). Humans on the edge of the Alaskan Arctic. In B. M. Auerbach, C. E. Hilton, & L. W. Cowgill (Eds.), *The foragers of Point Hope: The biology and archaeology of humans on the edge of the Alaskan Arctic* (pp. 1–8). Cambridge University Press.

Holt, B., Whittey, E., Niskanen, M., Sládek, V., Berner, M., & Ruff, C. (2018). Temporal and geographic variation in robusticity. In C. Ruff (Ed.), *Skeletal variation and adaptation in Europeans: Upper paleolithic to the twentieth century* (pp. 91–132). John Wiley & Sons, Inc.

Hu, J., Xin, H., Chen, Z., Zhang, Q., Peng, Y., & Jin, Z. (2019). The role of menisci in knee contact mechanics and secondary kinematics during human walking. *Clinical Biomechanics*, *61*, 58–63.

Jeffrey James, L., Peter, C., & Vivienne, H. (2017). Sexual dimorphism of the first rib: A comparative approach using metric and geometric morphometric analyses. *Journal of Forensic Sciences*, *5*, 1251-1258.

Jennings, J. (1974). *Prehistory of North America*. McGraw-Hill.

Justice, L. C., & Temple, D. H. (2019). Bioarchaeological evidence for social maturation in the mortuary ritual of Ipiutak and Tigara hunter-gatherers: Lifespan perspectives on the emergence of personhood at Point Hope, Alaska. *American Antiquity*, *84*(2), 234–251.

Kanabur, V. (2012). Identification of the sex of human hip bone by metric analysis of its anterior border. *Biomedical Research*, *23*(2), 211–214.

Kelly, P. M., & Diméglio, A. (2008). Lower-limb growth: How predictable are predictions? *Journal of Children's Orthopaedics: Official Journal of the European Paediatric Orthopaedic Society (EPOS)*, *2*(6), 407-415.

Kersh, M. E., Ploeg, H.-L., & Pandy, M. G. (2015). The dependence of knee joint stability on the cruciate and collateral ligaments. *Movement & Sport Sciences*, *90*, 37–54.

Klingenberg, C. P. (2020). Walking on Kendall's shape space: Understanding shape spaces and their coordinate systems. *Evolutionary Biology*, *47*(4), 334-352.

Klingenberg, C. P. (2016). Size, shape, and form: Concepts of allometry in geometric morphometrics. *Development Genes and Evolution*, *226*(3), 113–137.

Klingenberg, C. P. (2013). Visualizations in geometric morphometrics: How to read and how to make graphs showing shape changes. *Hystrix, the Italian Journal of Mammalogy*, *24*(1), 15–24.

Klingenberg Christian Peter, & Marugán-Lobón Jesús. (2013). Evolutionary covariation in geometric morphometric data: Analyzing integration, modularity, and allometry in a phylogenetic context. *Systematic Biology*, *62*(4), 591–610.

Kuzminsky, S. C., Tung, T. A., Hubbe, M., & Villaseñor-Marchal, A. (2016). The application of 3D geometric morphometrics and laser surface scanning to investigate the standardization of cranial vault modification in the Andes. *Journal of Archaeological Science: Reports*, *10*, 507–513.

Lanyon, L. (1980). The influence of function on the development of bone curvature. An experimental study on the rat tibia. *Journal of Zoology*, *192*, 457–466.

Lee, R. (1979). *The !Kung San: Men, women and work in a foraging society*. Cambridge University Press.

Lieberman, D. (2002). Neandertal and early modern human mobility patterns. In T. Akazawa, K. Aoki, & O. Bar-Yosef (Eds.), *Neandertals and modern humans in western Asia* (pp. 263–275). Springer.

Lisee, C., Slater, L., Hertel, J., & Hart, J. M. (2019). Effect of sex and level of activity on lower-extremity strength, functional performance, and limb symmetry. *Journal of Sport Rehabilitation*, *28*(5), 413–420.

Loy, A., Cataudella, S., & Corti, M. (1996). Shape changes during the growth of the Sea Bass, Dicentrarchus labrax (Teleostea: Perciformes), in relation to different rearing conditions.

In L. Marcus, M. Corti, A. Loy, G. Naylor, & D. Slice (Eds.), *Advances in morphometrics* (pp. 399–405). Plenum.

Lynch, J., Cross, P., & Heaton, V. (2017). Sexual dimorphism of the first rib: A comparative approach using metric and geometric morphometric analyses. *Journal of Forensic Sciences*, *62*(5), 1251–1258.

Lyon, G. (2014). *A brief narrative of an unsuccessful attempt to reach Repulse Bay*. Cambridge University Press.

Macintosh, A., Davies, G., Stock, T., & Pinhasi, R. (2015). Declining tibial curvature parallels ∼6150 years of decreasing mobility in central european agriculturalists. *American Journal of Physical Anthropology*, *157*(2), 260–275.

Marean, C. W., Cawthra, H. C., Cowling, R. M., Esler, K. J., Fisher, E., Milewski, A., Potts, A. J., Singels, E., & Vynck, J. D. (2014). Stone age people in a changing South African Greater Cape Floristic Region. In N. Allsopp, J. Colville, & A. Verboom (Eds.), *Fynbos: Ecology, Evolution, and Conservation of a Megadiverse Region* (pp. 164–199). Oxford University Press.

Marchi, D. (2007). Relative strength of the tibia and fibula and locomotor behavior in hominoids. *Journal of Human Evolution*, *53*(6), 647–655.

Martín-Serra, A., Figueirido, B., & Palmqvist, P. (2014). A three-dimensional analysis of morphological evolution and locomotor performance of the carnivoran forelimb. *PloS One*, *9*(1), 1–20.

Mathiassen, T. (1927). *Archaeology of the central Eskimos: The Thule culture and its position within the Eskimo culture. Report of the Fifth Thule Expedition 1921-24*. Gyldendalske Boghandel, Copenhagen.

Mays, S., Ives, R., & Brickley, M. (2009). The effects of socioeconomic status on endochondral and appositional bone growth, and acquisition of cortical bone in children from 19th century Birmingham, England. *American Journal of Physical Anthropology*, *140*(3), 410–416.

Meissner, M. H., Moneta, G., Burnand, K., Gloviczki, P., Lohr, J. M., Lurie, F., Mattos, M. A., McLafferty, R. B., Mozes, G., Rutherford, R. B., Padberg, F., & Sumner, D. S. (2007). The hemodynamics and diagnosis of venous disease. *Journal of Vascular Surgery*, *46*(6), 4–24.

Meloni, M. (2019). *Impressionable biologies: From the archaeology of plasticity to the sociology of epigenetics*. Routledge.

Merbs, C. (2018). The discovery and rapid demise of the Sadlermiut. In D. Temple & C. Stojanowski (Eds.), *Hunter-gatherer adaptation and resilience: A bioarchaeological perspective* (pp. 302–327). Cambridge University Press.

Mitteroecker, P., & Gunz, P. (2009). Advances in geometric morphometrics. *Evolutionary Biology*, *36*(2), 235–247.

Mitteroecker, P., Gunz, P., Windhager, S., & Schaefer, K. (2013). A brief review of shape, form, and allometry in geometric morphometrics, with applications to human facial morphology. *Hystrix*, *24*(1), 59–66.

Moorrees, C., Fanning, E., & Hunt. (1963). Age variation of formation stages for ten permanent teeth. *Journal of Dental Research*, *42*, 1490–1502.

Moorrees, C., Fanning, E., & Hunt, E. (1963). Formation and resorption of three deciduous teeth in children. *American Journal of Physical Anthropology*, *21*(2), 205–213.

Murphy, E. M., & Le Roy, M. (2017). *Children, death and burial: Archaeological discourses*. Oxbow Books.

Navarro-Romero, M. T., Muñoz, M. de L., Alcala-Castañeda, E., Terreros-Espinosa, E., Domínguez-de-la-Cruz, E., García-Hernández, N., & Moreno-Galeana, M. Á. (2020). A novel method of male sex identification of human ancient skeletal remains. *Chromosome Research: Chromatin, Chromosomes and Genomes*, *28*(3), 277

Nealis, S., & Seeman, M. (2015). Dental attrition at the Indian Knoll (15oh2) and Black Earth (11sa87) sites: Extreme wear as a stressor in late archaic populations of the Ohio Valley. *Southeastern Archaeology*, *34*(1), 57–70.

Neumann, G. (1952). Archaeology and race in the American Indian. In J. Griffin (Ed.), *Archeology of the Eastern United States* (pp. 13–34). University of Chicago Press.

Noble, J., Cardini, A., Flavel, A., & Franklin, D. (2019). Geometric morphometrics on juvenile crania: Exploring age and sex variation in an Australian population. *Forensic Science International*, *294*, 57–68.

Oettle, A. C., Pretorius, E., & Steyn, M. (2005). Geometric morphometric analysis of mandibular ramus flexure. *American Journal of Physical Anthropology*, *3*, 623–629.

Optical Measuring Techniques GOM. (2019). GOM Inspect.

Osipov, B., Harrington, L., Cowgill, L., Temple, D., Bazaliiskii, V. I., & Weber, A. W. (2017). Regional variation and sexual dimorphism in the ontogeny of humeral asymmetry among prehistoric hunter-gatherers. *American Journal of Physical Anthropology*, *162*, 306–306.

Pandey, N., Bhola, S., Goldstone, A., Chen, F., Chrzanowski, J., Terranova, C. J., Ghillani, R., & Jepsen, K. J. (2009). Interindividual variation in functionally adapted trait sets is established during postnatal growth and predictable based on bone robustness. *Journal of Bone and Mineral Research, 24*(12), 1969-1980.

Pfeiffer, S. (2007). The health of foragers: People of the Later Stone Age, southern Africa. In M. Cohen & G. Crane-Kramer (Eds.), *Ancient health: Skeletal indicators of agricultural and economic intensification* (pp. 223–236). University Press of Florida.

Pfeiffer, S., & Harrington, L. (2011). Bioarchaeological evidence for the basis of small adult stature in southern Africa: Growth, mortality, and small stature. *Current Anthropology*, *52*(3), 449–461.

Pfeiffer, S., & Harrington, L. (2018). Regional continuity and local challenges to resilience among holocene hunter-gatherers of the Greater Cape Floristic Region, South Africa. In C. M. Stojanowski & D. H. Temple (Eds.), *Hunter-gatherer adaptation and resilience: A bioarchaeological perspective* (pp. 26–46). Cambridge University Press.

Powell, M. (1996). Health and disease in the Green River archaic. In K. Carstens & P. Watson (Eds.), *Of caves and shell mounds* (pp. 119–131). University of Alabama Press.

R Core Team. (2018). *R* (Version 3.5.0) [Computer software].

Rainey, F. (1941). The Ipiutak culture at Point Hope, Alaska. *American Anthropologist*, *43*(3), 364–375.

Rantalainen, T., Weeks, B. K., Nogueira, R. C., & Beck, B. R. (2015). Effects of bone-specific physical activity, gender and maturity on tibial cross-sectional bone material distribution: A cross-sectional pQCT comparison of children and young adults aged 5–29 years. In *Bone*, 72, 101–108.

Rantalainen, T., Weeks, B. K., Nogueira, R. C., & Beck, B. R. (2016). Long bone robustness during growth: A cross-sectional pQCT examination of children and young adults aged 5–29 years. *Bone*, *93*, 71–78.

Rein, T. R., & Harvati, K. (2014). Geometric morphometrics and virtual anthropology: Advances in human evolutionary studies. *Anthropologischer Anzeiger; Bericht Uber Die Biologisch-Anthropologische Literatur*, *71*(1), 41-55.

Rosas, A., & Bastir, M. (2002). Thin-plate spline analysis of allometry and sexual dimorphism in the human craniofacial complex. *American Journal of Physical Anthropology*, *117*(3), 236–245.

Roseman, C., & Auerbach, B. (2015). Ecogeography, genetics, and the evolution of human body form. *Journal of Human Evolution*, *78*, 80–90.

Rothschild, A. (1979). Mortuary behavior and social organization at Indian Knoll and Dickson mounds. *American Antiquity*, *44*(4), 658-675.

RStudio Team (2016). RStudio: Integrated development for R Studio, Inc., Boston, MA. http://www.rstudio.com/

Ruff, C. (1980). Age differences in craniofacial dimensions among adults from Indian Knoll, Kentucky. *American Journal of Physical Anthropology*, *53*, 101–108.

Ruff, C. B., & Hayes, W. C. (1982). Subperiosteal expansion and cortical remodeling of the human femur and tibia with aging. *Science*, *217*(4563), 945–948.

Ruff, C., & Hayes, W. (1983). Cross-sectional geometry of Pecos Pueblo femora and tibiae--a biomechanical investigation: II. sex, age, and side differences. *American Journal of Physical Anthropology*, *60*, 383–400.

Ruff, C. (1987). Sexual dimorphism in human lower limb bone structure: Relationship to subsistence strategy and sexual division of labor. *Journal of Human Evolution*, *16*(5), 391–416.

Ruff, C. B., & Hayes, W. C. (1988). Sex differences in age-related remodeling of the femur and tibia. *Journal of Orthopaedic Research: Official Publication of the Orthopaedic Research Society*, *6*(6), 886–896.

Ruff, C. (2003). Long bone articular and diaphyseal structure in old world monkeys and apes. *American Journal of Physical Anthropology*, *120*(1), 16–37.

Ruff, C. B., Holt, B. M., Sladek, V., Berner, M., Murphy, W. A., Zur Nedden, D., Seidler, H., & Recheis, W. (2006). Body size, body proportions, and mobility in the Tyrolean Iceman. *Journal of Human Evolution*, *51*(1), 91–101.

Ruff, C. (2018). Biomechanical analyses of archaeological human skeletons. In A. Katzenberg & A. Grauer (Eds.), *Biological anthropology of the human skeleton* (pp. 189–224). John Wiley & Sons, Inc.

Ryan, K., & Young, J. (2013). Identification of a probable Aarnguaq in a Sadlermiut grave from Native Point, Southampton Island, Nunavut, Canada. *Arctic Anthropology*, *50*(1), 20–48.

Scheuer, L., & Black, S. (2004). *The juvenile skeleton*. Academic Press.

Scholtz, Y., Steyn, M., & Pretorius, E. (2010). A geometric morphometric study into the sexual dimorphism of the human scapula. *Homo: Internationale Zeitschrift Fur Die Vergleichende Forschung Am Menschen*, *61*(4), 253–270.

Schuh, A., Kupczik, K., Gunz, P., Hublin, J., & Freidline, S. E. (2019). Ontogeny of the human maxilla: A study of intra-population variability combining surface bone histology and geometric morphometrics. *Journal of Anatomy*, *235*(2), 233–245.

Shackelford, L. (2014). Bone strength and subsistence activities at Point Hope. In C. Hilton, B. Auerbach, & L. Cowgill (Eds.), *The foragers of Point Hope: The biology and archaeology of humans on the edge of the Alaskan Arctic* (pp. 181–211). Cambridge University Press.

Sládek, V., Berner, M., & Sailer, R. (2006). Mobility in Central European Late Eneolithic and Early Bronze Age: Tibial cross-sectional geometry. *Journal of Archaeological Science*, *33*(4), 470–482.

Small, C., Brits, D., & Hemingway, J. (2016). Assessing the effects of tooth loss in adult crania using geometric morphometrics. *International Journal of Legal Medicine*, *130*(1), 233–243.

Smith, B. (1991). Standards of human tooth formation and dental age assessment. In M. Kelley & C. Larsen (Eds.), *Advances in Dental Anthropology* (pp. 143–168). New-York: Wiley-Liss Inc.

Smith, M. Z., Goettsch, B. M., Van Ramshorst, R. D., O'Brien, J. A., Jaque, S. V., & Sumida, K. D. (2008). Resistance training and bone mineral density during growth. *International Journal of Sports Medicine*, *29*(4), 316–321.

Sommer, M., & Sommer, D. (2017). Archaeology and developmental psychology: A brief survey of ancient Athenian toys. *American Journal of Play*, *9*(3), 341–355.

Sonoda, K. (2016). Constructing social learning in interaction among the Baka hunter-gatherers. In *Social learning and innovation in contemporary hunter-gatherers: Evolutionary and ethnographic perspectives* (p. 113). Springer Japan.

Sorensen, V., & Leonard, R. (2001). Neandertal energetics and foraging efficiency. *Journal of Human Evolution*, *40*(6), 483–495.

Sorrentino, R., Maria, G. B., Figus, C., Nicholas, B. S., Turley, K., William Harcourt-Smith, Timothy, M. R., & Benazzi, S. (2020). Exploring sexual dimorphism of the modern human talus through geometric morphometric methods. *PloS One*, *15*(2), 1-17.

Staheli, L., & Engel, G. (1972). Tibial torsion: A method of assessment and a survey of normal children. *Clinical Orthopaedics and Related Research*, *86*, 183–186.

Stavit, S. (2007). A syndrome characterized by intra-uterine lower limb dislocation, gracile bones, clubfeet, and other skeletal features. *American Journal 0f Medical Genetics, 143*(4), 395-398.

Stock, J., & Pfeiffer, S. (2001). Linking structural variability in long bone diaphyses to habitual behaviors: Foragers from the southern African Later Stone Age and the Andaman Islands. *American Journal of Physical Anthropology*, *115*(4), 337–348.

Stock, J. (2006). Hunter-gatherer postcranial robusticity relative to patterns of mobility, climatic adaptation, and selection for tissue economy. *American Journal of Physical Anthropology*, *131*(2), 194–204.

Tian, M., Herbert, R. D., Hoang, P., Gandevia, S. C., & Bilston, L. E. (2012). Myofascial force transmission between the human soleus and gastrocnemius muscles during passive knee motion. *Journal of Applied Physiology*, *113*(2), 517–523.

Trinkaus, E. (1975). Squatting among the neandertals: A problem in the behavioral interpretation of skeletal morphology. *Journal of Archaeological Science*, *2*(4), 327–351.

Trinkaus, E. (1993). Femoral neck-shaft angles of the Qafzeh-Skhul early modern humans, and activity levels among immature Near Eastern Middle Paleolithic hominids. *Journal of Human Evolution*, *25*(5), 393–416.

Turner, M. S., & Smillie, I. S. (1981). The effect of tibial torsion of the pathology of the knee. *The Journal of Bone and Joint Surgery. British Volume*, *63-B*(3), 396–398.

Ubelaker, D. (1978). *Human skeletal remains: Excavation, analysis, interpretation*. Chicago: Aldine Publishing Company.

Vieira, T. M. M., Minetto, M. A., Hodson-Tole, E., & Botter, A. (2013). How much does the human medial gastrocnemius muscle contribute to ankle torques outside the sagittal plane? *Human Movement Science*, *32*(4), 753–767.

Ward, S. (2005). Dental biology of the Carlston Annis shell mound population. In W. Marquardt & P. Watson (Eds.), *Archaeology of the Middle Green River Region, Kentucky* (pp. 515–628). University of Kentucky.

Webb, W. (1946). *Indian Knoll, site Oh 2, Ohio County, Kentucky: Vol. 4, no. 3, pt. 1*. Dept. of Anthropology, University of Kentucky.

Webster, M., & Sheets, H. D. (2010). A practical introduction to landmark-based geometric morphometrics. In J. A. G. Hunt (Ed.), *Quantitative methods in paleobiology: Vol. 16* (pp. 163–188). The Paleontology Society.

Weinstein, K. J. (2017). Morphological signatures of high-altitude adaptations in the Andean archaeological record: Distinguishing developmental plasticity and natural selection. *Quaternary International*, *461*, 14–24.

West-Eberhard, M. J. (2005). Developmental plasticity and the origin of species differences. *Proceedings of the National Academy of Sciences of the United States of America*, *102*, 6543–6549.

Wickham, H. (2016). *ggplot2: Elegant graphics for data analysis*. Springer-Verlag New York.

Wilson, L. A., MacLeod, N., & Humphrey, L. T. (2008). Morphometric criteria for sexing juvenile human skeletons using the ilium. *Journal of Forensic Sciences*, *53*(2), 269–278.

Wilson, L. A. B., & Humphrey, L. T. (2015). A virtual geometric morphometric approach to the quantification of long bone bilateral asymmetry and cross-sectional shape. *American Journal of Physical Anthropology*, *158*(4), 541–556.

Wilson, L. A. B., Ives, R., Cardoso, H. F. V., & Humphrey, L. T. (2015). Shape, size, and maturity trajectories of the human ilium. *American Journal of Physical Anthropology*, *156*(1), 19–34

Wilson, L. A. B., & Humphrey, L. T. (2017). Voyaging into the third dimension: A perspective on virtual methods and their application to studies of juvenile sex estimation and the ontogeny of sexual dimorphism. *Forensic Science International*, *278*, 32–46.

Wilson, L. A. B., Ives, R., & Humphrey, L. T. (2017). Quantification of 3D curvature in the iliac crest: Ontogeny and implications for sex determination in juveniles. *American Journal of Physical Anthropology*, *162*(2), 255–266.

Winters, H. (1974). *Indian Knoll*. University of Tennessee Press.

Wolff, J. (1986). *The law of bone remodelling*. Springer Berlin Heidelberg.

Woodburn, J. (1982). Social dimensions of death in four African hunting and gathering societies. In J. Parry & M. Bloch (Eds.), *Death and the regeneration of life* (pp. 187–210). Cambridge University Press.

Yang, P., Sanno, M., Ganse, B., Koy, T., Brüggemann G., Müller, L., & Rittweger, J. (2014). Torsion and antero-posterior bending in the in vivo human tibia loading regimes during walking and running. *PloS One*, *9*(4), 1-13.

Zelditch, M., Swiderski, D. L., & Sheets, H. D. (2012). *Geometric morphometrics for biologists: A primer* (2nd ed.). Elsevier Academic Press.

Zhang, S., Huang, W., Zeng, Y., Shi, W., Diao, X., Wei, X., & Ling, S. (2018). Gear shifting of quadriceps during isometric knee extension disclosed using ultrasonography. *BioMed Research International*, *2018*, 1–7.

3D Systems Inc. (2019). Geomagic Design X.

Appendix A: Tibia Alignment Protocol

Regardless of the model side, Geomagic Design X did not automatically align the fused XRL models in proper anatomical alignment. Following the steps outlined by Dr. Alison Murray's Rapidform Protocol, anatomical alignment was achieved manually using the "Interactive Alignment" function (3D Systems Inc. 2019). "Interactive Alignment" allowed the model to be adjusted by manipulating the orientation of the model (3D Systems Inc. 2019). This alignment was refined by redefining the coronal and sagittal planes of the model.

Geomagic Design X automatically generated two planes that divided the tibiae into separate surfaces: Front (for later A-P alignment) and Right (for later M-L alignment) (3D Systems Inc. 2019). These two planes allowed for the model to be seen in one of six random viewpoints by pressing the ALT key in conjunction with numbers 1 to 6 (3D Systems Inc. 2019). These viewpoints, through refinement, would be readjusted to the anterior, posterior, medial, lateral, proximal and distal orientations of the model.

To ensure proper anterior-posterior alignment, a new coronal (front) plane was created in proximal view using the "Ref. Plane" function and titled Coronal Plane 1 (3D Systems Inc. 2019). A new plane could then be drawn between the two proximal tibial plateau condylar surfaces (3D Systems Inc. 2019). The method used to draw the new plane was set to "Draw Line" (3D Systems Inc. 2019). The old Front plane was replaced with Coronal Plane 1 using the "Datum Match" function (3D Systems Inc. 2019). The front plane was then deleted. To further refine the coronal plane, the function "Ref. Vector" was used to add a reference vector via method of "Pick Multiple Points" (3D Systems Inc. 2019). Two points were placed on the model

to ensure the entire length of the model adhered to the A-P coronal plane. The first point was placed directly between the proximal condylar surfaces along Coronal Plane 1; the second point was placed on the distal surface of the model as close to the midpoint as possible (3D Systems Inc. 2019). These two points generated a dotted reference line (vector) down the entire length of the model. Orientating the model medially, a new plane titled Coronal Plane 2 was traced using "Ref. Plane" along the dotted reference vector (3D Systems Inc. 2019). The function "Datum Match" was again used to replace Coronal Plane 1 with the refined A-P alignment of Coronal Plane 2 (3D Systems Inc. 2019). This process was repeated as needed to ensure full A-P alignment.

With A-P alignment complete, a new plane was required to ensure proper sagittal medial-lateral alignment (M-L). A new reference vector was created using "Ref. Vector" (3D Systems Inc. 2019). The same steps described for A-P alignment were followed for M-L alignment. A single point was placed on the proximal surface and distal surface along Coronal Plane 2 as close to the sagittal midline as possible distally (3D Systems Inc. 2019). With a reference vector created, the model was rotated into anterior view. A new plane was then drawn over the dotted reference vector and titled "Sagittal Plane 1" (3D Systems Inc. 2019). The automatically created Right plane was replaced with Sagittal Plane 1 using "Datum Match" and was deleted (3D Systems Inc. 2019). In anterior view, the newly-drawn plane divided the model into a medial half and a lateral half. Just as with A-P alignment, the steps for M-L alignment were repeated as necessary to refine the M-L orientation. Using the ALT key combined with numbers 1-6, the model could then be rotated into the desired correct

anatomical viewpoint. Correct anatomical alignment is required for the models to be measured in GOM Inspect (Optical Measuring Techniques GOM, Germany, 2019).

Once the anterior-posterior coronal plane and medial-lateral sagittal plane were created, the model was exported as an anatomically aligned PLY file using the “Export” function (3D Systems Inc. 2019).

Appendix B: R Code

This appendix details the R code used for this thesis' analyses. Annotations are provided above the applicable section and provide an overview of what is occurring in the code. These annotations are marked with the '#' symbol. All code is in blue and marked with the '>' symbol. Code A1 contains *italicized* words, names and R objects that would vary in name/identifier from person by person.

Below is the working directory and packages required for analysis.

```
> setwd("~/Desktop/Tibiae/R Code")
> library("geomorph")
> library("ggplot2")
> library("shapes")
```

 # Code A1. This is the measurement error test code. The function summary() was used to display the MS values of procD.lm(). These values were used in the MS equations detailed in Zelditch et al. (2012). A measurement error test was conducted for both the non-adult and adult samples. The non-adult test is detailed below as an example.

```
> data <- read.csv("Error Test Subadult.csv",
            header = T,  sep = ",")
> dat.mat <- as.matrix(data[3:38])
> indiv <- as.factor(data[,1])
> dat.array <- arrayspecs(dat.mat, 12, 3)
> GPA <- gpagen(dat.array, PrinAxes = F, print.progress = T)
> mod <- summary(procD.lm(GPA$coords ~ indiv))
> summary(mod)
```

 # Code B1. This is the code to read the non-adult sample csv file. This was then converted into a data frame and then a data matrix. Column names and row names were retained from the csv file.

```
> SubadultData <- read.csv("~/Desktop/MA /SubadultsOnly.csv", header = T, row.names = 1,
sep = ",")
> SubadultData.mat <- as.matrix(SubadultData[5:40])
```

A 3D array was constructed for GPA using the arrayspecs() function. '12' represents the total number of landmarks in this analysis, and '3' represents the number of array dimensions.

```
> SubadultData.array <- arrayspecs(SubadultData.mat, 12, 3)
```

This code is for Generalized Procrustes Analysis and Principal Component Analysis.

```
> GPA_SubadultData <- gpagen(SubadultData.array, PrinAxes = T, max.iter = NULL, ProcD = T, Proj = T, print.progress = T)
> pca.SubadultData <- plotTangentSpace(GPA_SubadultData$coords, warpgrids = T, label = T)
```

The first two PCs for the non-adult sample were extracted for later use in the PC scatter plots.

```
> pca.SubadultData$pc.summary
> pca.CMB.frame <- as.data.frame(pca.SubadultData$pc.scores[,1:2])
> PC1 <- pca.CMB.frame$PC1
> PC2 <- pca.CMB.frame$PC2
```

This code set up the variables that were used in the PC scatter plot. Each non-adult was given a unique symbol and color depending on the population.

```
> pop.facs <- factor(c("Native Point", "Later Stone Age", "Indian Knoll", "Point Hope"))
> CMB.color <-
as.factor(c(15,15,15,15,15,15,15,15,15,17,17,17,17,17,17,17,17,17,17,17,17,18,18,18,18,18,18,
18,18,18,18,16,16,16,16,16,16,16,16,16,16))
> allData.shape <-
as.factor(c(1,1,1,1,1,2,2,2,2,1,1,1,1,1,2,2,2,2,2,2,1,1,1,1,1,2,2,2,2,2,1,1,1,1,2,2,2,2,2,2))
> pops <- pop.facs[CMB.color]
> Populations.s <- factor(pops, levels = c("Native Point", "Later Stone Age","Indian Knoll", "Point Hope"))
```

This code constructed the non-adult PC scatter plot. PC1 was bound to the x-axis, and PC2 was bound to the y-axis. Each population's unique shape was coded using geom_point(). Each individual's population color was coded using scale_color_manual(). The plot's title was created using ggtitle(), and theme() altered its position. labs() created a subtitle and subheadings for the x and y axes. scale_shape_manual() designated the legend names, shape and color of each population in the legend.

```
> ggp.CMB <- ggplot(pca.CMB.frame, aes(x = PC1, y = PC2)) + geom_point(aes(shape =
Populations.s , col = Populations.s), size = 3)  + scale_color_manual(values = c("Blue", "Red",
"Orange", "green")) + ggtitle("Principal Component Analysis of Non-Adult Sample") +
theme(plot.title = element_text (hjust = 0.5)) + labs(subtitle = "PC1 Vs PC2 (cumulative
proportion of shape variance = 61.6%)", x = "PC1 (43.6%)", y = "PC2 (18%)") +
scale_shape_manual(values = c(15,4,17,5), labels = c("Native Point", "Later Stone Age","Indian
Knoll", "Point Hope"))
```

This code created the scatter plot legend.

```
> ggp.CMB + guides(col = guide_legend(title = "Population")) + labs(shape = "Population")
```

This code extracted the minima and maxima shape extremes of PC1 and PC2 in the non-adult sample.

```
> sub.PC1.min <- pca.SubadultData$pc.shapes$PC1min
> sub.PC1.max <- pca.SubadultData$pc.shapes$PC1max
> sub.PC2.min <- pca.SubadultData$pc.shapes$PC2min
> sub.PC2.max <- pca.SubadultData$pc.shapes$PC2max
```

The code allowed for the visual comparison of the minima and maxima shape extremes of PC1 and PC2.

```
> plotRefToTarget(sub.PC1.min, sub.PC1.max, method = "points", mag = 2, label = T, axes = T)
> plotRefToTarget(sub.PC2.min, sub.PC2.max, method = "points", mag = 2, label = T, axes = T)
```

 # Code B2. The code used for the adult sample was largely the same as that of the non-adult sample. However, imaging of minima and maxima PC shape extremes was not required.

```
> comb.Adults <- read.csv("~/Desktop/MA/comb.Adults.csv", header = T,row.names = 1, sep = ",")
> comb.Adults.mat <- as.matrix(comb.Adults[5:40])
> comb.Adults.array <- arrayspecs(comb.Adults.mat, 12, 3)
> GPA_combAdults  <- gpagen(comb.Adults.array , PrinAxes = T, max.iter = NULL, ProcD = T, Proj = T, print.progress = T)
> pca.Adults <- plotTangentSpace(GPA_combAdults$coords, warpgrids = T, label = T)

> pca.Adults.frame <- as.data.frame(pca.Adults$pc.scores[,1:2])
> PC1 <- pca.Adults.frame$PC1
> PC2 <- pca.Adults.frame$PC2
> pca.Adults$pc.summary

> CMB.Acolor <- as.factor(c(15,18,16,15,15,16,16,15,17,18,16,16,15,15,17,17,18,18,15,15,17,17,18,18))
> pop.fac <- factor(c("Native Point", "Later Stone Age","Indian Knoll", "Point Hope"))
> pop <- pop.fac[CMB.Acolor]
> Populations <- factor(pop, levels = c("Native Point", "Later Stone Age","Indian Knoll", "Point Hope"))
```

```
> ggp.CMBA <- ggplot(pca.Adults.frame, aes(x = PC1, y = PC2)) + geom_point(aes(shape =
Populations , col = Populations), size = 3)  + scale_color_manual(values = c("Blue", "Red",
"Orange", "green")) + ggtitle("Principal Component Analysis of Adult Sample") +
theme(plot.title = element_text (hjust = 0.5)) + labs(subtitle = "PC1 Vs PC2 (cumulative
proportion of shape variance = 63.2%)", x = "PC1 (37.7%)", y = "PC2 (25.5%)") +
scale_shape_manual(values = c(15,4,17,5), labels = c("Native Point", "Later Stone Age","Indian
Knoll", "Point Hope"))
```

 # Code B3. The code used for the adults by sex sample. This code was largely the same as that of the non-adult and adult samples. However, a two-tiered legend for sex and population was added to this sample's PC scatter plot. Instead of color-coding by population, this sample's PC scatter plot color-coded by sex. Also, the non-adult code for minima and maxima PC shape change code was not required.

```
> AdultsBySex <- read.csv("~/Desktop/MA /AdultsBySex.csv", header = T,row.names = 1, sep =
",")
> Asex.mat <- as.matrix(AdultsBySex[5:40])
> Asex.array <- arrayspecs(Asex.mat, 12, 3)
> GPA_Asex <- gpagen(Asex.array , PrinAxes = T, max.iter = NULL,
                     ProcD = T, Proj = T, print.progress = T)
> pca.Asex <- plotTangentSpace(GPA_Asex$coords, warpgrids = T, label = T)

> pca.A.frame <- as.data.frame(pca.Asex$pc.scores[,1:2])
> PC1 <- pca.A.frame$PC1
> PC2 <- pca.A.frame$PC2
> pca.Asex$pc.summary

> sex.fac <- factor(c("Male", "Female"))
> sex.color <- as.factor(c(1,2,1,2,1,2,1,2,1,2,1,2,1,2))
> A.shape <- as.factor(c(15,15,15,15,17,17,17,17,18,18,18,18,16,16))
> sex.fac <- factor(c("Male", "Female"))
> Sex <- sex.fac[sex.color]
> s <- factor(Sex, levels = c("Male", "Female"))

> ggp.CMBS <- ggplot(pca.A.frame, aes(x = PC1, y = PC2)) + geom_point(aes(shape = A.shape,
col = s), size = 3)  + scale_color_manual(values = c("Blue", "Green")) + ggtitle("Principal
Component Analysis of Combined Adults of Identified Sex") + theme(plot.title = element_text
(hjust = 0.5)) + labs(subtitle = "PC1 Vs PC2 (cumulative proportion of shape variance = 59.5%)",
```

```
x = "PC1 (40%)", y = "PC2 (19.5%)") + scale_shape_manual(values = c(15,4,17,5), labels =
c("Native Point", "Later Stone Age","Indian Knoll", "Point Hope"))

> ggp.CMBS + guides(col = guide_legend(title = "Sex")) + labs(shape = "Population")
```

 # Code C1. The code used for the non-adult sample's Pearson correlation tests is detailed below. As age and size were variables of interest in this thesis, the dental ages of the non-adult sample were extracted from the parent data frame. Age was compared with shape change, represented by PC score, to see if the two variables correlated. A confidence level of 95% was input for these tests. (NOTE: Requires Code B1)

```
> SubadultAge <- c(SubadultData$Dental.Age)
> cor.test(SubadultAge, pca.SubadultData$pc.scores[,1], method = "pearson", conf.level = 0.95)
> cor.test(SubadultAge, pca.SubadultData$pc.scores[,2], method = "pearson", conf.level = 0.95)
> cor.test(SubadultAge, pca.SubadultData$pc.scores[,3], method = "pearson", conf.level = 0.95)

# The code below was used to determine if size, represented by Csize, correlated with shape
change.
> cor.test(GPA_SubadultData$Csize, pca.SubadultData$pc.scores[,1], method = "pearson",
conf.level = 0.95)
> cor.test(GPA_SubadultData$Csize, pca.SubadultData$pc.scores[,2], method = "pearson",
conf.level = 0.95)
> cor.test(GPA_SubadultData$Csize, pca.SubadultData$pc.scores[,3], method = "pearson",
conf.level = 0.95)

# This code was used to determine if Csize correlated with age.
> cor.test(SubadultAge, GPA_SubadultData$Csize, method = "pearson", conf.level = 0.95)
```

 # Code C2. This t-test code was used to determine if males and females from the adults by sex sample differed in Csize and shape change. (NOTE: Requires Code B3)

```
> CMBadults_Sex <- c(1,2,1,2,1,2,1,2,1,2,1,2,1,2)
> t.test(GPA_Asex$Csize ~ CMBadults_Sex, var.equal = T)
> t.test(pca.Asex$pc.scores[,1] ~ CMBadults_Sex, var.equal = T)
> t.test(pca.Asex$pc.scores[,2] ~ CMBadults_Sex, var.equal = T)
> t.test(pca.Asex$pc.scores[,3] ~ CMBadults_Sex, var.equal = T)
```

 # Code C3. This code was required to determine if Csize correlated with shape change in the adult sample. (NOTE: Requires Code B2)

```
> cor.test(GPA_combAdults$Csize, pca.Adults$pc.scores[,1], method = "pearson", conf.level = 0.95)
> cor.test(GPA_combAdults$Csize, pca.Adults$pc.scores[,2], method = "pearson", conf.level = 0.95)
> cor.test(GPA_combAdults$Csize, pca.Adults$pc.scores[,3], method = "pearson", conf.level = 0.95)
```

 # Code D1. A scatter plot of PC1 and PC2 shape change during growth, represented by dental age, was created using the code below (NOTE: Requires code B1).

```
> ages <- SubadultData$Dental.Age
> PC1_Age <- ggplot(pca.CMB.frame, aes(x = ages, y = PC1)) + geom_point() + ggtitle("Non-Adult Sample: PC1 and Age") + theme(plot.title = element_text (hjust = 0.5)) + scale_shape_manual(values = c(15))
> PC1_Age + labs( x = "Dental Age (Years)", y = "PC1")

> PC2_Age <- ggplot(pca.CMB.frame, aes(x = ages, y = PC2)) + geom_point() + ggtitle("Non-Adult Sample: PC2 and Age") + theme(plot.title = element_text (hjust = 0.5)) + scale_shape_manual(values = c(15))
> PC2_Age + labs( x = "Dental Age (Years)", y = "PC2")
```

 # Code E1. This code extracted and formatted the relevant variables that would be later used in the maturation analysis. A new GPA was conducted on the non-adult sample with the individuals listed in descending order from youngest to oldest by dental age.

```
# First, the Csize and mean shape of the 5 youngest non-adult individuals were extracted from the new csv file. These functioned as the starting point for the size and shape maturations.
> SubAgeDesc <- read.csv("~/Desktop/MA /SubadultsAgeDescending.csv", header = T, row.names = 1, sep = ",")
> comb.Youngest <- as.matrix(SubAgeDesc[1:5,5:40])
> comb.Youngest.array <- arrayspecs(comb.Youngest, 12, 3)
> GPA_comb.Youngest  <- gpagen(comb.Youngest.array , PrinAxes = T, max.iter = NULL, ProcD = T, Proj = T, print.progress = T)
> comb.Youngest.mean <- mshape(GPA_comb.Youngest$coords)
> comb.Youngest.Csize <- (GPA_comb.Youngest$Csize)

# Second, the Csize of each non-adult individual was extracted and written into a csv file.
> comb.age <- as.matrix(SubAgeDesc[5:40])
> comb.age.array <- arrayspecs(comb.age, 12, 3)
```

```
> GPA_comb.age  <- gpagen(comb.age.array , PrinAxes = T, max.iter = NULL, ProcD = T, Proj = T, print.progress = T)
> write.csv(GPA_comb.age$Csize, "SubAdultsCOMBCS.csv")

# Last, the mean GPA shape of each non-adult individual was extracted.
> GPA_comb.age  <- gpagen(comb.age.array , PrinAxes = T, max.iter = NULL, ProcD = T, Proj = T, print.progress = T)
> CMBage_mean <- mshape(GPA_comb.age$coords)
```

 # Code E2. This code was used to extract the entire adult sample's average Csize and mean shape. The adults functioned as the endpoint of the size and shape maturations.

```
> comb.Adults <- read.csv("~/Desktop/MA /comb.Adults.csv", header = T, row.names = 1, sep = ",")
> comb.Adults.mat <- as.matrix(comb.Adults[5:40])
> comb.Adults.array <- arrayspecs(comb.Adults.mat, 12, 3)
> GPA_combAdults  <- gpagen(comb.Adults.array , PrinAxes = T, max.iter = NULL, ProcD = T, Proj = T, print.progress = T)
> comb.Adults.mean <- mshape(GPA_combAdults$coords)
> comb.Adults.Csize <- (GPA_combAdults$Csize)
> comb.Adults.Csize.mean <- mean(comb.Adults.Csize)
> write.csv(comb.Adults.Csize.mean, "AdultMeanCS.csv")
```

 # Code E3. This code performed the maturation analysis of shape using the Sliding Average Approach employed by Wilson et al. (2015). The mean shape of the 5 youngest non-adults (the start point) against non-adult 1 was listed as PD0. The procrustes distance of each individual was measured against the next using the procdist() function. (NOTE: Requires Code E1 and Code E2).

```
> PD0 <- procdist(comb.Youngest.mean, GPA_comb.age$coords[,,1], type = "full", reflect = F)
> PD1 <- procdist(GPA_comb.age$coords[,,1], GPA_comb.age$coords[,,2], type = "full", reflect = F)
> PD2 <- procdist(GPA_comb.age$coords[,,2], GPA_comb.age$coords[,,3], type = "full", reflect = F)
> PD3 <- procdist(GPA_comb.age$coords[,,3], GPA_comb.age$coords[,,4], type = "full", reflect = F)
> PD4 <- procdist(GPA_comb.age$coords[,,4], GPA_comb.age$coords[,,5], type = "full", reflect = F)
> PD5 <- procdist(GPA_comb.age$coords[,,5], GPA_comb.age$coords[,,6], type = "full", reflect = F)
```

```
> PD6 <- procdist(GPA_comb.age$coords[,,6], GPA_comb.age$coords[,,7], type = "full", reflect
= F)
> PD7 <- procdist(GPA_comb.age$coords[,,7], GPA_comb.age$coords[,,8], type = "full", reflect
= F)
> PD8 <- procdist(GPA_comb.age$coords[,,8], GPA_comb.age$coords[,,9], type = "full", reflect
= F)
> PD9 <- procdist(GPA_comb.age$coords[,,9], GPA_comb.age$coords[,,10], type = "full", reflect
= F)
> PD10 <- procdist(GPA_comb.age$coords[,,10], GPA_comb.age$coords[,,11], type = "full",
reflect = F)
> PD11 <- procdist(GPA_comb.age$coords[,,11], GPA_comb.age$coords[,,12], type = "full",
reflect = F)
> PD12 <- procdist(GPA_comb.age$coords[,,12], GPA_comb.age$coords[,,13], type = "full",
reflect = F)
> PD13 <- procdist(GPA_comb.age$coords[,,13], GPA_comb.age$coords[,,14], type = "full",
reflect = F)
> PD14 <- procdist(GPA_comb.age$coords[,,14], GPA_comb.age$coords[,,15], type = "full",
reflect = F)
> PD15 <- procdist(GPA_comb.age$coords[,,15], GPA_comb.age$coords[,,16], type = "full",
reflect = F)
> PD16 <- procdist(GPA_comb.age$coords[,,16], GPA_comb.age$coords[,,17], type = "full",
reflect = F)
> PD17 <- procdist(GPA_comb.age$coords[,,17], GPA_comb.age$coords[,,18], type = "full",
reflect = F)
> PD18 <- procdist(GPA_comb.age$coords[,,18], GPA_comb.age$coords[,,19], type = "full",
reflect = F)
> PD19 <- procdist(GPA_comb.age$coords[,,19], GPA_comb.age$coords[,,20], type = "full",
reflect = F)
> PD20 <- procdist(GPA_comb.age$coords[,,20], GPA_comb.age$coords[,,21], type = "full",
reflect = F)
> PD21 <- procdist(GPA_comb.age$coords[,,21], GPA_comb.age$coords[,,22], type = "full",
reflect = F)
> PD22 <- procdist(GPA_comb.age$coords[,,22], GPA_comb.age$coords[,,23], type = "full",
reflect = F)
> PD23 <- procdist(GPA_comb.age$coords[,,23], GPA_comb.age$coords[,,24], type = "full",
reflect = F)
> PD24 <- procdist(GPA_comb.age$coords[,,24], GPA_comb.age$coords[,,25], type = "full",
reflect = F)
```

```
> PD25 <- procdist(GPA_comb.age$coords[,,25], GPA_comb.age$coords[,,26], type = "full",
reflect = F)
> PD26 <- procdist(GPA_comb.age$coords[,,26], GPA_comb.age$coords[,,27], type = "full",
reflect = F)
> PD27 <- procdist(GPA_comb.age$coords[,,27], GPA_comb.age$coords[,,28], type = "full",
reflect = F)
> PD28 <- procdist(GPA_comb.age$coords[,,28], GPA_comb.age$coords[,,29], type = "full",
reflect = F)
> PD29 <- procdist(GPA_comb.age$coords[,,29], GPA_comb.age$coords[,,30], type = "full",
reflect = F)
> PD30 <- procdist(GPA_comb.age$coords[,,30], GPA_comb.age$coords[,,31], type = "full",
reflect = F)
> PD31 <- procdist(GPA_comb.age$coords[,,31], GPA_comb.age$coords[,,32], type = "full",
reflect = F)
> PD32 <- procdist(GPA_comb.age$coords[,,32], GPA_comb.age$coords[,,33], type = "full",
reflect = F)
> PD33 <- procdist(GPA_comb.age$coords[,,33], GPA_comb.age$coords[,,34], type = "full",
reflect = F)
> PD34 <- procdist(GPA_comb.age$coords[,,34], GPA_comb.age$coords[,,35], type = "full",
reflect = F)
> PD35 <- procdist(GPA_comb.age$coords[,,35], GPA_comb.age$coords[,,36], type = "full",
reflect = F)
> PD36 <- procdist(GPA_comb.age$coords[,,36], GPA_comb.age$coords[,,37], type = "full",
reflect = F)
> PD37 <- procdist(GPA_comb.age$coords[,,37], GPA_comb.age$coords[,,38], type = "full",
reflect = F)
> PD38 <- procdist(GPA_comb.age$coords[,,38], GPA_comb.age$coords[,,39], type = "full",
reflect = F)
> PD39 <- procdist(GPA_comb.age$coords[,,39], GPA_comb.age$coords[,,40], type = "full",
reflect = F)
> PD40 <- procdist(GPA_comb.age$coords[,,40], GPA_comb.age$coords[,,41], type = "full",
reflect = F)
> PD41 <- procdist(GPA_comb.age$coords[,,41], CMBage_mean, type = "full", reflect = F)
> PD42 <- procdist(GPA_comb.age$coords[,,41], comb.Adults.mean, type = "full", reflect = F)
```

In descending order, each PD along with the individual's dental age were manually saved into a new csv file titled "*R - Shape Maturation*.csv"

To calculate the cumulative procrustes distance (trajectory length) for the shape maturation analysis, the code below was required.

```
> R_Shape_Maturation <- read.csv("~/Desktop/R Maturation /R - Shape Maturation.csv", header = T, row.names = 1)
> DistValue.youngest <- (R_Shape_Maturation[1,2])
> DistValue.1 <- sum(R_Shape_Maturation[1:2,2])
> DistValue.2 <- sum(DistValue.1, R_Shape_Maturation[2:3,2])
> DistValue.3 <- sum(DistValue.2, R_Shape_Maturation[3:4,2])
> DistValue.4 <- sum(DistValue.3, R_Shape_Maturation[4:5,2])
> DistValue.5 <- sum(DistValue.4, R_Shape_Maturation[5:6,2])
> DistValue.6 <- sum(DistValue.5, R_Shape_Maturation[6:7,2])
> DistValue.7 <- sum(DistValue.6, R_Shape_Maturation[7:8,2])
> DistValue.8 <- sum(DistValue.7, R_Shape_Maturation[8:9,2])
> DistValue.9 <- sum(DistValue.8, R_Shape_Maturation[9:10,2])
> DistValue.10 <- sum(DistValue.9, R_Shape_Maturation[10:11,2])
> DistValue.11 <- sum(DistValue.10, R_Shape_Maturation[11:12,2])
> DistValue.12 <- sum(DistValue.11, R_Shape_Maturation[12:13,2])
> DistValue.13 <- sum(DistValue.12, R_Shape_Maturation[13:14,2])
> DistValue.14 <- sum(DistValue.13, R_Shape_Maturation[14:15,2])
> DistValue.15 <- sum(DistValue.14, R_Shape_Maturation[15:16,2])
> DistValue.16 <- sum(DistValue.15, R_Shape_Maturation[16:17,2])
> DistValue.17 <- sum(DistValue.16, R_Shape_Maturation[17:18,2])
> DistValue.18 <- sum(DistValue.17, R_Shape_Maturation[18:19,2])
> DistValue.19 <- sum(DistValue.18, R_Shape_Maturation[19:20,2])
> DistValue.20 <- sum(DistValue.19, R_Shape_Maturation[20:21,2])
> DistValue.21 <- sum(DistValue.20, R_Shape_Maturation[21:22,2])
> DistValue.22 <- sum(DistValue.21, R_Shape_Maturation[22:23,2])
> DistValue.23 <- sum(DistValue.22, R_Shape_Maturation[23:24,2])
> DistValue.24 <- sum(DistValue.23, R_Shape_Maturation[24:25,2])
> DistValue.25 <- sum(DistValue.24, R_Shape_Maturation[25:26,2])
> DistValue.26 <- sum(DistValue.25, R_Shape_Maturation[26:27,2])
> DistValue.27 <- sum(DistValue.26, R_Shape_Maturation[27:28,2])
> DistValue.28 <- sum(DistValue.27, R_Shape_Maturation[28:29,2])
> DistValue.29 <- sum(DistValue.28, R_Shape_Maturation[29:30,2])
> DistValue.30 <- sum(DistValue.29, R_Shape_Maturation[30:31,2])
> DistValue.31 <- sum(DistValue.30, R_Shape_Maturation[31:32,2])
> DistValue.32 <- sum(DistValue.31, R_Shape_Maturation[32:33,2])
> DistValue.33 <- sum(DistValue.32, R_Shape_Maturation[33:34,2])
```

```
> DistValue.34 <- sum(DistValue.33, R_Shape_Maturation[34:35,2])
> DistValue.35 <- sum(DistValue.34, R_Shape_Maturation[35:36,2])
> DistValue.36 <- sum(DistValue.35, R_Shape_Maturation[36:37,2])
> DistValue.37 <- sum(DistValue.36, R_Shape_Maturation[37:38,2])
> DistValue.38 <- sum(DistValue.37, R_Shape_Maturation[38:39,2])
> DistValue.39 <- sum(DistValue.38, R_Shape_Maturation[39:40,2])
> DistValue.40 <- sum(DistValue.39, R_Shape_Maturation[40:41,2])
> DistValue.41 <- sum(DistValue.40, R_Shape_Maturation[41:42,2])
> DistValue.Oldest <- sum(DistValue.41, R_Shape_Maturation[42:43,2])
> Cumulative.Dist <- DistValue.Oldest
```

The distance values (excluding cumulative PD) were combined into a single numeric R object.

```
> DistanceValueEachIndividual <- c(DistValue.youngest, DistValue.1, DistValue.2, DistValue.3,
DistValue.4, DistValue.5, DistValue.6, DistValue.7, DistValue.8, DistValue.9, DistValue.10,
DistValue.11, DistValue.12, DistValue.13, DistValue.14, DistValue.15, DistValue.16,
DistValue.17, DistValue.18, DistValue.19, DistValue.20, DistValue.21, DistValue.22,
DistValue.23, DistValue.24, DistValue.25, DistValue.26, DistValue.27, DistValue.28,
DistValue.29, DistValue.30, DistValue.31, DistValue.32, DistValue.33, DistValue.34,
DistValue.35, DistValue.36, DistValue.37, DistValue.38, DistValue.39, DistValue.40,
DistValue.41, DistValue.Oldest)
```

This code was used to create the sliding shape maturation groups from the preceding procrustes distance values in the above R object. Each maturation group contained 5 individuals, with an overlap of 2 individuals per group. proc.group.1 contains the average distance of individuals 1-5, and proc.group.2 contains the average distance of individuals 3-7. (Note: Due to data format distances 1-5 were located in data cells 2-6).

```
> proc.group.1 <-mean(DistanceValueEachIndividual[2:6])
> proc.group.2 <- mean(DistanceValueEachIndividual[4:8])
> proc.group.3 <- mean(DistanceValueEachIndividual[6:10])
> proc.group.4 <- mean(DistanceValueEachIndividual[8:12])
> proc.group.5 <- mean(DistanceValueEachIndividual[10:14])
> proc.group.6 <- mean(DistanceValueEachIndividual[12:16])
> proc.group.7 <- mean(DistanceValueEachIndividual[14:18])
> proc.group.8 <- mean(DistanceValueEachIndividual[16:20])
> proc.group.9 <- mean(DistanceValueEachIndividual[18:22])
> proc.group.10 <- mean(DistanceValueEachIndividual[20:24])
> proc.group.11 <- mean(DistanceValueEachIndividual[22:26])
> proc.group.12 <- mean(DistanceValueEachIndividual[24:28])
```

```
> proc.group.13 <- mean(DistanceValueEachIndividual[26:30])
> proc.group.14 <- mean(DistanceValueEachIndividual[28:32])
> proc.group.15 <- mean(DistanceValueEachIndividual[30:34])
> proc.group.16 <- mean(DistanceValueEachIndividual[32:36])
> proc.group.17 <- mean(DistanceValueEachIndividual[34:38])
> proc.group.18 <- mean(DistanceValueEachIndividual[36:40])
> proc.group.19 <- mean(DistanceValueEachIndividual[38:42])
```

Each maturation group's procrustes distance by the cumulative procrustes distance was divided using this code, before being multiplied by 100. This resulted in the maturation % for each maturation group.

```
> maturity.group.1 <- (proc.group.1/Cumulative.Dist)*100
> maturity.group.2 <- (proc.group.2/Cumulative.Dist)*100
> maturity.group.3 <- (proc.group.3/Cumulative.Dist)*100
> maturity.group.4 <- (proc.group.4/Cumulative.Dist)*100
> maturity.group.5 <- (proc.group.5/Cumulative.Dist)*100
> maturity.group.6 <- (proc.group.6/Cumulative.Dist)*100
> maturity.group.7 <- (proc.group.7/Cumulative.Dist)*100
> maturity.group.8 <- (proc.group.8/Cumulative.Dist)*100
> maturity.group.9 <- (proc.group.9/Cumulative.Dist)*100
> maturity.group.10 <- (proc.group.10/Cumulative.Dist)*100
> maturity.group.11 <- (proc.group.11/Cumulative.Dist)*100
> maturity.group.12 <- (proc.group.12/Cumulative.Dist)*100
> maturity.group.13 <- (proc.group.13/Cumulative.Dist)*100
> maturity.group.14 <- (proc.group.14/Cumulative.Dist)*100
> maturity.group.15 <- (proc.group.15/Cumulative.Dist)*100
> maturity.group.16 <- (proc.group.16/Cumulative.Dist)*100
> maturity.group.17 <- (proc.group.17/Cumulative.Dist)*100
> maturity.group.18 <- (proc.group.18/Cumulative.Dist)*100
> maturity.group.19 <- (proc.group.19/Cumulative.Dist)*100
```

Maturity group values are combined into a numeric R object

```
> MaturityPercent <- c(maturity.group.1, maturity.group.2, maturity.group.3, maturity.group.4,
maturity.group.5, maturity.group.6, maturity.group.7, maturity.group.8, maturity.group.9,
maturity.group.10, maturity.group.11, maturity.group.12, maturity.group.13,
maturity.group.14,
maturity.group.15, maturity.group.16, maturity.group.17, maturity.group.18,
maturity.group.19)
```

The average dental age of each maturation group was averaged using the mean() function. age.group.1 contains the average dental age of individuals 1-5, and age.group.2 contains the average dental age of individuals 3-7.

```
> age.group.1 <- mean(R_Shape_Maturation[2:6,1])
> age.group.2 <- mean(R_Shape_Maturation[4:8,1])
> age.group.3 <- mean(R_Shape_Maturation[6:10,1])
> age.group.4 <- mean(R_Shape_Maturation[8:12,1])
> age.group.5 <- mean(R_Shape_Maturation[10:14,1])
> age.group.6 <- mean(R_Shape_Maturation[12:16,1])
> age.group.7 <- mean(R_Shape_Maturation[14:18,1])
> age.group.8 <- mean(R_Shape_Maturation[16:20,1])
> age.group.9 <- mean(R_Shape_Maturation[18:22,1])
> age.group.10 <- mean(R_Shape_Maturation[20:24,1])
> age.group.11 <- mean(R_Shape_Maturation[22:26,1])
> age.group.12 <- mean(R_Shape_Maturation[24:28,1])
> age.group.13 <- mean(R_Shape_Maturation[26:30,1])
> age.group.14 <- mean(R_Shape_Maturation[28:32,1])
> age.group.15 <- mean(R_Shape_Maturation[30:34,1])
> age.group.16 <- mean(R_Shape_Maturation[32:36,1])
> age.group.17 <- mean(R_Shape_Maturation[34:38,1])
> age.group.18 <- mean(R_Shape_Maturation[36:40,1])
> age.group.19 <- mean(R_Shape_Maturation[38:42,1])
```

This code combined each age group into a single numeric R object.

```
> Age <- c(age.group.1, age.group.2, age.group.3, age.group.4, age.group.5, age.group.6,
age.group.7, age.group.8, age.group.9, age.group.10, age.group.11, age.group.12,
age.group.13, age.group.14, age.group.15, age.group.16, age.group.17, age.group.18,
age.group.19)
```

The average dental age of each group and their MaturityPercent were combined into a single data frame to be plotted alongside the maturation analysis for size.

```
> df.shape <- data.frame(Age, MaturityPercent)
```

 # Code E4. This code was used for the maturation analysis of size. The Csize of the 5 youngest non-adults, along with the Csizes of every individual non-adult, were manually combined in a csv file titled “R - Size Maturation.csv". (NOTE: Requires Code E3).

```
> R_Size_Maturation <- read.csv("~/Desktop/R Maturation /R - Size Maturation.csv", header =
T, row.names = 1)

# The Csize of every non-adult was re-expressed as a percentage of average adult Csize. (NOTE:
The calculation of a cumulative trajectory length for size is not required when using Csize.)
> size.percent.youngest <-(R_Size_Maturation[1,1]/comb.Adults.Csize.mean)*100
> size.percent.1 <- (R_Size_Maturation[2,1]/comb.Adults.Csize.mean)*100
> size.percent.2 <- (R_Size_Maturation[3,1]/comb.Adults.Csize.mean)*100
> size.percent.3 <- (R_Size_Maturation[4,1]/comb.Adults.Csize.mean)*100
> size.percent.4 <- (R_Size_Maturation[5,1]/comb.Adults.Csize.mean)*100
> size.percent.5 <- (R_Size_Maturation[6,1]/comb.Adults.Csize.mean)*100
> size.percent.6 <- (R_Size_Maturation[7,1]/comb.Adults.Csize.mean)*100
> size.percent.7 <- (R_Size_Maturation[8,1]/comb.Adults.Csize.mean)*100
> size.percent.8 <- (R_Size_Maturation[9,1]/comb.Adults.Csize.mean)*100
> size.percent.9 <- (R_Size_Maturation[10,1]/comb.Adults.Csize.mean)*100
> size.percent.10 <- (R_Size_Maturation[11,1]/comb.Adults.Csize.mean)*100
> size.percent.11 <- (R_Size_Maturation[12,1]/comb.Adults.Csize.mean)*100
> size.percent.12 <- (R_Size_Maturation[13,1]/comb.Adults.Csize.mean)*100
> size.percent.13 <- (R_Size_Maturation[14,1]/comb.Adults.Csize.mean)*100
> size.percent.14 <- (R_Size_Maturation[15,1]/comb.Adults.Csize.mean)*100
> size.percent.15 <- (R_Size_Maturation[16,1]/comb.Adults.Csize.mean)*100
> size.percent.16 <- (R_Size_Maturation[17,1]/comb.Adults.Csize.mean)*100
> size.percent.17 <- (R_Size_Maturation[18,1]/comb.Adults.Csize.mean)*100
> size.percent.18 <- (R_Size_Maturation[19,1]/comb.Adults.Csize.mean)*100
> size.percent.19 <- (R_Size_Maturation[20,1]/comb.Adults.Csize.mean)*100
> size.percent.20 <- (R_Size_Maturation[21,1]/comb.Adults.Csize.mean)*100
> size.percent.21 <- (R_Size_Maturation[22,1]/comb.Adults.Csize.mean)*100
> size.percent.22 <- (R_Size_Maturation[23,1]/comb.Adults.Csize.mean)*100
> size.percent.23 <- (R_Size_Maturation[24,1]/comb.Adults.Csize.mean)*100
> size.percent.24 <- (R_Size_Maturation[25,1]/comb.Adults.Csize.mean)*100
> size.percent.25 <- (R_Size_Maturation[26,1]/comb.Adults.Csize.mean)*100
> size.percent.26 <- (R_Size_Maturation[27,1]/comb.Adults.Csize.mean)*100
> size.percent.27 <- (R_Size_Maturation[28,1]/comb.Adults.Csize.mean)*100
> size.percent.28 <- (R_Size_Maturation[29,1]/comb.Adults.Csize.mean)*100
> size.percent.29 <- (R_Size_Maturation[30,1]/comb.Adults.Csize.mean)*100
> size.percent.30 <- (R_Size_Maturation[31,1]/comb.Adults.Csize.mean)*100
> size.percent.31 <- (R_Size_Maturation[32,1]/comb.Adults.Csize.mean)*100
> size.percent.32 <- (R_Size_Maturation[33,1]/comb.Adults.Csize.mean)*100
```

```
> size.percent.33 <- (R_Size_Maturation[34,1]/comb.Adults.Csize.mean)*100
> size.percent.34 <- (R_Size_Maturation[35,1]/comb.Adults.Csize.mean)*100
> size.percent.35 <- (R_Size_Maturation[36,1]/comb.Adults.Csize.mean)*100
> size.percent.36 <- (R_Size_Maturation[37,1]/comb.Adults.Csize.mean)*100
> size.percent.37 <- (R_Size_Maturation[38,1]/comb.Adults.Csize.mean)*100
> size.percent.38 <- (R_Size_Maturation[39,1]/comb.Adults.Csize.mean)*100
> size.percent.39 <- (R_Size_Maturation[40,1]/comb.Adults.Csize.mean)*100
> size.percent.40 <- (R_Size_Maturation[41,1]/comb.Adults.Csize.mean)*100
> size.percent.41 <- (R_Size_Maturation[42,1]/comb.Adults.Csize.mean)*100
```

The size maturation percent of each non-adult was combined into a single R object.

```
> Size.MaturityEachIndividual <- c(size.percent.youngest, size.percent.1, size.percent.2,
size.percent.3, size.percent.4, size.percent.5, size.percent.6, size.percent.7, size.percent.8,
size.percent.9, size.percent.10, size.percent.11, size.percent.12, size.percent.13,
size.percent.14, size.percent.15, size.percent.16, size.percent.17, size.percent.18,
size.percent.19, size.percent.20, size.percent.21, size.percent.22, size.percent.23,
size.percent.24, size.percent.25, size.percent.26,size.percent.27, size.percent.28,
size.percent.29, size.percent.30, size.percent.31, size.percent.32, size.percent.33,
size.percent.34, size.percent.35, size.percent.36, size.percent.37, size.percent.38,
size.percent.39, size.percent.40, size.percent.41)
```

Each maturation group's Csize was averaged using the code below. Each group consisted of 5 individuals, with an overlap of 2 individuals per group.

```
> size.group.1 <- mean(Size.MaturityEachIndividual[2:6])
> size.group.2 <- mean(Size.MaturityEachIndividual[4:8])
> size.group.3 <- mean(Size.MaturityEachIndividual[6:10])
> size.group.4 <- mean(Size.MaturityEachIndividual[8:12])
> size.group.5 <- mean(Size.MaturityEachIndividual[10:14])
> size.group.6 <- mean(Size.MaturityEachIndividual[12:16])
> size.group.7 <- mean(Size.MaturityEachIndividual[14:18])
> size.group.8 <- mean(Size.MaturityEachIndividual[16:20])
> size.group.9 <- mean(Size.MaturityEachIndividual[18:22])
> size.group.10 <- mean(Size.MaturityEachIndividual[20:24])
> size.group.11 <- mean(Size.MaturityEachIndividual[22:26])
> size.group.12 <- mean(Size.MaturityEachIndividual[24:28])
> size.group.13 <- mean(Size.MaturityEachIndividual[26:30])
> size.group.14 <- mean(Size.MaturityEachIndividual[28:32])
> size.group.15 <- mean(Size.MaturityEachIndividual[30:34])
```

```
> size.group.16 <- mean(Size.MaturityEachIndividual[32:36])
> size.group.17 <- mean(Size.MaturityEachIndividual[34:38])
> size.group.18 <- mean(Size.MaturityEachIndividual[36:40])
> size.group.19 <- mean(Size.MaturityEachIndividual[38:42])
```

The size groups were combined into a single R object.

```
> Size.MaturityPercent <- c(size.group.1, size.group.2, size.group.3, size.group.4, size.group.5,
size.group.6, size.group.7, size.group.8, size.group.9, size.group.10, size.group.11,
size.group.12, size.group.13, size.group.14, size.group.15, size.group.16, size.group.17,
size.group.18, size.group.19)
```

The average dental age of each group and its Size.MaturityPercent were combined into a single data frame to be plotted in a graph alongside the maturation analysis for shape.

```
> df.size <- data.frame(Age, Size.MaturityPercent)
```

 # Code E5. This code was used to plot shape and size maturation side by side in a single graph. A 'loess' regression was included for each maturation. (NOTE: Requires Code E3 and Code E4).

```
> shape.size.plot <- ggplot() + geom_point(data = df.shape, aes(x=Age, y=MaturityPercent),
color = "orange") + geom_smooth(data=df.shape, aes(x=Age, y=MaturityPercent), colour="red",
size=0.3, se = F, method = "loess") + scale_x_continuous(name = "Dental Age (Years)") +
scale_y_continuous(name = "Maturation %") + geom_smooth(method = "loess",  size = 0.2,
color = "red", se = F) + geom_point(data=df.size, aes(x=Age, y=Size.MaturityPercent), color =
"blue") + geom_smooth(data=df.size, aes(x=Age, y=Size.MaturityPercent), colour="red",
size=0.3, se = F, method = "loess") + ggtitle("Shape and Size Maturation") + theme(plot.title =
element_text(hjust = 0.5, face = "bold"))
```

Appendix C: Sliding Average Approach

This appendix outlines an example of the sliding average approach outlined by Wilson et al. (2015). The R code used to perform these calculations is found in Appendix B.

Start = mean shape of the youngest 5 non-adults.
Oldest = shape of the oldest non-adult.
Adult = adult mean shape.

Cumulative trajectory length (CL) is the total Procrustes Distance (->) between each individual and represents complete maturity.

CL = (*Start* -> 1) + (1 -> 2) + (2 -> 3) + ... (40 -> *Oldest*) + (*Oldest* -> *Adult*)

The Procrustes Distance of individual 2 along the trajectory is determined as follows:

Distance 2 = (*Start* -> 1) + (1 -> 2)

To ensure that each maturation group did not plot beyond the next group, the distances and ages were averaged to act as a smoothing function:

Individual	**Age**	**Procrustes Distance**
Start	Mean age of youngest 5	Mean distance of youngest 5
1	7.5	0.01107942
2	8.5	0.0303826
3	9.5	0.05780099
4	9.5	0.08167349
5	9.5	0.10643309
6	9.5	0.12823181
7	10.5	0.14935043

Etc.

Groups were then created by averaging the ages and Procrustes distances of the individuals within.

Group 1 = Mean distance of individuals 1 - 5

Group 2 = Mean distance of individuals 3 - 7
Etc.

Group	**Mean Age**	**Mean Distance**
1	(7.5 + 8.5 + 9.5 + 9.5 + 9.5) /5	(0.01107942 + 0.0303826 + 0.05780099 + 0.08167349 + 0.10643309) /5
2	(9.5 + 9.5 + 9.5 + 9.5 + 10.5) /5	(0.05780099 + 0.08167349 + 0.10643309 + 0.12823181 + 0.14935043) /5

Etc.

After group age and distance is determined, the group mean distance is re-expressed as a percentage of total maturity.

Maturation Group 1 = (Group 1 Mean Distance / CL) * 100
Maturation Group 2 = (Group 2 Mean Distance / CL) * 100
Etc.

These calculations were repeated for every maturation group and plotted alongside its group age.

Appendix D: PC Summary

Table A. See below a PC summary of the non-adult population. Each PC along with its proportion of variance and its percentage of variance are listed below. The PC cut-point was a proportion of variance less than 10%. The cut-point is indicated by a blue line and the preceding PC is written in bold.

Principal Components	Proportion of Variance	Cumulative Proportion of Variance (%)
PC1	0.4364	0.4364
PC2	0.18004	0.61644
PC3	**0.11891**	**0.73534**
PC4	0.07339	0.80874
PC5	0.04459	0.85332
PC6	0.0304	0.88372
PC7	0.02203	0.90575
PC8	0.01843	0.92418
PC9	0.01598	0.94015
PC10	0.01353	0.95368
PC11	0.01117	0.96485
PC12	0.00758	0.97243
PC13	0.00665	0.97908
PC14	0.00582	0.9849
PC15	0.00481	0.98971
PC16	0.00272	0.99243
PC17	0.00215	0.99457
PC18	0.00166	0.99624
PC19	0.00123	0.99747
PC20	0.00097	0.99843
PC21	0.00071	0.99914
PC22	0.00053	0.99967
PC23	0.00017	0.99984

PC24	0.00007	100

Table B. See below a PC summary of the adult population. Each PC along with its proportion of variance and its percentage of variance are listed below. The PC cut-point was a proportion of variance less than 10%. The cut-point is indicated by a blue line and the preceding PC is written in bold.

Principal Components	Proportion of Variance	Cumulative Proportion of Variance (%)
PC1	0.37732	0.37732
PC2	0.25558	0.6329
PC3	**0.11293**	**0.74583**
PC4	0.08559	0.83142
PC5	0.04594	0.87737
PC6	0.02945	0.90682
PC7	0.02651	0.93332
PC8	0.0169	0.95023
PC9	0.01599	0.96622
PC10	0.00906	0.97529
PC11	0.00749	0.98278
PC12	0.0049	0.98767
PC13	0.00422	0.9919
PC14	0.00303	0.99493
PC15	0.00159	0.99652
PC16	0.00121	0.99774
PC17	0.00107	0.99881
PC18	0.00054	0.99935
PC19	0.00037	0.99972
PC20	0.00013	0.99985
PC21	0.0001	100